UNIVERSITY OF CALIFORNIA

Santa Barbara

Microfabrication of Biomimetic Structures for Neural Interfaces

A dissertation submitted in partial satisfaction of the

requirements for the degree Doctor of Philosophy

in Electrical and Computer Engineering

by

Samuel Jack Beach

Committee in charge:

Professor Luke Theogarajan, Chair

Professor Forrest Brewer

Professor Chris Palmstrøm

Professor Matthew Turk

December 2014

The dissertation of Samuel Jack Beach is approved.

_____

Forrest Brewer

_____

Chris Palmstrøm

_____

Matthew Turk

_____

Luke Theogarajan, Committee Chair

December 2014

Microfabrication of Biomimetic Structures for Neural Interfaces

by

Samuel Jack Beach

ACKNOWLEDGEMENTS

I wish to thank and acknowledge many people who made my doctoral work possible and supported me and my work. Foremost, I would like to thank my parents and grandparents for making education an important part of my life and supporting me through my bachelors, masters, and certificate programs and as I worked towards the completion of this dissertation.

I also wish to extend my gratitude and acknowledge Dr. Theogarajan, who welcomed me into his group upon his arrival at UCSB and offered me the chance to make his dreams tangible realities. Dr. Theogarajan supported me through hardships in my personal life as well as difficulties in my research projects. His support has been critical in enabling me to expand my skills in microfabrication with industry experiences and in allowing me access to UCSB's state-of-the-art Nanotech Cleanroom facility and the California Nanosystems Institute at UCSB. Without his financial support in the form of Graduate Student Researcher positions as well as technical specialist positions, none of my research would have been possible. I will always remember the diverse research background about which Dr. Theogarajan has been kind enough to teach me. Dr. Theogarajan's guidance and insights have always motivated me to push to find solutions within my research.

I also wish to thank my dissertation committee members, Professor Forrest Brewer, Professor Chris Palmstrøm, and Professor Matthew Turk for their insights and support.

I would like to acknowledge all my current and former colleagues, particularly Mohamed Elzeftawi, Andrew Merithew, Avantika Sodhi, Saeed Mirzaeian, Sukru Yemenicioglu, Sarah Grundeen, Justin Rofeh, Luis Chen, Chin-Hsuan Chen, Weibin Cue. My microfabrication endeavors in particular were greatly enhanced by the meaningful conversation and suggestions of Avantika Sodhi, Sukru Yemenicioglu, Ashfaque Uddin and Justin Rofeh. Additionally, without the help of Sarah Grundeen none of the biological in vitro investigations of my devices would have been possible. I must also thank Wesley Collins, Justin Rofen and April Yates for their help in suggesting edits for this manuscript.

Finally, I would like to acknowledge the many interns who have contributed to my projects under my mentorship Christopher Nakamoto, Jason Farkas, Zach Pritchard, Aaron Lovato, Cara Hale-Hanes, Jenny Willis, Justin Balter, Veronica Zhu, Christopher Bascomb, Rano Sidhu, and Daniel Vong. Without the assistance of Christopher Nakamoto and Aaron Lovato, my research might never have achieve the milestones that have been reached.

I would also like to thank the staff UCSB's Nanotech cleanroom, where so much of my research was conducted. In particular, I would like to acknowledge Dr. Brian Thibeault, Ning Cao, Bill Mitchell, Don Freeborn, and Jack Whaley for their insightful conversations, technical assistance, and support of my projects. It was only through their assistance that my research goals in the clean room were met.

I also thankfully acknowledge the financial support of the Institute for Collaborative Biotechnologies, the National Institutes of Health, the California

NanoSystems Institute Challenge Grant, International Business Machines Corporation, and Intel Corporation.

This dissertation is dedicated to my parents, Glenna and Albert Beach who have given me the curiosity to address research questions and the drive and determination to see them through.

VITA OF SAMUEL JACK BEACH

December 2014

EDUCATION

University of California, Santa Barbara

Bachelors of Science in Electrical Engineering, Sept 2007
Graduated summa cum laude, Undergraduate G.P.A. 3.89/4.0

Masters of Science in Electrical and Computer Engineering, June 2009

Graduate Program in Management Practices, June 2010

Doctor of Philosophy in Electrical and Computer Engineering, December 2014
Graduate G.P.A 3.98/4.0

PROFESSIONAL EMPLOYMENT

June 2007 - Sept 2008: CPIMA Research Intern, IBM Almaden Research Center, San Jose CA

2007 - 2011: Teaching Assistant, Department of Electrical and Computer Engineering, University of California, Santa Barbara

June 2008 - Sept 2008: Research Intern, IBM Research Division, IBM Almaden Research Center, San Jose CA

June 2010 - Sept 2010: Process Engineer, Etch Process Development, IBM Microelectronics Albany Nanotech, Albany NY (Graduate Technical Intern)

Part-time 2010-2013: Fabrication Leader for NNIN Chip Camps

2011 - 2014: Graduate Student Researcher, University of California, Santa Barbara

Summers 2012-2014: Mentor for INSET, NNIN (National Nanotechnology Infrastructure Network) REU, NNIN RET internship programs

Sept 2012 - March 2013: Process Engineer, High Volume Manufacturing, Intel AzFSM, Chandler AZ (Graduate Technical Intern)

April-Sept 2014: Assistant Specialist, University of California, Santa Barbara

Sept 2014: Rotational Engineer | Senior Lithography Development Engineer, Intel Corporation, Chandler AZ.

PUBLICATIONS

Mohamed Elzeftawi, Samuel Beach, Le Wang, Luke Theogarajan, *A 1.3_W 0.0075mm2 Neural Amplifier and Capacitor-Integrated Electrodes for High Density Neural Implant Recording*, Biomedical Circuits and Systems Conference (BioCAS), 2012 IEEE.

Avantika Sodhi, Samuel J. Beach, Luis Chen, Matt Jacob-Mitos, Jonathan E. Roth, John Bowers, Luke Theogarajan, *Heterogeneous optoelectronic integration using locally polymerized imprinted hard mask*, SPIE Proceedings vol. 8628, March 6, 2013.

AWARDS

University of California College of Engineering Merit Scholarships (2x)

Department of Homeland Security Graduate Fellowship (declined award conditions)

SMART DOD Fellowship (declined award conditions)

UCSB ECE Department Teaching Assistant Recognition Award

GEM Masters Fellowship award supported by IBM

GEM PhD Fellowship award supported by Intel

ABSTRACT

Microfabrication of Biomimetic Structures for Neural Interfaces

by

Samuel Jack Beach

Interfacing with the brain is a challenging problem. While many innovative methods for providing input and output to neural systems have been developed and demonstrated successfully in human patients, these invasive systems use less biologically compatible means than are realizable. Materials and mechanisms which are closer mimics to biological systems in their behaviors can lead to more stable and effective medical prosthetic and research devices.

Retinal prosthetics, as well as Cochlear implants, are neural implants which provide stimulation via electrical impulses. Currents passing across neurons trigger neurons to begin firing or generating action potentials down their axons, stimulating neurons with dendrites connected to those axons terminals. This scheme transduces the desired simulation into neural firing spikes, but the majority of applied current is shunted around neurons rather than contributing to stimulation. Excess current contributes to the power and thermal budgets of neural simulation devices, which are implanted in tissue, limiting their functionality. Additionally, the electrical contacts

which provide a source and return for the stimulation currents are subject to degradation over time, as currents are repeatedly applied during stimulation events. Stimulation of neurons via local delivery of potassium in excess of available intercellular potassium can be used in place of direct electrical stimulation and promises to be a more biologically compatible method.

Several forms of neural recording devices have been developed and the widest know and highest density is the Utah Array, a 3D array of silicon spires, which can record from their tips when inserted into neural tissue. While this 3D array topology can access a field of neural activity, the stiffness of these silicon spires is very different than that of neural tissue, which can lead to an unwanted inflammatory response. Conductive polymer pillars made of softer materials that are a closer match to neural tissues, while mirroring the same density and insertion length as the Utah Array, may provide a better recording mechanism due to their improved mechanical compatibility with neural tissues.

This thesis investigates microfabrication schemes to produce biomimetic structures that can enable neural simulation and recording devices which feature greater biological stability and improve utility.

TABLE OF CONTENTS

LIST OF FIGURES

I. Motivations and Introduction to Microfabrication of Biomimetic Structures for Neural Interfaces

A. Developing a Greater Understanding of the Human Brain

The brain and its incredibly complex functions are of interest to the world. How the brain works, how neuronal circuits function, and how the basic neuronal code operates are all ongoing questions. A better understanding of the brain can lead to knowledge about how decision making, perception, and even consciousness come about. Knowledge about how neural circuits work will certainly also play a role in advancing treatments for many debilitating diseases and physiological conditions.

Current knowledge about the human brain and its mechanisms has led to innumerable drug treatments for conditions afflicting people around the world as well as a growing number of devices to correct or stabilize damaging activities occurring in the brain. These include arresting seizures and tremors as well as some forms of migraines.

The study of the mind and brain has been called, “The last frontier in science” by Professor Michael Tarr of Carnegie Mellon University. He has pointed out that, “Although the field has made enormous progress over the past several decades, understanding of the basic principles of thought and brain function are still far more unknown than known," going as far as suggesting that understanding the human brain “is a significant step in understanding what makes humans human.”

It is imaginable that with greater study of the human brain, improved treatments or even cures could be found for degenerative neural diseases such as Alzheimer's and other dementia causing conditions, as well as degenerative disorders of the central nervous system such as Parkinson's.

The BRAIN Initiative (Brain Research Through Advancing Innovative Neurotechnologies) aims to direct the scientific community to investigate the human brain and create a map of the neural landscape of the brain with a scope that reaches down to the level of individual neurons and neuronal circuits. This initiative aims to reproduce the fruitful results of the human genome mapping project by focusing the scientific community on this goal and providing funding to develop innovative neurotechnologies that will enable the desired leap in understanding of the human brain. These neurotechnologies may be investigative, but may also directly result in improvements in therapeutic technologies that address the brain.

When discussing the prospect of a full mapping of brain activity and gaining an understanding of the emergent properties of the neural circuits of the brain, A. Paul Alivisatos writes, "Understanding how the brain works is arguably one of the greatest scientific challenges of our time". It is with this challenge in mind that this dissertation focuses on developing improved methods to interface with and learn about the human brain and its neuronal circuitry. It is hoped that investigation of these novel simulating input interfaces and recording output interfaces may one day lead to improved human medical prosthetics and enable greater understanding of the brain and its neuronal circuitry.

B. Microfabrication of Biomimetic Structures for Neural Interfaces

Novel neural interfaces can be developed by designing structures while using biomimetic principles and applying microfabrication techniques.

1. Microfabrication Techniques

Very precise devices and structures can be formed through the use of microfabricaition techniques which can enable a desired interface to be formed. These techniques come from the huge expansion of human knowledge related to semiconductor and specifically silicon processing techniques that drove the computer revolution, as well as advancements in MEMS (mico-mechanical machine systems) and related chemical microfabricaition processing and functionalization techniques. Specifically, these techniques allow for the generation of ultra-thin membranes, nanoscopic porous films, and patterns of deep high aspect ratio voids in solid crystals. These techniques additionally allow easy patterning of conductive and dielectric layers, enabling devices which can be directly connected to electronic circuits.

2. Biomimetic Principles

The idea of biomimetics is to essentially imitate, mimic, or mirror biology through synthetic means to solve problems. In general, this idea has been applied when looking to nature for inspiration to problems and then designing systems that synthetically reproduce the biological solution found in nature. In the case of interfacing with biological systems, the meaning may become more precise and

change slightly as the problems being faced generally result from differences and conflicts existing between the interfacing systems behaviors, properties, and operating principles and those of the cells, tissue, or biological system within which the interface is being established. By looking at the way the human brain operates and mimicking its operations, interfaces, and the mechanical properties of its tissues, neural interfaces can be developed that are more compatible with the human brain and specifically the cells and tissues within which interfaces are being created. In this case, mimicking the tissues properties or the neurons behaviors can potentially aid in the functionality, bio-compatibility, and lifetime of the device.

Mimicking the electrochemical membrane potentials that are integral to neuron firing potentials and the function of neuronal circuits in order to stimulate neuronal firing activity is one potential biomimetic innovation in the realm of neural stimulation. Normally, currents are driven from a source to a return electrode with the current shunting through intercellular fluid or electrolyte between neurons near the stimulation device. This process triggers some neurons along the path to become stimulated and fire, but most of the current is simply shunted around the neurons and doesn't have an effect. This means that a significant amount of the power used to stimulate the target neurons is wasted needlessly using up thermal budget and power budget. Additionally, repeated stimulation using electric currents can degrade the electrodes being used, causing electroplating of the nearby tissue and the release of electrode materials that can be cytotoxic. The application of cations to the local

intercellular fluid increases the local external concentration nearby the neurons and causes the neurons to begin firing.

Mimicking the mechanical properties of brain tissues is another possible avenue to enhance neural recording interfaces. In this case, the standard materials used are so stiff compared to brain tissue that they can cause excessive and unwanted damage both during implantation, as well as over the lifetime of the device. This occurs as the material is inserted into the softer brain tissue and creates a track of traumatic damage over time due to the small micro motion of the brain in a moving skull causing wear against the much softer tissue being moved against the stiffer implant material. By designing implants that are as soft as possible to minimize the difference between the mechanical properties of the implants and tissues involved, while still being stiff enough to successfully be inserted in the brain, implants of greater biocompatibility can be created. Additionally, as the inflammatory and isolating response of brain tissue to trauma results in the growth of glial support cells which seal off the source of the trauma, devices that minimize this trauma should additionally benefit from enhanced recording functionality and recording longevity.

C. Sensory Loss and Simulating Ion Pumps

The loss of a sensory organ or system and the information that system provides to the brain can have a devastating impact on an affected individual, limiting their access to the sensory information available in the world around them and degrading their quality of life. This comprises a significant problem, with the World Health

Organization for example estimating that fully 0.6% of the world's population is blind.

1. Stimulating Neural Interfaces and Implants

A number of stimulating neural prosthetic systems have been developed to treat several different sensory organ failures. These stimulating interfaces are implanted to restore lost function due to neural damage and sensory loss. The Cochlear Implant is one such device used to restore the effect and sensation of hearing. In the case of this device, direct electrical stimulation of the cochlea via an implanted electrode array is used to restore hearing. While the Cochlear Implant is one of the most successful stimulating implants used to restore sensory loss, with 324,000 implanted patients worldwide as of 2012 according to NIH reporting, stimulating implants have also been made to restore other sensory systems and to arrest adverse neural activity.

Some examples of this alternate but similarly important stimulating goal include stimulating systems developed to arrest undesired neural activity linked to Parkinson's tremors, epileptic seizures, and some forms of intense migraines. These implanted systems have shown great promise in treating and limiting those debilitating conditions.

One such sensory system where work is ongoing to restore sensory function is the vision system. Most often, the cause of blindness is related to the optical and sensing elements of the eye failing. In these instances, the neural cells in the retina and the nerves connecting the retina to the visual cortex remain intact. Two diseases which result in the loss of photoreceptors and blindness or severe vision loss in over a

million people each year, but which leave untouched nerves in the retina that can be stimulated are retinitis pigmetosa and macular degeneration. Each of these has a very different cause, but both can be treated with direct stimulation of the neurons in the retinal tissue.

2. Electrical Neural Stimulation

All of the above stimulating neural interfaces use direct electrical stimulation to trigger a biological electrochemical response in nerves or neurons to effectively transduce the desired signal into the action potentials used by the neuronal circuits of the brain. This stimulation is manifested as currents that are driven access the target tissue from one electrode to another. Significantly, most of this current travels around nerve cells or neurons by following the path of least resistance along the intercellular fluid between them. This process is inefficient as most current circumvents the cells of interest. Unnecessary power is wasted stimulating the target neurons in this manner, which increases the thermal and power budget of the stimulating interface. The repeated application of these electrical currents degrades the electrodes over time and can cause electroplating of the nearby tissue and the release of electrode materials that can be cytotoxic. For these reasons, a mechanism that does not breakdown electrodes over time, shunt excess current around cells, generate excessive heat, or require excessive power would be more ideal and more biologically compatible.

3. Ionic Neural Stimulation

Ionic neural stimulation offers an alternative method to electrical neural stimulation. By momentarily adding potassium cations to the intercellular fluid near a neuron, the local concentration of potassium ions immediately outside a neuron can be increased to the point that the neuron begins firing. Preliminary experiments demonstrating this possible avenue for neural stimulation were carried out by Professor Luke Theogarajan[1], demonstrating both stimulation of neural firing in rabbit retinal cells when potassium was added to their intercellular solution, (see Figure 1) as well as the dose response curve (see Figure 2) which indicates that doubling the local concentration of potassium is sufficient to generate firing.

Figure 1. Time delayed response to the addition of potassium to local intercellular fluid around rabbit retina.

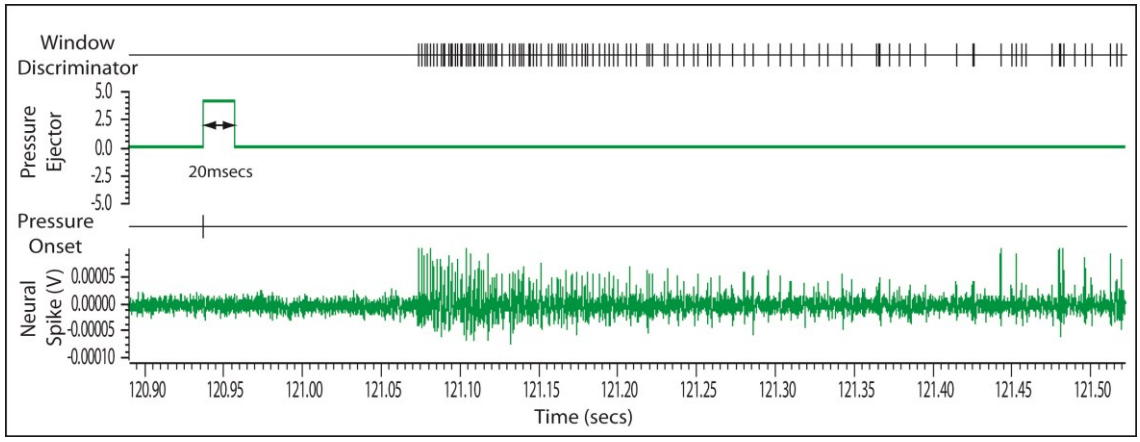

Figure 2. Dose-response curve for neural firing spikes verses concentrations of potassium.

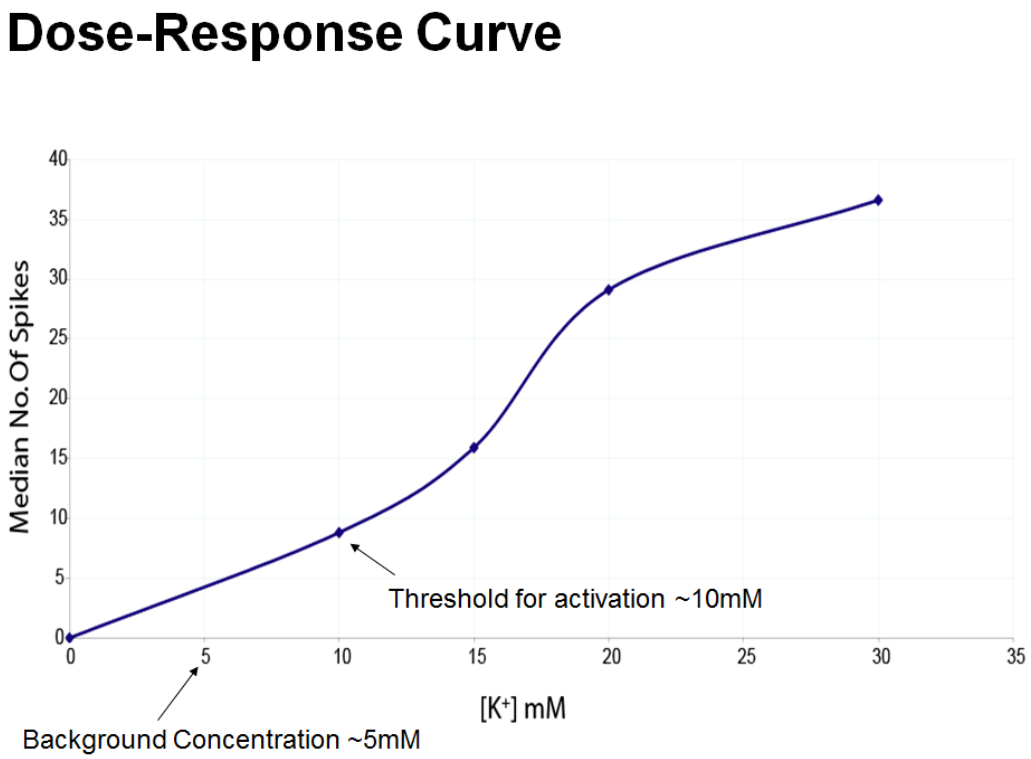

Due to the low background concentration of potassium present in intercellular fluid, doubling the concentration locally at the surface of a simulating neural interface is an intriguing and achievable goal.

Unlike electrical stimulation which can damage tissues over time or the use of neurotransmitters which would have be stored for the lifetime of the device and slowly released, posing a health risk should the interface malfunction or leak, ionic stimulation has few potential downsides. Potassium can be slowly sequestered and concentrated from the potassium already present in extracellular fluid and then released in pulses significant enough to double the local concentration at the point of desired ionic stimulation.

4. Ion Pump Based Neural Stimulation

Given the motivations behind increasing local potassium concentrations to trigger neuronal firing, a synthetic electrically gated ion pump would be an ideal device to form the basis of a stimulation neural interface. A scheme can be envisioned (see Figure 3) which ties CMOS control electronics to an array of pixels containing electrically gated ion pumps, continuously active potassium sequestration pumps, and a storage matrix for the sequestered potassium.

Figure 3. Complete envisioned electrically gated potassium ion pump stimulation neural interface scheme.

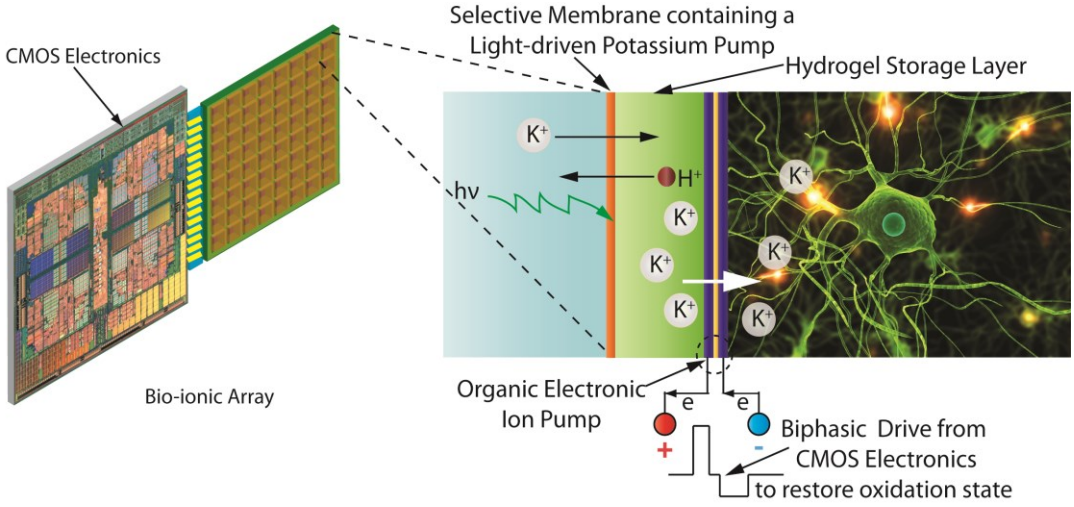

This scheme also uses an electrically conductive conjugate polymer (PEDOT:PSS) to support the electrically gated transport of ions, and is motivated by earlier work demonstrating simple two dimensional ion pumps.[2] However, due to the oxidation-reduction process that takes place during each ion transport event, it is necessary to design the system to be biphasic so that, on average, an equivalent number of carriers are transported in the reverse direction between stimulation

events. Additionally, the requirement for biphasic operation to preserve the functional state of the conjugate polymer also means that the pump must be selective to potassium while it is in the restoration phase between stimulation events. This is because ions will be transported from the intercellular fluid back into the reservoir, leaving substantially more sodium ions available for transport which could contaminate the potassium reservoir. As sodium maintains a far greater concentration than potassium in intercellular fluid, trying to stimulate neurons by altering sodium concentration locally would be quite difficult. Thus, the only way to ensure continuing operation of the envisioned device is to ensure that the pump has some selectivity to potassium over sodium during the restoration phase of the pump's operation.

5. Planar Ion Pump Based Neural Stimulation

Initially, a number of planar pump designs based on conductive polymer electrodes were investigated and optimized. These investigations showed that diffusion within the conductive polymer was a limiting factor in devices that required ions to diffuse some distance within the polymer. Additionally, these investigations highlighted the instability of planar devices where layers of different materials are placed along the direction of transport and the applied field. The interfaces between these layers tended to hydrate and delaminate, causing device failure. From these investigations it became clear that a thin lateral device (see Figure 4) which transports ions perpendicular to the layers making up the device's structure would be more ideal. In this case, the interfaces of layers are less likely to be hydrated and

delaminated. Additionally, this lateral device can be made to have a much larger cross section for transport and the thickness of the transport region can be minimized to reduce the required voltage needed to produce a desired electric field.

Figure 4. Model of a simple lateral ion pump devices.

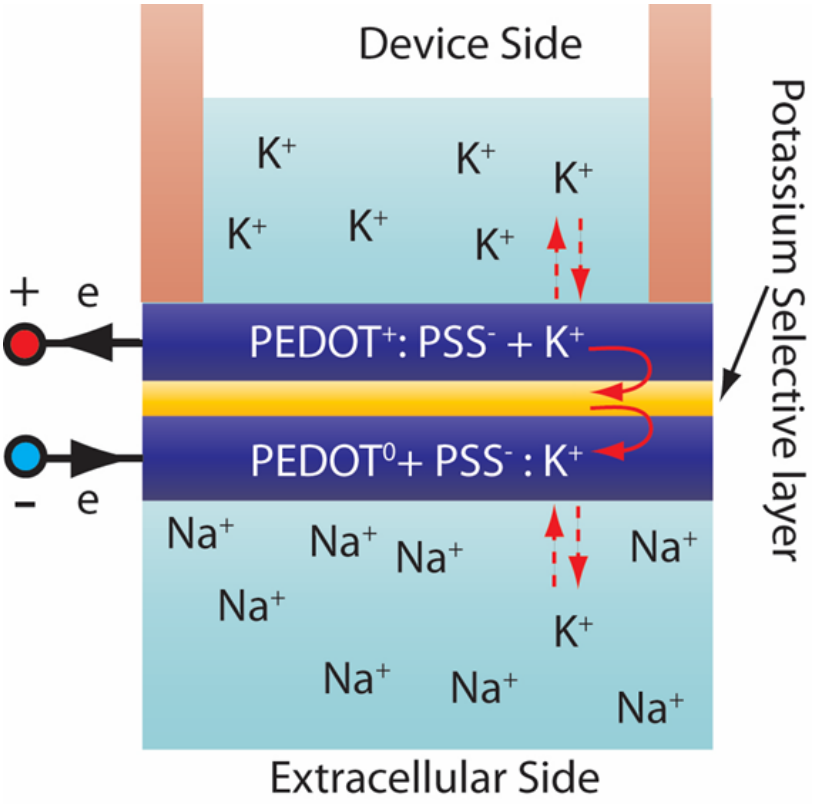

6. Nanoporous Track-Etched Polycarbonate Arrays

Initial investigations of thin film lateral devices focused on commercial track-etch polycarbonate membranes and patterned holey thin-film silicon nitride membranes. Nanoporous membranes were determined to be optimal, as these could minimize transport thickness and maximize transport area while providing a structurally stable scaffold capable of hosting softer, more flexible chemistries and

matrix materials capable of diffusive transport. A scaffold was necessary as chemistries that were found to be flexible enough to allow diffusive transport tended to form films that were unstable, especially when exposed to liquids. By placing selective chemistries in and on top of a nanoporous scaffold, the chemistry can still transport ions but the combined film gains the structural support of the scaffold material.

Using polycarbonate membranes, lateral thin-film conductive polymer ion pumps were fabricated which did not suffer from hydration and delamination issues and used the porous voids in the polycarbonate layer as the device's transport region. After examination of the stability of these pumps however, the limited chemical attachment routes available using polycarbonate track-etch membranes and the limited chemical, thermal, and mechanical stability of the material were shown to render polycarbonate unideal as a material from which to continue development. A more chemically, thermally, and mechanically stable nanoporous scaffold material was determined to be required for continued development. Additionally, an ideal material needed a chemistry for which many different chemical attachment routes for chemical functionalization of selective chemistries exist.

7. Suspended Anodized Aluminum Nanoporous Arrays

Given the need for a thin nanoporous membrane that is chemically, thermally, and mechanically stable, one major focus of this work has been the development of a cost effective fabrication scheme that can produce this sort of membrane integrated into a stable silicon handle that maximizes the mechanical integrity of the devices.

Simple nanopores in a stable membrane would meet many of these requirements, however the methods used to produce membranes are serial and not economical. While these methods are sufficient to make one or several nanopores in an individual membrane, these methods become unfeasible when producing the millions of nanopores needed to provide a large transport area in a scaffold. The formation of anodized alumina in combination with microfabrication techniques has led to the development of a fabrication scheme that can produce suspended anodized aluminum nanoporous arrays meeting all the required criteria.

While applicable to the selective ion transport scheme discussed previously, these devices are also a useful investigative tool for all sorts of transport experiments where chemical, thermal, and structural stability of the scaffold is desired along with a high transport area containing nanometer scale pores in a thin transport membrane. Chapter II focuses on the different fabrication schemes developed to produce the necessary suspended anodized aluminum nanoporous arrays, while Chapter IV focuses on demonstrative testing of these arrays while investigating ion transport selectivity when under an applied field. Finally, Chapter VI touches on a few possible future avenues for these devices.

D. Peripheral Nervous System Failure and Recording Neural Electrodes

Recent staggering advances in microfabrication along with our developing understanding of neural diseases have begun to enable the design of sophisticated devices that benefit patients suffering from neurodegenerative diseases. Most of

these devices, as already mentioned above, have mainly concentrated on stimulating the remaining healthy layers of the appropriate neural network to partially restore normal function. This method is most applicable with the central nervous system, however when dealing with the peripheral nervous system this approach does not work as well and an alternative approach must be taken. For diseases associated with the peripheral nervous system, it is not sufficient to stimulate neural tissue as faults exist between the brain and the peripheral nervous system. Thus, it is essential to record relevant neural activity from the brain in order to have any chance of restoring lost function. In this case, recording from the brain may be able to complete the feedback-loop that has been degraded or is absent due to disease or trauma. By recording the appropriate relevant neural activity associated with control over a part of the peripheral nervous system that is no longer responsive, control might be restored via implanted simulating interfaces or an alternative system might be implemented to return to patients some of the control over interactions with their environment that they have lost.

1. Recording Neural Interfaces

By developing recording neural interfaces it may be possible to stimulate intact areas of patients' nervous systems beyond the point where damage or trauma has occurred. While this may be a more distant goal, recorded neural activity can also be used to allow patients suffering from peripheral nervous system failure to interact with their environments and control robotic or computerized systems designed to improve their lives. In these cases, recorded relevant neural activity is translated into

control signals for a system and the patient is trained along with the translation model to provide feedback to drive the system being run from the recorded signals in near real time. Such systems could include computer cursors, other human computer interaction systems specifically designed to work well with direct neural recording interfaces, motorized system such as wheelchairs, and robotic systems such as multi-axis arms. Of course, the ultimate ideal restoration scheme would be the ability to regain direct control over the parts of the patients' peripheral nervous system that have stopped responding.

One other avenue that neural recording interfaces may enable is the possibility to map the neural code and gain a greater understanding of how the neural circuitry of the brain operates. In particular, by combining recording neural interfaces along with stimulating neural interfaces, complete input-output systems may be implanted in neuronal tissues allowing for in-depth study of these networks of neural circuits and a more complete understanding of the brain.

The ability to provide a closed feedback system to a prosthesis that uses neural activity directly recorded from the relevant part of the brain associated with the activity is essential for its success. The electrical domain is ideal for recording, unlike the stimulation domain where additional challenges such as the need to prevent faradic reactions from occurring at the electrodes must be taken into consideration. Neural recording interfaces pose their own challenges however, and due to the need to access specific regions of neural activity these recording systems must be implanted on a much larger scale to record the greatest amount of potentially

useful neural activity. As mentioned before, the Cochlear Implant is among the best stimulating neural interfaces developed today and it provides only 21 electrodes. Neural recording interfaces feature hundreds of electrodes and these electrodes have to be implanted deep into neural tissue to record the most relevant neural activity. Ideally, being able to record from as large a population as possible in the area of interest provides the best odds of establishing good recording sites where neural plasticity may enhance the resulting output signals given sufficient feedback training. Additionally, the largest number of recording sites possible would be optimal for effectively mapping neural signals and the operation of neural circuity.

2. Challenges of Recording Neural Interfaces

In order to reach the areas of neural activity of most interest it is necessary to be able to record from a depth of at least 1mm within the tissue of the brain. As removal of this depth of tissue would critically damage the area of interest and reduce normal functioning of the remaining neural tissue, it is ideal to penetrate into the brain tissue with neural recording electrodes that have a small cross-section while the main body of the recording neural interface sits against the outer surface of the brain. As trauma can result from the insertion and continuing existence of such an implanted recording neural interface, these implants need to be designed to minimize trauma and the corresponding isolating inflammatory response which can limit the quality of neural activity that is recorded. The recording neural interfaces also need to be generally biocompatible so that the neural tissue they are implanted in is not harmed by some element that is cytotoxic or otherwise harms the population of neurons or their

supporting glial cells. Finally, to operate within the electrical domain and capacitively couple to electrical signals propagating from neuronal action potentials through intercellular fluid, it is necessary that these recording neural interfaces be electrically conductive and able to route capacitive signals into recording circuitry. In turn, this circuitry must be able to efficiently transmit the recorded neural activity out of the brain and to a data processing system that can convert the recorded activity into control signals for a given stimulation or external interface such as a cursor or robotic arm. Ideally, such a scheme should use wireless power and data communication methods such that the patient is free to move and is not hindered by tethered cabling. Additionally, several health benefits exist should no ports into the skull be required for regular operation as an enclosed system is the best route to minimize possible paths of contagion and infection.

3. Recording Neural Interface Scheme

From the above criteria determined necessary for an optimal recording neural interface, a scheme (see Figure 5 and Figure 6) has been devised. This high density recording neural interface array scheme includes aspects that range from wireless data and power transmission to customized amplification and signal acquisition CMOS electronics. The envisioned device consists of a thin, flexible, and biocompatible integrated package that is implanted on the surface of the brain and contains a high density array of recording neural interface electrodes. These electrodes penetrate into the brain to record from the appropriate regions of neural circuity. The resulting signals are amplified by custom CMOS electronics integrated

within the implant, which also digitizes and wirelessly transmits the recordings to a relay unit located on the outside of the skull in order to remove the need for tethered cables.

The electrodes are fabricated form flexible materials to minimize the damage caused due to shear stress during insertion and to also minimize damage post insertion due to micro motion based shear stress. Additionally, the use of flexible materials helps to eliminate the fibrous and glial encapsulation that are responses related to trauma from insertion and micro motion damage. By developing flexible recording neural interface electrodes, it is hoped that better chronic implants with improved recording quality and longer lifetimes will result.

The focus of this work is on the actual recording neural interface electrodes rather than the complete envisioned system. Thus, the custom CMOS electronics as well as wireless data, power circuitry, and external data telemetry module are not the focus of this work. Instead, the development of a fabrication scheme for independent, biocompatible, conductive, and flexible recording neural electrodes that can be integrated with custom CMOS electronics and other components is the focus of this work.

Figure 5. Complete envisioned high density recording neural interface

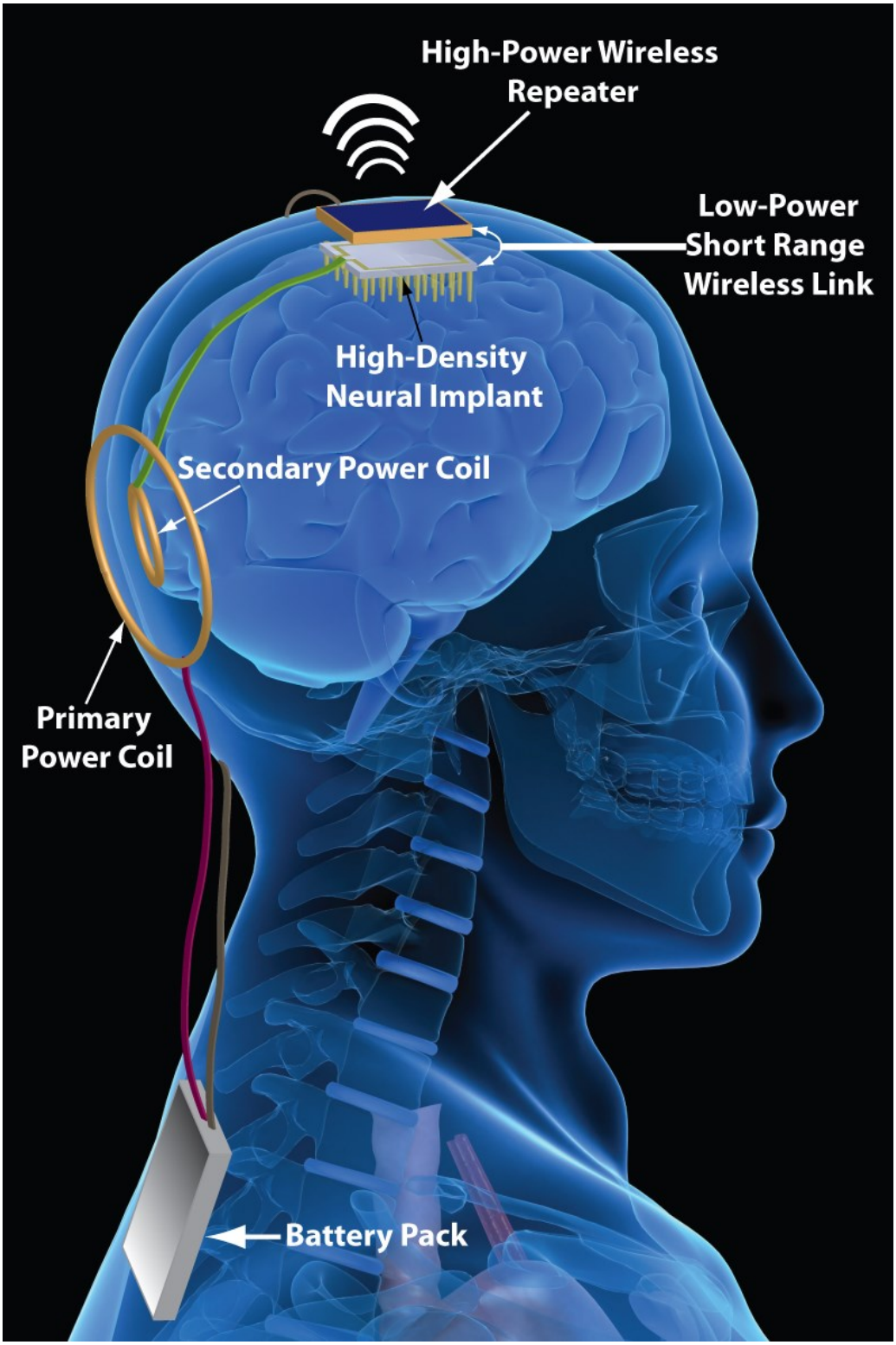

Figure 6. Envisioned high density recording neural interface integrated with thinned CMOS electronics in a thinned silicon handle with interconnects.

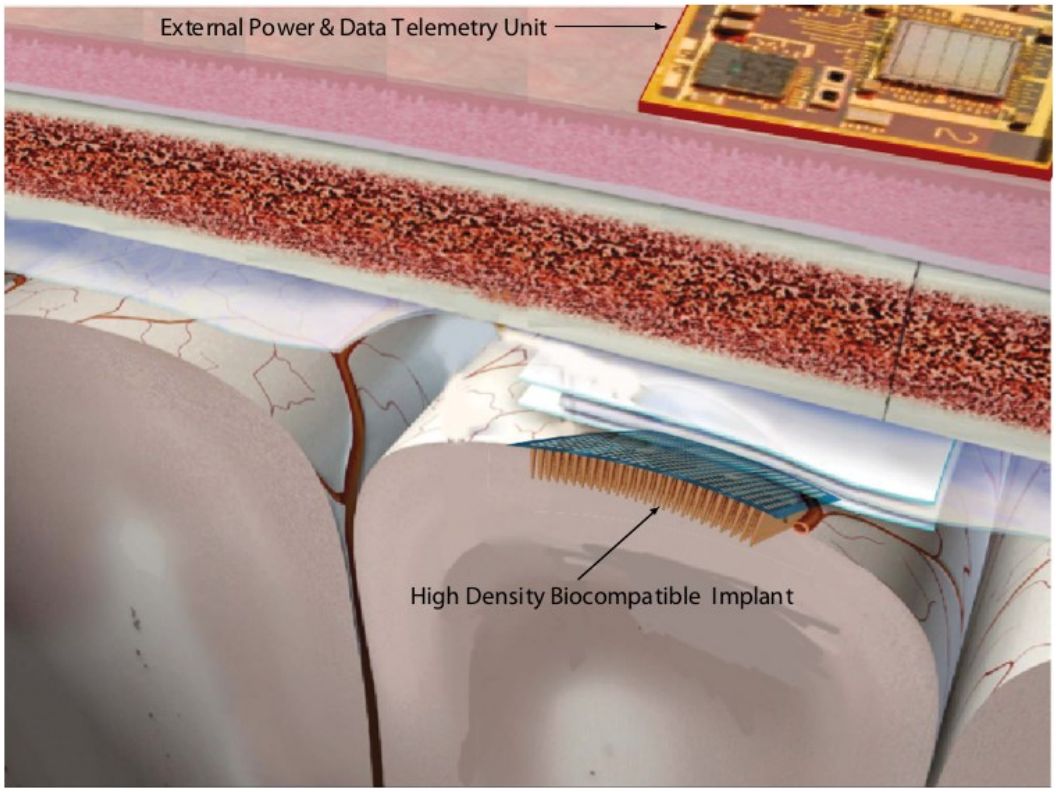

4. Recording Neural Interface Electrodes

Focusing on the development and fabrication of a recording neural interface as entailed above is a daunting task. Critical to this development and fabrication scheme is the necessity that the resulting structures be at least 1mm tall and be able to penetrate brain tissue while also being conductive and as flexible as possible. This flexibility results in the material requiring a low Young's Modulus. Additionally, in order to minimize trauma and damage to the tissue being penetrated by the electrodes, it is necessary that these pillars be as narrow, and thus as high aspect

ratio, as possible while still having sufficient structural support to be successfully inserted into the brain tissue of interest.

In order to determine the best type of recording neural interface electrode array structure to pursue, it is worth looking at the currently most often used implant types. The two most common chronic implant types are the Utah Array and the Michigan Array, which are named after the universities where they were initially developed. The Utah Array consists of a number of equal height spires of silicon on a silicon substrate. These spires can be micromachined and fabricated using a number of different techniques, but in all cases the result is a field of spires with the mechanical properties of silicon that are formed from a substrate they are attached to which also has the same mechanical properties. As the modulus of silicon is ~200 GPa and the modulus of brain tissue is between one and several hundred KPa there is a huge mismatch between the two which results in unnecessary trauma during insertion and after insertion due to the micro motion of the brain. A flexible electrode array which minimizes this modulus mismatch is a better solution.

The alternative design is the Michigan Array, which is generally implemented as a single flat spike of silicon machined from a thin wafer. This single spike features multiple recording sites along at least one of its two planar surfaces. Additionally, the Michigan Array can be built on a flexible tether so that once implanted the spike itself is not mechanically fixed to a large structure on the surface of the brain. While the ability to partially mechanically decouple the Michigan Array from components left on the surface of the brain is advantageous in helping reduce some of the

associated chronic micro motion damage, the array can only record from a narrow linear field into which it has been implanted. Because the Michigan array is also fabricated from a silicon structure, it is still subject to the same insertion trauma and a large portion of the micro motion trauma associated with the mismatch between the implanted array and the brain tissue it is penetrating.

From a recording perspective, the field recording format present in the Utah Array design is better for recording activity across whole regions of neural circuity. This renders it better for both creating a high density recording neural interface array and for mapping neural activity. For this reason, the structures developed and fabricated in this work will focus on this format of recording structures that record from a field of neural tissue.

5. Flexible Polymer Electrodes

In order to fabricate an array of flexible electrodes, a flexible material needs to be selected as a basis from which to develop a fabrication scheme and produce the desired recording neural interface arrays. Using COMSOL modeling, (see Figure 7) several materials were compared to determine the best route for development. While stiffer materials often used in microfabrication such as silicon and SU-8 (a common structural photo-patternable epoxy) both quickly fail under a uniform force applied to the modeled electrodes, the third electrode modeled using PDMS (Polydimethylsiloxane), a common flexible siloxane based rubber, can continue to deform without a point of mechanical failure. Based on these and other simulation results, PDMS was further investigated. With a modulus around 3 MPa, the most

commonly used laboratory version of PDMS, Dow Corning Sylgard 184, has a much smaller mismatch to brain tissue than that between silicon and brain tissue.

Figure 7. Simulated mechanical properties of penetrating electrodes made from three popular microfabrication materials. Both silicon and SU-8 that have high modulus fail early by breaking at the base when a uniform force is applied to the electrodes. PDMS, however, shows deformational failure rather than breakage. Deformation failure is defined as the point where the aspect ratio in any dimension changed by 30%.

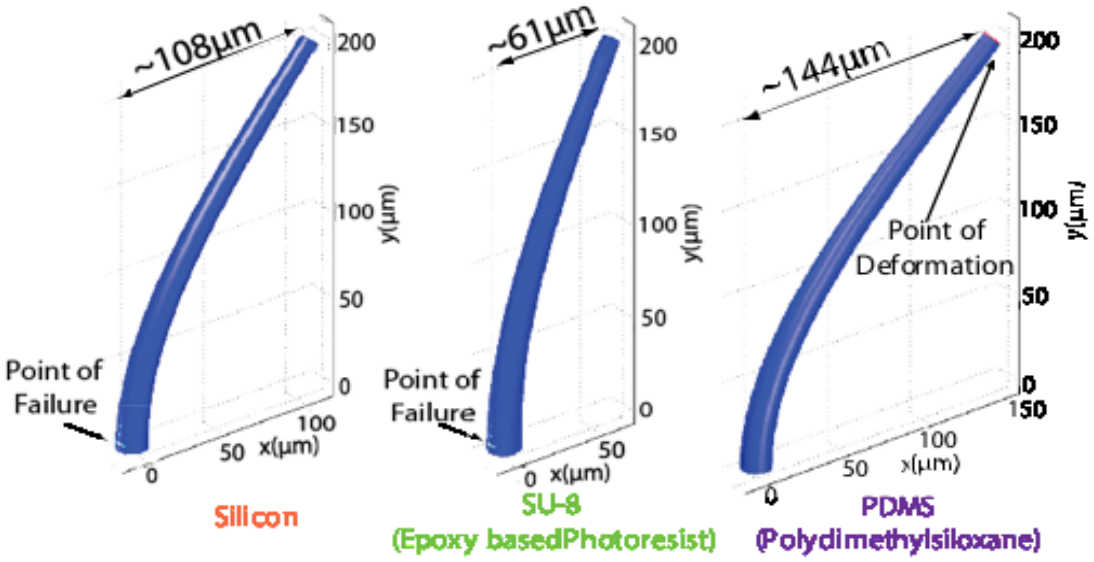

It is clear that flexible electrodes are required to support brain plasticity and minimize trauma when the electrodes are being inserted and after they are implanted. For these reasons, it is important to investigate polymer based flexible electrodes made from polymers such as PDMS. Calculating the bucking force for a 100 micron diameter electrode pillar that is 1 mm tall, the resulting force the pillar can withstand before buckling is determined to be 36 µN to 297 µN, depending on whether the

pillar sticks into the surface it is being compressed against or glances off. In the case of implantation, the surface texture of the tissues involved should make glancing off the surface very unlikely. In comparison, the force required to penetrate a 100 micron diameter section of the Pia-arachnoid membrane layer, which is the final protective layer left in place over the brain tissue during an implantation procedure, is 4-40 mN. This seemingly makes pillars made from PDMS too soft to properly insert, but this is not the case. A variety of absorbable coatings[3] and aging polymers are under development that can temporarily impart additional structural integrity to softer materials that are being implanted in brain tissue and facing this issue. One such temporary structural coating that has been demonstrated with some success is crystalline sucrose. In such a coating scheme, an array of electrode pillars can be inverted and slowly drawn from a heated and saturated solution of sucrose, which will dry to form a hard coating over the pillars. Then, to protect the added structural layer from immediately dissolving in intercellular fluid during the insertion process, the coated pillars can be drawn from a bath of mineral oil. The oil layer slows the degradation of the sucrose coating long enough for the insertion to be completed. Given such available techniques, flexible PDMS based polymer electrodes are a major focus of this work. Chapter III focuses on the development of fabrication schemes to produce flexible conductive polymer neural recording electrodes that meet the height and aspect ratio requirements outlined above and further investigates methods to produce electrodes that are conductive, independent, and capable of being connected to planar interconnect structures for neural recordings. Chapter V focuses

on investigations and experiments demonstrating the functionality of the resulting recording neural electrodes fabricated using the scheme developed. Finally, Chapter VI briefly touches on future possibilities associated with these recording neural electrodes.

II. Fabrication of Suspended Anodized Aluminum Nanoporous Arrays

Working from the anodization methods found in literature and widely standardized, several generations of devices have been designed and fabricated. The goal of these schemes has been to provide the structure to support the creation of the envisioned ion selective electrically gated pump. Secondarily, these devices serve as a general research mechanism to understand biological and chemical reaction as they occur on a thin nanoscopic scaffold. Both of these goals may provide insight both into basic experimental research as well as cognitive neuroscience.

Fabrication of these nanopourous arrays is by no means a trivial task. With each new generation of devices and each revision and improvement to the fabrication schemes involved, utility, yield, uniformity, and cost (in terms of labor, materials, and clean room time) have been further optimized. A stable and functional device for which device-to-device and wafer-to-wafer uniformity is high, feature membranes are both sturdy and chemically stable, and individual pores are all of similar dimensions at the nanoscopic scale is ideal.

A. Fabrication of Nanoporous Alumina Films

The initial attempts to produce nanoporous arrays of alumina focused on the anodization process itself without concern to providing access to the underside of the nanoporous alumina film. These studies were conducted on small samples framed by 3M 470 electroplating masking tape protecting a ring of copper tape and anodized while varying the anodization time, acid solution, and applied voltage. Results were determined by optical inspection of the resulting porous surface as well as SEM imaging of the pores. A high degree of variation and disorder was seen from sample to sample and from near masked edge to center. Occasional contamination by copper conductive tape would lead to an unwanted current path and affect the uniformity of the anodization. This would occur when protective electroplating masking tape delaminated and exposed to the copper to the anodization process. This would both deteriorate the conductor supplying current to the aluminum sample being etched, increasing resistance, and also poison the anodization solution with copper ions.

As the envisioned pores needed to be small enough to easily react and fill with small molecule chemistries that would allow for selectivity, the goal of initial studies was to determine the best conditions for producing uniform small-diameter pores given the available anodization apparatus. Optimal conditions were determined to be low voltages (10 V applied) in 6 wt.% sulfuric acid aqueous solution at ~2 ºC for 1.5-2 hours followed by at least one half hour soak in deionized water. As voltage increases, the solution becomes more able to etch through oxide layers, and the resulting fields in the pores tend to increase the pore diameters and interpore spacing.

As voltage drops, it is harder to etch into formed oxides and the etch rate drops. While there are generally five chemistries widely used for making porous aluminum, testing of the three safer and more accessible chemistries (oxalic acid, phosphoric acid, and sulfuric acid) verified that sulfuric acid resulted in the smallest pore diameters. Low temperatures for long etch times provided best uniformity at these desired pore sizes when combined with standard 3-6% acid concentrations.

B. Fabrication of First Generation Nanoporous Arrays

With the anodization method verified, the first generation of nanoporous arrays focused on providing a successful integration scheme that would mate a nanoporous film with a window in a fixed silicon substrate acting as a support scaffold. Two methods were initially explored using an anodization-last approach. In this approach, windows were fabricated in silicon first, then the arrays were formed, and finally the membrane on which the arrays were formed was removed.

1. Handle and Dielectric Membrane Via Selective Wet Etch

The first of these approaches used a selective wet etch process using potassium hydroxide (KOH). KOH is known to selectively etch silicon preferentially along the <111> crystal plane and is known to etch silicon nitride at a much slower rate, making silicon nitride a good choice as a hard masking material. As KOH would easily etch aluminum and alumina, deposition of the metal for the nanoporous layer was performed after a solid membrane was formed. Starting with double side-polished <100> plane silicon, both sides were masked with silicon nitride. A pattern

to form square windows as well as to separate the wafer into dies was transferred into the back side of the wafer using contact lithography. Then the pattern was subsequently used to open areas of the back side of the silicon nitride using an inductively coupled plasma CF_4/O_2 etch followed by the removal of the resist. The pattern used accounted for the narrowing of the etch features as they etched deeper into the silicon wafer, meaning that patterned features were wider than the final desired membrane width. The resulting etch windows appeared as inverted pyramidal frustums and the cut lines defining device perimeters appeared as pointed trenches.

The KOH etch process (see Figure 8) results in suspended membranes in independent dies provided that the mask has been perfectly aligned to the <100> crystal plane of the silicon and that no defects exist in the silicon nitride layers. In most cases, defects in the nitride layers result in broken or damaged membranes. Additionally, significant areas of the protected silicon handle were removed, cratered, or otherwise made mechanically unsound for further processing. Similarly, any rotation of the masking pattern leads to the pyramidal KOH etch expanding under the masked areas to take on the shape of a larger pyramid aligned with the crystal planes of the silicon. This effect is particularly damaging when one considers the effect to the cut lines separating dies that run all along the wafer; in this case, a rotation may significantly increase the amount of area being etched and significantly reduce the size of resulting dies.

Figure 8. KOH selective wet etch processing scheme.

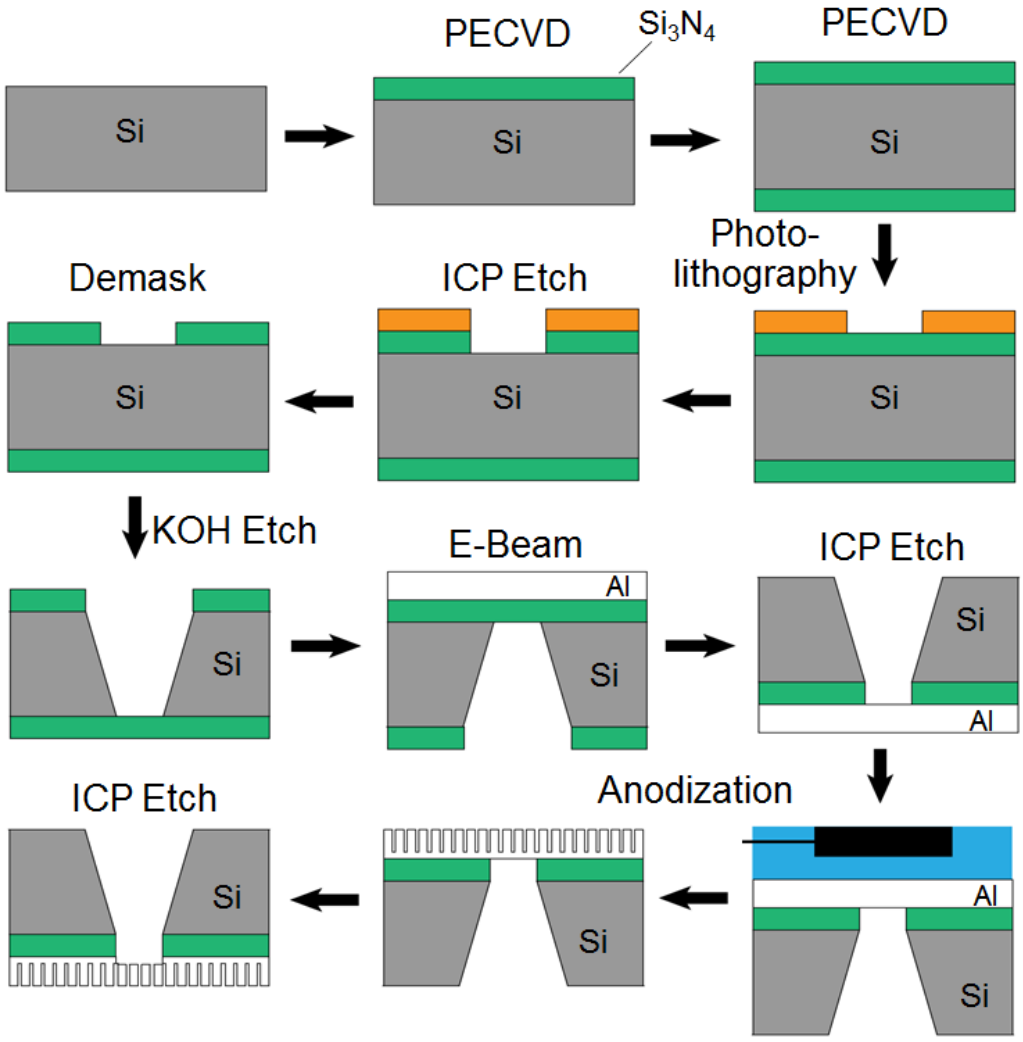

While the ability to make the region underneath the membrane an inverted pyramidal frustum with KOH provides benefits to spinning or otherwise depositing on or accessing the underside surface of the membrane and array, these benefits do not outweigh the resulting damage and low yield due to the destructive nature of the KOH etch process. It is for this reason that methods that avoid wet plane-selective etches have been investigated.

2. Handle and Membrane Via Deep Reactive Ion Etch

As an alternative to the KOH process and techniques related to the pillar deep silicon mold process, the Bosch deep reactive ion etching process is well suited to open windows in silicon substrate. This method (see Figure 9) can be used to form windows as well as die cut lines, but, unlike KOH, it does not yield a plane-selective etch. Starting with a double-sided polished silicon wafer, a stopping layer of silicon nitride or silicon dioxide is deposited on the topside, and a hard masking layer of silicon dioxide is deposited on the bottom side of the wafer. Using lithography, a pattern for cut lines and square windows is transferred into photoresist and then subsequently transferred into the silicon dioxide hard mask using a vertical oxide etch with an inductively coupled plasma containing CHF_3 and O_2.

Once the pattern is transferred into the hard mask, the Bosch deep reactive silicon etch is carried out against the patterned bottom side of the wafer. The Bosch etch is a cyclic process which alternates between a plasma of SF_6 and argon as an etch gas mixture and a plasma of C_4F_8 and argon as a passivation gas mixture. As the etch proceeds, the sample is routinely checked for optical transmission through the membrane and remaining silicon. The etch continues until all silicon under the dielectric membrane layer in the window area is removed, along with passivation defects resulting from the Bosch etch (e.g. grassing or fluorocarbon-passivated spires).

These near vertical etched lines and windows are quite clean and free of major defects. While center-to-edge etch uniformity across the wafer varies more than that

of a wet etch, the overall uniformity achieved with this procedure is much better than that of KOH. Additionally, defects in the Bosch etch present themselves as differences in etch diameters or as debris in the voids being etched, rather than defects in the mask seen in the case of the KOH etch. These defects can generally be removed by continuing to etch once the front side dielectric membrane has initially been reached. In this case, open windows grow slightly wider and their membranes grow thinner, while most defects are removed and smaller windows widened.

Figure 9. Bosch first processing scheme.

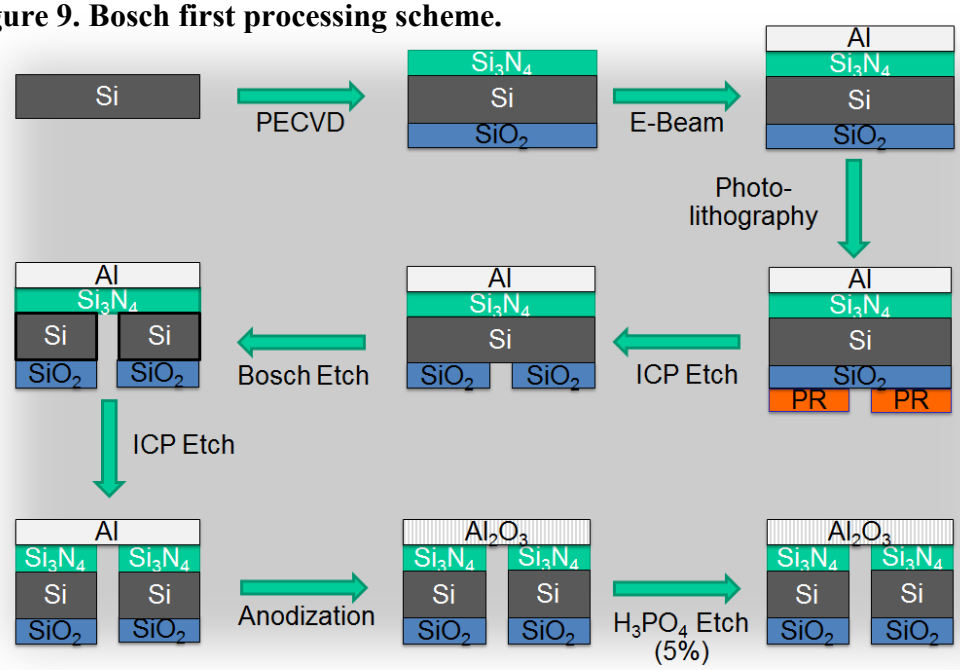

3. Anodization Last Following Window Fabrication

Once the silicon die with a suspended dielectric membrane over the backside window has been properly manufactured, aluminum can be deposited via electron beam metal evaporation and then anodized. In the case of the KOH process, aluminum can only be deposited on the topside of the die following the etch process.

In the Bosch process, aluminum can be deposited before the Bosch deep reactive ion etch, keeping the interface between the dielectric membrane and aluminum pristine; however, the ability to conduct window inspections using transmission microscopy to verify etch end point is lost in this case.

Samples are anodized using the optimal conditions described earlier with the edges of each die masked off with electroplating masking tape and copper conductive tape (also masked off) providing the electrical connection for the anodization. The complexities of the masking and the need for an electrical connection to the dies that is otherwise insulated from the solution determine that few dies can be anodized at a time without risking significant uniformity issues and possible copper contamination. Each of the separate dies need equivalent resistance paths to the power supply in order to properly be anodized and each copper contact to the aluminum must be properly masked off, as the failure of one contact results in copper contamination of the entire bath. Removing the anodization bath solution from the devices can be accomplished by placing the anodized devices in deionized water at room temperature with a stir bar, allowing 20 minutes for dissolved material as well as acid residues to diffuse.

After the anodization is complete, exemplary samples can be sacrificed to gold palladium sputtering and SEM imaging of the suspended membrane areas to verify pore diameter, surface morphology, and the amount of defects at the nanoscale. SEM imaging alone would not be particularly destructive to the devices at this point, however surface charging on the micron thickness insulating film makes SEM

imaging an impossibility without the reactive ion driven sputter deposition of a conformal conductive gold palladium coating on top of the nanoporous aluminum.

The dielectric membrane that the aluminum has been deposited onto must be removed along with the dense oxide layer formed by the self-termination of the anodization process, which is immediately above the original dielectric. The removal of the underlying dielectric membrane is accomplished by protecting the top surface with photoresist followed by mounting the dies topside down with oil on a carrier substrate and exposing the backside to inductively coupled plasma. Either a plasma consisting of CF_4 and O_2 for silicon nitride or a plasma consisting of SF_6 and argon for silicon dioxide is applied. These gas mixtures are selective to the specific dielectrics vs alumina, allowing the etch to stop on the alumina layer immediately under the inverted membrane. Devices made using the Bosch and KOH process schemes both relied on silicon nitride dielectric layers to form the support membrane under the alumina nanopores so that the dielectric removal process was common to both schemes and the resulting devices would be similar from the dielectric up through the nanoporous alumina film.

4. Difficulties in an Anodization Last Approach

The anodization last fabrication schemes outlined previously provide a good means of manufacturing the substrate membrane, but ultimately limit the yield of final nanoporous array devices. This occurs because the window fabrication process is also used in parallel to form the individual device die. Hence, once the fabrication process is complete, the starting wafer is no longer a mechanically stable single piece

but rather many dies held together by bridges of silicon between die. With the dies in this configuration and with the complexities of connecting and masking multiple dies, yield and nanoporous array quality suffer. A scheme allowing for whole wafers to be fabricated without relying on serial processing of individual dies and while also maintaining better nanoporous alumina quality would be more ideal.

C. Fabrication of Second Generation Nanoporous Arrays

The first generation nanoporous arrays were able to provide suspended nanoporous alumina membranes in a silicon window that successfully conducted ionic currents between solutions in a test cell. However, the anodization last processing scheme, when combined with defining the dies while etching the silicon windows, made producing the needed inventory of uniform nanoporous arrays impractical. The approach essentially required individual dies to be contacted, masked, and anodized sequentially or in very small batches. The masking and contacting process involved manually cutting and placing those materials on each array perimeter by hand. This had the effect of making each nanoporous array more like a work of art than a reliable device.

Clearly the anodization scheme initially used in the first generation devices was insufficient and needed to be replaced with a more uniform and more parallelized method. Additionally, whole wafer processing needed to be maintained through the entire processing scheme to maximize uniformity.

The processing scheme for second generation devices aimed to overcome the yield and uniformity issues identified during and after fabrication runs using the first generation processing schemes.

1. Anodization First Fabrication Process

As so many yield and quality issues stemmed from serial processing of small, already defined dies through the anodization process, an anodization first processing scheme (see Figure 10) was the next logical step towards improving yields and quality of the devices. This change in the process scheme was also beneficial as numerous anodization experiments had been carried out on small samples and a fixed anodization process providing desired results was already determined. By anodizing whole wafers before the Bosch process has been employed to define backside windows and cut lines in the silicon, issues stemming from tape delamination and copper contamination can be limited. This is because the ratio of wafer perimeter to surface area is smaller than the ratio for already defined dies. As the distance from the edge of the masked copper contacted region to the defined die areas increases, there is also some improvement in uniformity in comparison to very small exposed areas, but still less improvement than is desired. Anodization slows in areas further from the contact that experience greater resistance in the final stages of anodization, leading to decreased applied potential and altering the resulting pores.

Figure 10. Bosch last processing scheme.

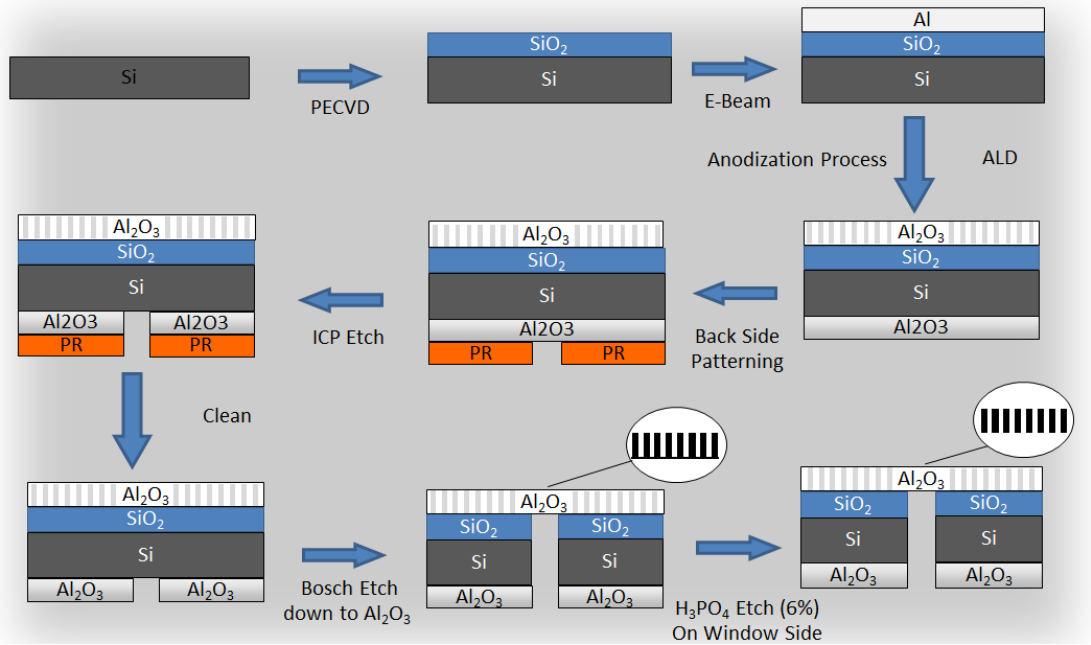

The stack required for the anodization first approach begins with high quality dielectric layers that serve two purposes: to block current from being supplied through the silicon substrate during anodization and to act as a stopping layer for the later Bosch etch. As this layer will eventually need to be etched to open through nanopores and will not need to support itself as a free-standing membrane at any time in the process scheme, a very thin high quality dielectric stack is preferable. A stack of SiO_2, Al_2O_3, and SiO_2 is deposited using atomic layer deposition via an Oxford Flexal deposition tool without breaking vacuum, which insures the quality of the interfaces of the dielectric stack. The first layer of SiO_2 is used to form a good interface to the underlying silicon wafer. The second layer consisting of Al_2O_3 is used for its quality both as a dielectric and as a very strong etch stopping layer for the Bosch etch process. The final SiO_2 layer is used to block the anodization process from interacting with the Al_2O_3 layer should there be any potential on the substrate.

Upon this dielectric stack a micron thick aluminum layer can be deposited using E-beam or sputter deposition. Using the conditions mentioned previously, the complete metal on dielectric stack can be anodized all the way down to an additional hard stopping layer of alumina at the bottom of the nanopores, just above the deposited dielectric layers. Anodizing the stack for a longer period slightly increases pore diameter while not affecting the spacing between the pores. Further, it has the benefit of ensuring that the pores terminate at the base of the anodized aluminum after having consumed all the aluminum.

2. Improving Uniformity with a Potential Grid

While an anodization first approach is a quality and yield improvement over the original anodization last scheme, the variation in distance from the masked contact to the exposed aluminum that is converted to nanoporous alumina leads to variations in the applied field and the formation of the nanoporous alumina. To reduce the distance from the contacts to all of the aluminum to be anodized, an equipotential conducting grid can be used to supply a uniform voltage at the edge of every die. This could hypothetically be accomplished by placing copper tape and masking tape across the wafer in a grid pattern, but this would in turn cause many of the issues observed in the anodization last approach. A better approach is the introduction of a patterned grid of buried metal lines, which will not be anodized, and, thus, will provide uniform potential across all dies on the wafer as the anodization progresses. Copper and masking tape can be excluded from the entire wafer with the exception

of one edge where the applied voltage is supplied the grid, minimizing the risk of copper shorting and demasking issues.

The potential distribution grid could be formed in a number of ways, including a buried conductive material that will not etch during the course of the anodization and is protected by a similarly etch-resistant dielectric layer to keep current from shunting from the grid into the anodization bath. The simplest way to accomplish this is to protect a part of the aluminum plane to be anodized with an insulating grid, so that a grid of aluminum remains conducting throughout the anodization process. Photoresist might be a sufficient protection layer to define and protect the potential grid, but to ensure the potential grid remains intact for the length of the anodization process and to further minimize the route of contamination, patterning a protective dielectric layer over these areas is preferred (see Figure 11). In this case, a stack of Al_2O_3 and SiO_2 is deposited via atomic layer deposition, with the first layer acting as an interface layer and the second layer providing the protection from the anodization bath. After this layer is deposited, a standard photoresist recipe is used to pattern photoresist over a grid, allowing the remainder of the deposited dielectric to be etched away down to the alumina layer via a vertical oxide etch. The etch uses an inductively coupled plasma containing CHF_3 and O_2 and is followed by the stripping of the remaining photoresist before anodization. Because the grid lies along the perimeter of every die to be defined by the Bosch etching process, the potential grid effectively ensures that each region that will be anodized to become a porous membrane is uniform (see Figure 12).

Figure 11. Bosch last processing scheme with potential grid.

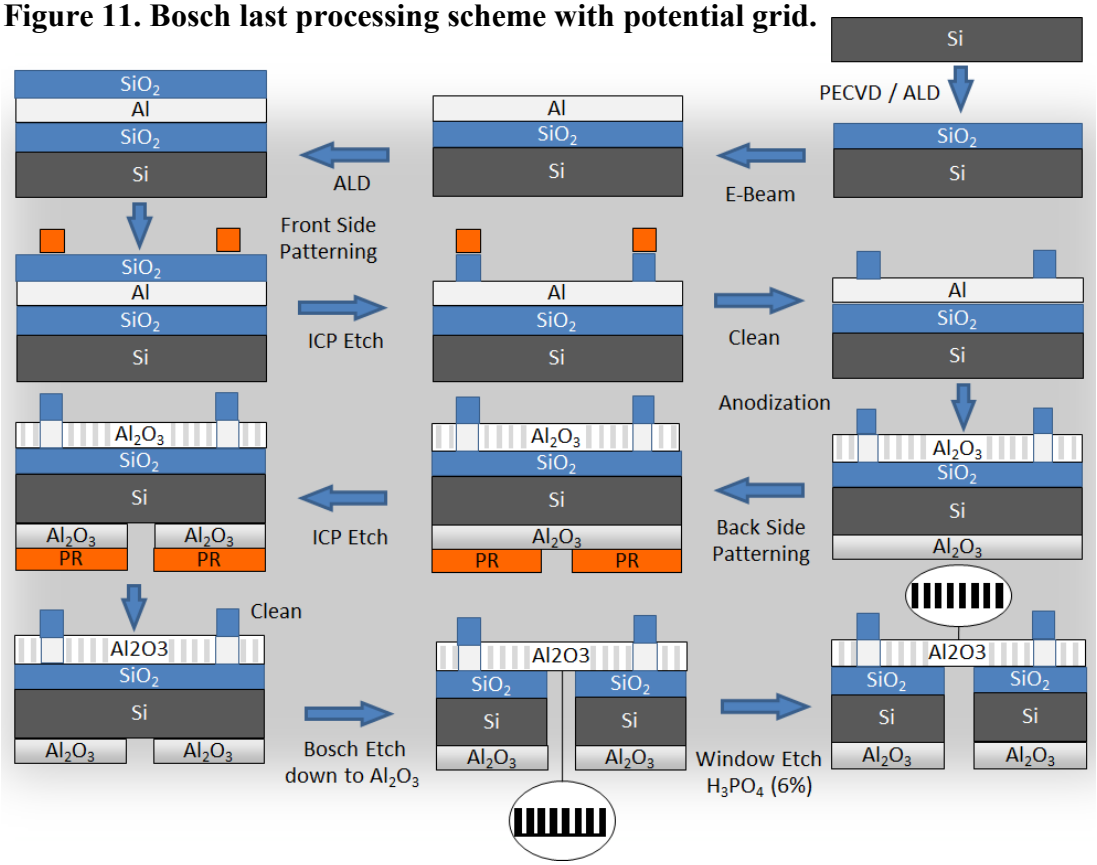

Figure 12. Anodized 100mm wafer with Bosch with potential grid.

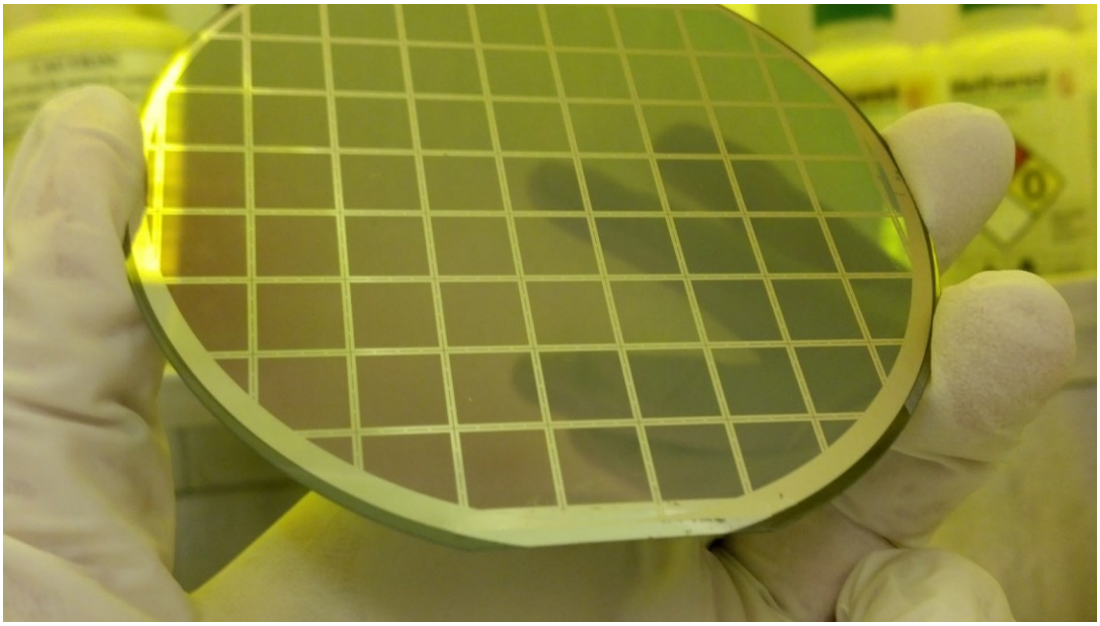

3. Bosch Last Silicon Window Formation

The process of Bosch last window formation is similar to the Bosch process in the Bosch first processing scheme, but the Bosch last scheme is more robust than the original approaches in a few respects. Trying to stop the etch process on a nitride layer that is necessarily strong enough to not break in subsequent processing steps can be difficult, particularly in instances such as the removal of the post-Bosch etch wafer from the carrier wafer to which it is mounted. Similarly, trying to stop on a dielectric stack containing an aluminum layer beneath it makes transmission microscopy impossible, greatly increasing the difficulty associated with finding an optimal point at which to stop the Bosch etch for a given wafer.

The addition of the nanoporous alumina layer prior to Bosch etching provides enhanced mechanical stability when compared to a thin nitride layer and allows the use of a thin SiO_2 and Al_2O_3 stack as the dielectric stopping layer, as mechanical support is provided by the nanoporous alumina film. This dielectric stopping layer is more robust to the Bosch etch chemistry and is more easily removed with a simple phosphoric wet etch following the Bosch process. Perhaps most importantly, the stack of dielectric and aluminum is converted into a primarily porous dielectric stack that is compatible with transmission microscopy, providing a simple means of determining the etch status and quality of windows being formed by the Bosch process.

4. Bosch Window Patterning for Improved Spin Profiles

While in many cases the ability of the Bosch process to etch near-vertical deep features is desirable in the process, the resulting depressions can be difficult to spin onto from the side of the wafer that has been exposed to the Bosch etch. Many materials spun into such depressions may never correctly coat the depressions trapping air bubbles as they spin across the depression. Alternately they may fill in the depression but remain so thick that baking or otherwise removing solvent will generate cracks in the material such that it cannot provide continuous coverage of the membrane at the bottom of the depression. If the final material stack desired for a device requires a continuous film on the bottom side of the membrane that needs to be spin coated, this is an unacceptable situation.

One improvement to overcome this issue is to manipulate the geometry of the windows being patterned by the Bosch etch to generate sloped ramps by which fluid may flow into and out of the window when being spun. This should cause less pooling of spun material and trapped bubbles than in the case of pure vertical sidewalls. Specifically, by creating a sun-shaped pattern (see Figure 13) by adding triangles to the outer edge of the standard round perimeter of the desired etch window, the reduction in gas transport of the reactant species as the triangles narrow causes a decreasing etch rate and thus a tapered depth. The sun-shaped pattern produces the desired ramps while still providing increased mechanical support to the membrane. In this particular case, a limitation of a particular process technology,

specifically the effect of gas transport limits in Bosch etching, is used as an advantage to provide tapering to the etch.

Figure 13. Enhanced Bosch pattern for solution transport. (top left: surface pattern, top right: mid-depth pattern, mid figure: cross section of failure modes, bottom: cross section of enhanced Bosch etch feature)

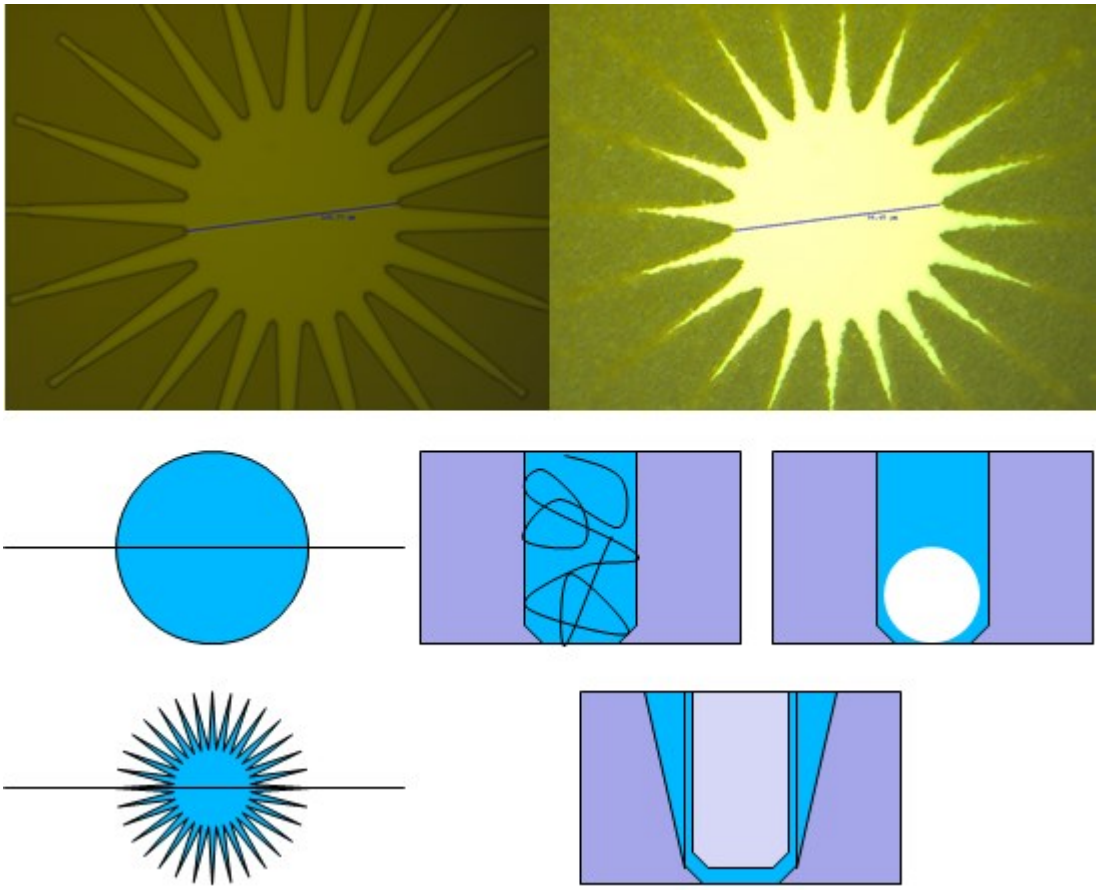

5. Glass Carrier-based Bosch Etching

Due to the variation between the etch rates of the windows used to provide access to the back side of the nanoporous alumina membranes and the cut lines employed to separate the wafer into individual devices, cut lines and the interactions between

them can begin to break through the silicon carrier and dielectric stopping layer long before the Bosch windows are fully opened. As no additional obstructions limit the gas flow of reactive species at the intersections of cut lines, even the relatively thick nanoporous alumina layer can be breached. As a result, this can lead to leaks between the helium cooling mechanism below the wafer and the process chamber above the wafer with the reactive plasma. Small leaks of helium and the associated drop in back side cooling pressure can be overcome by throttling back the needle cooling exhaust value. However, larger leaks can drop the helium cooling pressure below process control limits even if the cooling exhaust valve is closed completely.

Mounting the membrane side of the wafer being processed face down onto a carrier wafer using vacuum oil can remove the risk of substantial helium leaks from developing under the wafer being processed. The standard carrier wafer used in the Bosch process is a silicon wafer with a thick deposited layer of silicon dioxide. While such wafers do eliminate helium leaks and maintain good thermal contact, their inability to transmit visible light necessitates dismounting the wafer being processed from the carrier at any point where it is desirable to conduct transmission microscopy when looking for an endpoint.

Glass carrier wafers offer a substantial improvement in processing as they are sufficiently thermally conductive while removing the need to repeatedly dismount a wafer that is being Bosch etched from the carrier in order to check the progress of the etch using transmission microscopy. As each dismounting and mounting action can scratch, dirty, or otherwise mechanically damage the wafer being processed,

minimizing these events down to a single precision mounting and dismounting can positively impact die yield and quality as well as the mechanical stability of the resulting released nanoporous membranes.

6. Recovery of Cracked or Shattered Wafers

Additionally, the risk of the wafer shattering in the dismounting process is negated in the instance that it is only dismounted once the Bosch etch is determined to be completed. This is because the next processing step beyond this point is a wet phosphoric etch to open the terminating alumina layer, which is easily carried out via series processing just before each array is going to be used. However, due to the configuration of Bosch processing tools, continuing an incomplete etch on a cracked wafer becomes problematic and usually requires sets of individual dies to be processed in smaller quantities on an otherwise empty carrier wafer, leading to different plasma loading conditions. Occasionally, cracked wafers can continue to be processed as if they were whole but the height at the edge of the wafer must be kept continuous to avoid damaging the Bosch processing tool.

7. Pore Widening and Removal of Back Side Alumina Stopping Layer

Commonly, dilute phosphoric acid is used to widen porous anodized alumina. In the case that the anodization is allowed to completely consume the aluminum, the alumina stopping layer at the bottom of the anodization stack can also be removed using the same wet etch. This can be useful in the event that the alumina is being used to template nanostructures being grown upon a seed layer beneath the alumina

stopping layer. In the case that a suspended membrane requires that alumina stopping layer be removed to create through-pores, a dilute phosphoric etch can also be employed. However, placing the membrane in the wet etch will also widen the diameter of the nanopores, which may not be desirable.

In order to minimize the ultimate diameter of the alumina nanopores, which is desirable for a number of uses such as small molecule surface functionalization, only the back side can be exposed to a phosphoric wet etch while the already open front side of the membrane can instead be exposed to water. When working at the wafer scale the whole wafer can be phosphoric etch opened at once without exposing the front side of the membrane to significant widening by employing a photoresist or stable vacuum oil to keep the wafer attached to the Bosch carrier wafer. When working at the individual die scale, most apparatuses useful in testing these devices are also sufficient to allow selective etching of the back side of the die while wetting the front side with water.

8. Pore Shrinking via Atomic Layer Deposition

Along with forming nanometer-thick quality dielectric stacks on top of the silicon substrate or deposited metal stack, atomic layer deposition can also be used to shrink nanopores to dimensions smaller than that which is achievable by alumina anodization alone. To ensure penetration into the extremely high aspect ratio, nanopores' very slow reaction cycle times can be mated with a thermally driven water vapor process. In this process, TMA (tetrametyl-aluminum) is allowed to slowly chemically adsorb on exposed existing anodized alumina providing sufficient

time for transport of the precursor into the nanopores. This is followed by a purge and exposure to water vapor, which forms an alumina monolayer during each cycle.

9. Multistep Anodizations for Improved Pore Uniformity

One further improvement to the processing schemes for nanoporous alumina discussed above is the implementation of multi-step anodization to improve the ordering of the nanopores in the suspended alumina membrane. Two-step anodizations are most often carried on aluminum films with a thickness of hundreds of microns. Generally the majority of the film is anodized in a first anodization step using conditions selected for their ability to form desired regular interpore distances. While the exposed surface of the alumina may appear very chaotic, after significant anodization depth, the pores become aligned to each other as a result of the applied voltage conditions and the insulating nature of the consumed alumina. Using a combination of chromic acid and phosphoric acid, the first anodization layer can be quickly etch away while leaving the remaining alumina intact with a remaining imprint of the ordered nanopores. Then a second anodization can be performed, forming new pores at the depressions already left from the first anodization. Using this method with large thicknesses of alumina, very well-ordered pores can be formed for certain voltage and concentration conditions. However, in the case of thin film suspended nanoporous membranes that are being fabricated on a mechanically stable silicon frame, limited methods exist to deposit the necessary thicknesses of aluminum. While electroplating is one such potential option, it was not examined, as the necessary electrochemistry bath was not readily available.

As an alternative, the thickness of deposited aluminum thin films can be increased slightly and a short sacrificial anodization can be carried out. The formed nanoporous alumina film can then be etched back and the remaining aluminum can again be anodized to improve the ordering of the remaining film. An alumina etching 500mL aqueous solution containing 10g chromium trioxide and 20mL of 85% stock phosphoric acid was used at 75C when investigating this two-step process. This etch was carried out after a 30 minute anodization in 6% H2SO4 at 2C and 25v, and before a final anodization under the same conditions for 3 hours.

D. Fabrication of Planar Ion Pump Devices

While they are not specifically nanoporous alumina based devices, a number of planar two-dimensional devices have been produced for investigating ion pumps, selective ion pumps, and similar concepts. In this section the design of these devices is outlined.

1. PEDOT:PSS Gasket Based Devices

Using PEDOT:PSS (Poly(3,4-ethylenedioxythiophene) Polystyrene sulfonate) as an electrically driven ion transport layer and adhesive silicone rubber gaskets as wells for aqueous salt solutions, electric and ionic transport can be demonstrated. By applying over 20 V to a narrow region where all current is forced to flow, the PEDOT:PSS can be irreversibly oxidized, making the region highly resistive to electron transport, but still capable of drift-based ion transport. This oxidation can also be accomplished by placing a well over the area to be oxidized, supplying

bleach to the well, and applying a similar voltage across the edge of the PEDOT:PSS and the bleach solution.

These devices, while easy to fabricate, suffer from the eventual leakage of the well, which leads to delamination of the gasket from the PEDOT:PSS and eventually hydration across the oxidized PEDOT:PSS region. Additionally, due to the size of available adhesive silicone gaskets, the length of the over-oxidized region as well as the distance ions are required to diffuse before reaching the over-oxidized region can also limit ion transport.

2. Patterned PEDOT:PSS SU8 Devices

By pattering PEDOT:PSS and SU8 (SU-8 2000 series structural photo-patternable resist) using lithographic processing techniques, more robust planar devices can be fabricated, which are capable of more useful experimental investigations. In particular, SU8 can be employed to provide more stable wells that are less likely to delaminate as well as miniaturized devices that feature shorter drift and diffusion distances for ion transport. Additionally, photoresist masking can be used along with O_2 plasma etching to selectively pattern the PEDOT:PSS layer to define its dimensions. Alternatively, photoresist masking can be used to remove an area of PEDOT:PSS that would have been over-oxidized so that it can be replaced with a selective transport chemistry under investigation.

3. Planar Device Stability Issues

Like the gasket-based planar devices, patterned PEDOT:PSS and SU8 devices also suffer from delamination of the isolating SU8 patterned layer as well as hydration and delamination of the patterned PEDOT:PSS layer. Once either the substrate-PEDOT:PSS interface or the PEDOT:PSS-SU8 interface is breached by the aqueous salt solution being tested, or once the PEDOT:PSS film become sufficiently hydrated that a parallel channel develops, the transport through the PEDOT:PSS is supplanted by the other path.

These hydration and delamination issues can potentially be overcome with the addition of chemistries tuned to maintain adhesion at these interfaces. However, devices designed without exposed interfaces that are parallel to the direction of transport can greatly limit these issues. Such devices, where the transport of ions and the application of electric field is directly into the plane of the device rather than across it, also have the benefit of being able to be fabricated into very thin transport stacks. It is for these reasons, in addition to results discussed later suggesting that greater transport can be achieved in narrower transport widths, that suspended anodized aluminum nanoporous arrays were developed.

III. Fabrication of Flexible Conductive Polymer Neural Recording Electrodes

The fabrication of high aspect ratio conductive polymer recording electrodes is a daunting task. While on its surface many possible avenues seem viable as routes to

produce such devices, there are many difficulties that make most of these possible routes unfeasible given some practical experimentation. Ultimately a mold-based polymer casting scheme using silicon molds created through the Bosch etching process has been employed to fabricate the desired recording electrodes.

A. Direct Fabrication of Flexible Pillars

The simplest method for fabricating flexible pillars would appear to be to fabricate the structures directly from a material of the desired properties. In this scheme a layer of an appropriate material would need to be deposited as a film and then patterned so that only the desired pillar volume remained. As the most useful neural recording pillars need to be implantable in at least 1mm into neural tissue, these films and pillars need to be at least 1mm thick.

1. Mechanical Machining of Non-Pillar Volumes

Mechanical machining of 1mm thick flexible polymer films is a possibility. However, this requires all the material with the exception of the volume of the electrodes to be mechanically removed and the pillars to be formed sequentially. The bits used in the machining process need to be able to fit in between the defined pillars volumes to remove material while not disturbing or damaging the pillar volume itself and removing all unwanted film down to the substrate which also needs to be left in good condition. While working with hard material, machining these sorts of positive features is not difficult. With a flexible material, however, the material must be of similar modulus to that of neural tissues. Otherwise, the mechanical

motion of burs or bits will cause tangles and damage to the pillar volume will likely occur while in the process of removing unwanted film. It is for this reason that such a machining process was not selected to make the desired neural recording electrodes.

2. Laser Machining of Non-pillar Volumes

Laser machining is another option similar to mechanical removal of an excess volume of polymer film to define pillar volumes that has been considered. Using a CO_2 laser, undesired volumes can be removed by following cut patterns or a rasterized pattern, while pulse deration, frequency, and power level and be tuned ~~for~~ according to the desired material. Unlike mechanical machining of excess non-pillar volume, in this case there is no mechanical motion that may entangle and destroy desired pillar volume. As the laser process is essentially comprised of combustion of the polymer film along with ablation of the material under the beam, this process has a tendency to both combust and deform pillar areas as the beam spends time at the edge of each pillar. Additionally, the general heating of the film and more specifically the heating of film immediately around the pillars can induce further non-uniformities into the resulting pillar volumes are left after the films removal. The focus of the CO_2 laser is such that only one plane of material will be in focus, and, above and below that focus, the beam will spread exposing additional film for removal. Excess energy delivered to the substrate under the film can in the case of reflective materials damage the film limiting the use of metal interconnecting conductors that would be immediately under the film being removed. This otherwise could also cause damage to the substrate or additional energy transmitted into the

base of the pillar volumes being defined by the laser. For these reasons laser removal of the unwanted film volume surrounding pillar areas was determined to be unacceptable.

3. Photo Pattering of Structural Photoresists

Direct photo patterning was one initially very appealing method to produce polymer pillars. It was possible with sufficient synthetic chemistry such a photoresist system might be altered to meet the electrical and mechanical demands of a conducting flexible pillar array. Assumedly, conductivity and mechanical stability could be tuned via chemical or plating routes.

The photo patternable structural resist chosen was Microchem SU-8 2000 series. This epoxy-based system original developed by IBM at the Almaden Reaserch Center has seen widespread use, including use in complex MEMS devices. Studies with SU-8 including fabrication of very small diameter 25 micron pillars as well as larger diameter 100 micron pillar. SU-8 2150 specifically was used as it can be spun to thicknesses of 200 microns in a single layer, allowing only five layers of resist to form a 1mm structure.

The spinning, prebake, and post bake procedures required are complex for the highly viscous resist in particular, as at such thicknesses skin layers as well as gradients in remaining solvent density tend to occur. Patterning and developing each layer in sequence is not possible as it is impossible to build up material of any thickness while spinning on independent pillars on a substrate, due to the height of the first developed pillars being nearly equal to the height of additional layers. This

leads to the other two possible routes for multilayer patterning of the desired pillars: either spinning several layers with prebakes between and then attempting a very long exposure and development or prebaking and exposing each layer without subsequent developments until all layers have been spun on and exposed. Such extremely thick stack of resist is not easily exposed, as resist near the exposure source tends to filter out a great deal of the exposure energy. In the case of multiple exposures before development each exposure dose can be guaranteed but alignment between layers can become a problem, as the exposed structures are not well defined until they are developed. This is easily addressed with alignment marks on the substrate to reference against or by transferring the desired pillar pattern into a mask on the substrate. In the latter case, additional layers must be shot through the existing layers, but alignment is guaranteed. In either case, development of multi-layer stacks of narrow cross section structures, lacking cross structure supports, such as free-standing pillars proves very difficult. Interfaces between different layers of SU-8 tend to delaminate from one another under either exposure method, particularly given the amount of time and agitation required to develop the base layers of material that have been pre-baked repeatedly. Isopropanol is generally used to remove the remaining developer once development is finished, but this generates residues if any uncross-linked SU-8 remains. Substrate adhesion with SU-8 is also an issue for high aspect ratio structures with narrow bases, particularly as the structures are being developed. Occasionally, enough stress is present in the cross-linked materials that the pillar structures jet sideways and curl around rather than remaining upright as patterned.

While some of these issues can be overcome by permanent or temporary scaffolds between pillar structures and continuous base layers of adhesion promoting resist, Microchem Omnicoat, such schemes cannot be used to produce independent pillars that could be directly attached to an interconnected pad for neural recording connectivity. It is further noted that, in many circumstances, even continuous layers of much thinner and easier to work with SU-8 will tend to delaminate under aqueous conditions such as those that would be experienced when neural recording electrodes are inserted into the brain. Given the difficulty found in producing independent pillars of narrow cross sections, which lack a secondary structural support system, the decision was made to not continue further development along this route.

B. Methods for Fabricating Mold-Based Pillars

Following investigations into possible methods for direct patterning of pillars it was determined that a mold-based scheme would ultimately provide the best avenue to arrive at a reliable method for making 1mm tall and above polymer film pillar electrode structures. Molds have the advantage of being fabricated from harder materials while the different in the structural properties of materials can improve the process of mechanical separation between mold and cast pillar. Additionally, in many cases molds can be reused where a clean release of cast features has been achieved.

As only the volume of the pillars desired needs to be removed from the mold material, the mold-based approach is much more focused on the precise removal of desired pillar volume. Additionally, obstructions or deformations in the mold shape

can severely hinder the proper removal of cast materials as pillars can become caught on mold areas that narrow or protrude into the mold volume. Therefore, molds that are easily produced in bulk or parallel processes and feature the best mold and sidewall uniformity are ideal.

1. Drilling

While drilling was already explored as an option to directly fabricate pillars, it was also investigated for its use in producing the desired 1mm or greater thickness molds. While a bur is used to remove material bulk material, in the case of direct drilling of the desired pillar volume, a long high precision drill bit is required along with a high precision stage to produce a mold with the desired pillar dimensions and pitch. This was beyond the ability of the standard CnC machines found in machine shops such as the University of California Santa Barbara Physics machine shop. As a result, a mill operated by a physics group as well as example parts produced by a number of vendors were investigated. For ease of milling, metal brass or copper plates were drilled. The two external vendors' demo parts were unable to match the mold dimensions desired and tended to produce rough and non-planer molds. Both the surface roughness as well as the curvature of the parts made them unusable for casting pillars of the desired dimensions. A final attempt was made using the available mill, but the spindle was not sufficiently true and the rather expensive test bit was destroyed within a few holes. As mills, with the necessary precision to potentially keep the drill bits from immediately being destroyed upon initial use, are rather costly and quite specialized in their utility, no further attempts were made

along this route. In general, mechanical drilling of such narrow deep features is not suggested.

2. Laser Cutting

Laser cutting sheets of polymers or plastics were also investigated, but, similarly to the destructive nature of combustion and ablation observed when trying to remove fields of polymer films, uniform voids in the dimensions desired with vertical sidewalls are nearly impossible to produce. This is because of the focus and beam heating issue discussed earlier with the added detriment that combusted gases can only escape by movement up the beam path in the situation that the beam is covering the majority of the pillar mold area being cut. The issues with combusted products being trapped in the path of the beam leads to slower rate of material removal as well as local heating, which can further combust the material beyond the desired sidewalls of the pillar voids in the mold. Molds made in this manner tend to have burned out non-vertical upper surfaces and appear very rough. While laser cutting can be a great tool at larger, lower precision jobs, such as cutting soft PDMS gaskets for nanopump testing, it is not ideal for making small, high aspect ratio molds like those useful for neural recording arrays.

3. Strained Polystyrene Sheets

Strained polystyrene sheets have become quite well known in the microfluidics community since initial research was first conducted at UC Merced. They are also known for being the material used in the popular creative craft toy “Shrinky dinks.”

These strained polystyrene-based materials can be heated such that they draw in along their pressed in plane dimensions and expand along their vertical direction. As a result, in the microfluidics case, ink dots, other applied bumps, or cuts into the surface made at a low resolution can be converted into narrower, denser, and higher aspect ratio patterns. For microfluidics, this enables printing of higher aspect ratio features for PDMS casting masters using simple printers.

While strained polystyrene can be heated and drawn in in some cases as much as 20x in the strained in plane dimensions, even this is not sufficient to produce clean 1mm thick voids for molds. Inks or similar materials cannot be deposited in high enough densities while being conformal with the polystyrene surface to take advantage of the shrink.

Some of the problems associated with polystyrene can be overcome if rather than depositing ink on the polystyrene surface, the desired voids are directly removed. This can be accomplished by either the laser drilling method or mechanical drilling method, both of which are mentioned above. Unlike those processes, however, the lower aspect ratio and larger feature size available before the polystyrene is drawn back make such cutting attempts far more realizable. Since heating causes the strained polystyrene to draw back, uniform heating is critical to ensuring a flat polystyrene mold once the shrink is complete. This undermines the potential application of laser machining which would locally heat and possibly melt the sidewall material of the mold areas, possibly removing the necessary built-in strain needed for the shrink to occur.

To further investigate the use of strained polystyrene sheets as molds for flexible polymer pillar casting, a number were machined such that their post-shrink dimensions would approach the desired dimensions for the molds. These in turn were baked in an oven under normal atmosphere either in open air or with polished aluminum plates on either side to keep molds flat during the shrink process in order to avoid the formation of bubbles in the shrink process and to try to keep the ultimate shape planar. Thermally conductive weighted nonstick surfaces might have been optimal for this process, but they were not available.

As a starting point for flexible pillar electrodes, PDMS (Polydimethylsiloxane) which is a silicone rubber that is known to be biologically compatible and widely used in microfluidics applications as well as electronics potting applications, was chosen. Specifically, a very common formulation, Dow Corning Sylgard 184, was purchased and used as a starting material for pillar development. Sylgard, which has a Young's Modulus in the low MPa for a standard mixture, and a working life greater than 90 minutes, can be cured at a range of different temperatures and conditions making it an ideal starting material from which to work, particularly due to its ubiquity in the research community.

Shrunken polystyrene molds were placed in aluminum dishes and prepared and degassed. PDMS was poured into the dishes and then degassed repeatedly until all the mold voids were filled. The filled molds were then cured at 100 C for 35 minutes, as recommended by the manufacturer. The PDMS and the mold were cut out of the dish once cured and the thin layer of PDMS under the mold was removed,

making it possible to attempt to remove the mold and release the pillars. As the molds were not perfectly planar, and as the PDMS was well adhered to the mold, removal of the pillars from the mold was not successful when applying mechanical force. Cutting at the interface between the PDMS bulk and the mold tended to cut through the PDMS leaving a thin layer of PDMS attached to the mold. Mechanically disassociating the remaining PDMS tended to tear the pillar from the PDMS bulk, rather than release the pillars from the mold.

After several different attempts utilizing different methods of mechanically releasing the pillars, it was determined that all failed to be effective, and a chemical solution rather than a mechanical solution was sought. Several solvents that can over time swell and eventually dissolve polystyrene molds were investigated. While some of these were able to slowly remove the mold, freeing the PDMS, the PDMS did not prove particularly stable to these solvents and would also swell and deform irreversibly. This meant that even once all solvent was removed from the mold and PDMS, the result was not planar and generally did not reflect the original desired dimensions for the pillar array.

In parallel to this work, additional experiments were carried out evaporating metal films of gold and Titanium into the polystyrene molds. Using solvent-based methods, it was possible to transfer the evaporated metal to the chemically released pillars, but the uniformity and deformation issues following the solvent-based process remained.

While a broader search for the most appropriate selective etch chemistry to separate polystyrene from PDMS might have yielded improved results, the ultimate goal of being able to align and pattern the pillars directly to a substrate eventually terminated this avenue of investigation. A silicon substrate activated by an O_2 plasma process could be introduced and pushed into contact with the mold once the PDMS was degassed, leaving only a thin layer of PDMS between the mold and the desired substrate, but the solvents were not particularly helpful to maintaining the PDMS silicon substrate bond. Non-uniformities in the post-shrink positioning of the molds would always cause the released pillar to be at a random non-uniform spacing instead of a predictable, fixed pitch. This undermined the use of a fixed lithographic mask set for electrical contacts, as they would be impossible to mate to pillars fabricated in this process without significant tolerances being designed into the contacts. Similarly, the variations in flatness of these molds meant that without a good mechanism for the etch back or removal of excess PDMS or conductive flexible polymer film, the pillars would likely feature shorts bridging the array of pillars together. This investigation made it clear that a successful molding method must rely on a planar material that can be mechanically, rather than chemically, separated to be successful in the release process without negatively impacting the flexible polymer material.

C. Silicon Based Pillar Molds

Silicon based mold became the focus of the investigation for a method of producing mold to cast flexible polymer pillars, following feasibility problems found

with softer mold materials. In particular, the molding methods using soft materials like polystyrene produced irregularly spaced pillars that would not align well to lithographically-generated contact patterns, while other materials proved too difficult to produce the desired mold patterns successfully. This decision was made only after assessing the accessibility of methods for selectively deep etching hard planar materials such as glass or ceramics with the necessary etch ratios, and even considering current state of the art 3D printing platforms. Silicon is at the heart of the semiconductor industry and research has been focused on process techniques surrounding silicon for half a century making it a material from which to develop a process.

1. Bosch Etching of Molds

When determining the best route for creating deep narrow voids in silicon substrate for mold fabrication, three possible processes stand out. First, selective wet etches such as KOH (potassium hydroxide) and TMAH (tetramethylammonium hydroxide), which preferentially etch along certain crystal planes; second, dry etch processes designed for deep silicon etching; and third, photo- or laser-induced electrochemical etches. While the first of these methods is not sufficient to produce arrays of deep vertical circular features in silicon, the second and third are. As a deep reactive ion etching system was available in the UCSB Nanotech cleanroom and no well-characterized photo electrochemical etching system was readily available to investigate, the decision was made to focus the investigation on a dry etch technique.

Deep reactive ion etching, also called Bosch etching after the company's initial patent of the process in 1994, is a cyclic plasma etching technique that can produce near vertical sidewalls in large and in particularly small dimensions. The process is briefly described in relation to the nanoporous alumina membrane fabrication process scheme where it is also used, but will be examined in greater detail in these sections as the etch process scheme required to generate flexible polymer molds presents particularly interesting technical challenges. These challenges are associated with the aspect ratio as well as the desired depth of the etch in the case of fabricating the pillar molds in silicon.

The Bosch deep reactive ion etching process depends primarily on a directed chemical and kinetic etch of argon and SF_6 that supplies reactive free radicals of Fluoride. These radicals react to covert silicon into volatile SiF_4 which is then exhausted through the exhaust valve and low vacuum pump. This process on its own would lead to undesirable non-vertical results, as the etch would be only partially anisotropic depending on plasma conditions. However, this standard etch chemistry is combined with argon and a fluorocarbon chemistry such as C_4F_6 or C_4F_8 to isotropically passivate the exposed surface silicon bonds with fluorocarbon compounds. In industry, such etch and passivation chemistries are applied in different ratios during multi-step etching processes to achieve the desired, consistent etch profiles. In the case of the Bosch etch process, the two processing steps are applied in a sequential loop. The anisotropic nature of the etch combines with the

isotropic nature of the passivation step to produce near vertical sidewalls with very identifiable surface scalloping on those sidewalls in most instances.

Mask materials used to define areas that will be protected from the etch process include dielectric materials that are stable to SF_6 as well as other materials such as photoresists. Due to chamber contamination issues, etch stops or hard masks made of metals rather than oxides are prohibited in Bosch silicon deep reactive ion etching systems such as the one used in this investigation. Depending on the mask material being used, photolithography alone or photolithography along with dielectric deposition and reactive ion etching or wet chemical etching may be required to form the required etch mask. In the case of silicon dioxide or silicon nitride masks, a plasma etch chemistry of CF_4 and O_2 or CHF_3 and O_2 can be used to transfer the resist pattern into the dielectric hard mask.

2. Limitations of Bosch Etching

In general, the Bosch etch is a very useful technique for etching deep patterns into silicon either of large surface areas or small finer positive or negative features. Such uses include die-sized windows in silicon handles, thinning away complete silicon support substrates at a larger scale, etching small patterns to make voids, or removing unpattern bulks to leave hard masked pillars behind. Limitations on the Bosch process that occur when large areas are exposed to the etch process can be troubling. These include the loading down of the etch such that a uniform density of fluorine radicals is unable to reach the surface of the etch. Such effects lead to

sculpted etch areas which gradually curve up near the edge of the etch area and tend to be more pronounced at the edges of the wafer.

Additionally, as mentioned in the nanoporous alumina membrane fabrication scheme, grassing can be a significant problem for large areas where etch rate may slow down due to loading. Grassing refers to the formation of micro scale heavily passivated silicon spires, which feature sharp vertical topographies and as a result continuously experience greater passivation depositions than the etching species are able to remove. As a result, these spires appear to grow from the surface as the surface bulk is removed. Conditions allowing grass formation ultimately roughens the etch area with dense fields or "forests" of passivated silicon spires that the etch leaves behind. Most often, chemical residues on the wafer under etch or contaminates in the etch chamber from a previous run using excesses amount of passivation can be blamed for these events.

In the case that small areas are being exposed to the etch process, plasma loading and grassing as described above become much less of an issue. Small exposed areas and a low overall fraction of unmasked surface material ensures that sufficient reactant species are available to maintain the etch process and hinder these issues. However, other issues emerge under these circumstances, particularly at deep etch depths and narrow cross-sections.

The greatest limitation to the Bosch etching process for these processing scheme is the role gas transport plays in narrow etch cross-sections and at high aspect ratios. For etch features larger than 100 microns and even for short etch depths of hundreds

of microns at smaller feature sizes etch rate in the standard Bosch process recipe is stable and the limitations due to gas transport are not generally observed. However, for cross sections at or below 100 microns and at etch depths like those approaching the thickness of a standard 100mm wafer (~526 microns) gas transport limitations play a major role in determining the etch profile and etch rate.

Essentially, etch rate as well as passivation rate drop as gas transport into the deepening feature being etched becomes the limiting factor. While a bulk etch rate for the standard etch process might be around 2 microns of silicon per minute of active Bosch etch process time, that rate might drop to 0.7 microns of silicon per minute of etch time at several hundred microns into a 100 micron diameter etch feature. Additionally, as etches become slightly sloped rather than vertical while small deep cross sections are being etched, the features can grow wider than desired or narrower than desired as the etch proceeds into the silicon bulk. The effect can become so pronounced that a through etch of small features in a silicon handle may never finish while the hardmask is intact. This can happen if the passivation step slowly narrows the etch cross-section down to nothing or at some depth into the etched feature the passivation process begins to overwhelm the reactive etch species reaching the bottom of the etched feature.

These effects are particularly detrimental in cases where the etch cross-section is completely limited, such as when etching small circular cross-sections, and becomes much less of an issue where a narrow dimension exists only in one dimension, such as when a trench or street shaped cross section is being etched.

3. Bosch Etch Process Tuning for Narrow Deep Features

In many ways it is understandable that an etch technique designed to vertically etch silicon bulk primarily to sculpt MEMS structures would run into difficulties as gas transport, something for which the fixed repetitive process was not designed, becomes a limiting factor. However, by tuning the process parameters, the Bosch etch process can be corrected to cleanly etch deep narrow features, even at depths deeper than that of standard wafers such as 1-1.5 mm. Two easily accessible knobs that can be accessed to optimize the etch include gas flow rates used in the cyclic process steps and etch step length. Additionally, chamber pressure and applied RF power are two more variables that can be altered. However, due to the cyclic nature of the plasma process and the stress put on the RF components, these two variables were not modified from the standard process conditions. Either an extension of the active etch time or an increase in the flow of supplied SF6 etch reactant supply gas will increase the etch rate of the Bosch process as it etches deep features. In particular, a 30-50% increase in gas flow coupled with a 30% increase in etching time are sufficient to etch through 1mm thick wafers with etch patterns of 100um in diameter. These changes are made without reductions to Argon carrier gas flow or decreases in deposition process time; the cycle length is extended and the overall gas flow is increased. While a decrease in passivation gas flow or a decrease in passivation deposition time could also result in improved etch performance for the desired etch features, these changes could be detrimental to the performance of the Bosch etch, particularly shortening the overall cycle time, which would additionally

stress the matching network and other RF components whose response times are already at their limit during the standard Bosch process.

To effectively etch the required 1mm deep features, several different modified recipes were created which feature different degrees of etch enhancement. As an etch proceeds, more aggressive etches can be applied to further the etch depth while limiting the undesirable effects of more aggressive etch processes. Extending this concept, a more complex etch process recipe might slowly alter or morph etch conditions as the count of the etch cycles and etch time increases. This could provide the optimal etch cycle length and reactant gas flow as the etch deepened to keep etching vertically at a reliable etch rate. However, as such a complex etch recipe would approach the limits of the Bosch deep reactive ion etch system and be difficult to characterize, this additional experimentation and the ultimate fine tuning of the process was not carried out.

While grassing and other debris formation mechanisms play a lessor role in narrow etch features that do not load down the plasma process, such effects do play a role and can lead to defects that can partially or completely block a small number of the individual features being etched. This effect can diminish the yield of pillar voids in completed mold arrays as well as lead to irregularly shaped pillar voids that can be slower to etch and from which it can be difficult to release cast pillars. To pre-clean the chamber and minimize these issues, an automated pure O_2 dry etch recipe was created as a cleaning sequence using similar process conditions to the standard Bosch process. This was done so that a patterned wafer being processed could be loaded

into the Bosch etching system following the automated clean without moving in and out of manual operation mode or needing to wait for forced temperature ramps to be enforced on the Bosch deep reactive ion etcher's electrodes.

4. Limitations Due to Hard Mask Etch Selectivity

No matter the quality of the etch recipe or recipes involved, areas where bulk silicon removal is not desired must be protected. At a minimum, every etch/deposition cycle will etch away exposed silicon, particularly over large surfaces where gas transport is not an issue. Unless a masking material is completely invulnerable to etching by the chemical SF6 etch as well as the kinetic argon etch of the Bosch etching process, the hard mask will slowly be etched away cycle by cycle. The ratio or difference between the etch rate of the desired material being removed, in this case silicon, and the masking material is referred to as the etch ratio or the etch selectivity between the two materials. In silicon device processing, etch ratios between masking materials and materials being etched might be as low as 1:1, but when etching deep features, producing incredibly thick masking layers is impossible. If an etch is allowed to proceed after having removed the patterned hard mask material, the wafer will begin to be thinned in the exposed areas and plasma loading will begin to affect the etch rate of the areas where the etch is desired to proceed.

The most common masking materials for the Bosch deep reactive ion etching process are silicon dioxide and silicon nitride which have etch selectivities of ~200:1 and ~100:1 with respect to the etch rate of silicon in these conditions. While these are good selectivity values, even when using silicon dioxide a 200 micron deep etch

would require at least 1 micron of masking material to avoid the etch back of the bulk silicon located under the hard mask. Similarly, a 1mm deep etch would require at least 5 microns of silicon dioxide hard masking material to complete the etch. While 5 microns of silicon dioxide can reasonably be deposited on a wafer or thermally grown in the case of a virgin silicon wafer, this amount is only sufficient to protect the masked surfaces long enough for large features not effected by gas transport issues to be etched through to a depth of 1mm. The etch recipe tuning process described above results in etches with less passivation and greater etch speed, thus, in addition to a narrow feature requiring more etch time, the etch rate of the hard mask facing the aggressively tuned recipe is further increased. Several means of producing a hard mask capable of meeting the demands required to etch the desired narrow features to an etch depth of 1mm were investigated. As silicon nitride has a poorer selectivity than silicon dioxide it was excluded from the investigations. The growth rate of thermally grown silicon dioxide is limited by two mechanisms. The first of these is a reaction rate, which is limited as oxygen freely reacts with silicon to form silicon dioxide and the second is the diffusive transport rate of oxygen through formed silicon dioxide as it reaches towards the next available layer of silicon to react with. This diffusion transport rate quickly becomes the limiting factor when thermally growing thick layers of silicon dioxide and increases so quickly that a few microns can take days to grow under optimal conditions while thicker layers would take weeks. As a result, 6+ micron stacks of silicon dioxide used in investigating the molding process had to either be produced by PECVD

(plasma enhanced chemical vapor deposition) alone or by beginning with as much thermally grown oxide as possible and then adding to the grown layer with additional PECVD deposited oxide. As thermal oxide provides better selectivity it would have been preferable. Silicon dioxide stacks of 15+ microns approach the depth of hard mask material needed to complete the desired mold etch without widespread etch breakthrough in the masked areas. Unfortunately, at the silicon dioxide thicknesses required, patterning the silicon dioxide hard mask layer becomes difficult to complete in a single step process as many etch recipes to cleanly pattern such a thickness of SiO_2 will tend to combust the patterned photoresist long before etching through the full thickness of the SiO_2 being etched.

Additional hard masking stacks were also investigated that might provide an easier processing route or lead to a better quality etch. These included hybrid stacks of silicon dioxide and photoresists. In these cases, the remaining photoresists that had been used to pattern the silicon dioxide layer were left in place to be the top of the hard mask stack and initially slowed the consumption of the hard mask during the Bosch deep reactive ion etch. Using standard resists of thicknesses up to 11 microns such as thickly spun SPR 220-7 and 6-10 micron silicon dioxide layers, the hard mask stacks held up relatively well but were not able to completely remain intact for the necessary duration of the mold etch. One further improvement to this scheme was the replacement of standard resists with built into the silicon dioxide hard mask with a structural resist, SU-8, that is more robust to the SF6 etch chemistry employed and can be spun to produce much thicker layers. SU-8 has a tendency to delaminate from

surfaces, particularly when heated. This detrimental impediment to its use as a hard mask layer was addressed with the addition of a spun Omnicoat adhesion layer between the silicon dioxide base of the hard mask stack and the SU-8 layer of the stack. The addition of the Omnicoat layer also allowed the SU-8 hard mask film remaining at the end of the silicon etch to be removed with stripper, (Microposit 1165) exposing the more uniform remaining silicon dioxide masking layer which is a better surface for casting and releasing polymer pillars.

While these hybrid silicon dioxide and SU-8 dielectric stacks were capable of protecting the majority of the wafer surface, defects in the SU-8 layer which would form during the silicon etch would leave groves and holes etched into the silicon substrate. Additionally, delamination and enhanced hard mask consumption by the silicon etch at the edges of patterned areas would lead to broken mask corners and blown out areas of the pillar molds. These effects would result in irregular, wider features being etched into the upper parts of the silicon mold as the etch progressed and the exposed edges of the hard mask were consumed.

5. Angled Hard Mask Re-deposition

Two critical enhancements were required to overcome the widened features caused by enhanced removal of hard mask material at the edges of etch features as discussed above. First, a more selective hard mask was required to limit the problem. Second, a method was required to protect the area immediately below the hard mask surface so it would not be significantly etched into while the more aggressive etch recipes were applied to finish etching through the silicon remaining at the bottom of

the pillar volume. Due to the aggressive etch rate near the mouth of the etched features during the aggressive etch, both of these enhancements were required and neither would be successful alone.

After extensive investigation of possible methods to achieve these enhancements, it was determined that alumina could be used as a hard mask. While pure aluminum was not an acceptable hard mask due to chamber contamination concerns, nanofabrication facility staff eventual approved the use of alumina films in the facility's Bosch silicon deep reactive ion etch system. Alumina, with an etch selectivity of 10,000+:1 in a standard SF_6 based Bosch process, can be an incredible etch stop or hard mask material. The availability of alumina meant that nanometers rather than microns of hard mask material could be used to protect the surface of the silicon mold wafer. Complementary to the approval and successful tests verifying the etch selectivity of alumina in the deep silicon etch process, the availability of an ALD (atomic layer deposition) tool capable of depositing high quality alumina films enabled a transition to alumina as the hard mask material for forming the silicon molds. A stack of alumina, silicon dioxide, and alumina (50nm/3um/50nm) was chosen due to deposition limits imposed on the available ALD system.

Despite this structure, the alumina hard mask stack still suffered from undercutting in later portions of the silicon mold etch. Re-application of the hard mask, and particularly application of the hard mask onto the upper side walls of the etched holes in the silicon mold, was required. Standard methods of deposition and patterning were, however, impossible in this instance. If the base of the etch was

deposited with alumina and it was not selectively removed, the remaining silicon etch couldn't proceed. Additionally, few methods exist for protecting the extreme base of a deep feature to allow selective deposition on side walls and clean removal of the protecting material. A resist could be spun and then ashed back to a point at which it would only be present at some depth into the etch void, but deposition of a dielectric onto the surface and into the voids would entomb the resist under a layer of the deposited material or otherwise limit options for the removal of the resist. Chemical routes by which a hard mask might be deposited on the side walls would tend to operate at high enough temperatures to bake the remaining resist inside the mold voids.

One elegant solution to these problems is the electron beam evaporation of a dielectric onto a partially etch silicon mold wafer while the wafer is placed at an angle and rotated along its axes. Such a method, while uncommon to many process flows, takes advantage of the existing geometry that the mold etching process generates and uses the geometry as its own shadow mask. This innovative solution can thus cover any desired amount of already etched silicon mold depth through the adjustment of the angle at which the wafer is placed with respect to the source pocket. The deposited material masks both the patterned surface as well as the upper portions of the mold voids which see the greatest undercutting. As alumina is a far more economical source material than the metal organic alumina precursors used in ALD, thick lower quality depositions of such hard mask material can be deposited

using a dedicated dielectric electron beam deposition chamber with the correct tooling for angled rotational handling of substrates, if such a chamber is available.

It is worth noting that the facilities used during the completion of this work did not possess such a dedicated chamber with the necessary tooling and that, as a result, remasking deposition runs could only be carried out immediately before complete preventative maintenance measures were going to be carried out on the available metal deposition chamber with the necessary tooling in order to avoid excessive particle or flaking contamination issues.

In combination, a hard mask containing alumina and the above described masking technique (see Figure 14 and Figure 15) enables the fabrication of pillar mold voids sufficient for successful pillar releases. While it is possible to generate molds without using alumina as an initial hard mask, the process requires thick layers of silicon dioxide in place of the alumina. This necessitates the use of SU-8 as a patterning hard mask and a release coating due to the long silicon dioxide patterning etch required. For this reason, the use of alumina both in the primary masking step and the secondary re-masking step is heavily preferred.

Figure 14. Pillar Fabrication Scheme using SiO_2 and SU-8.

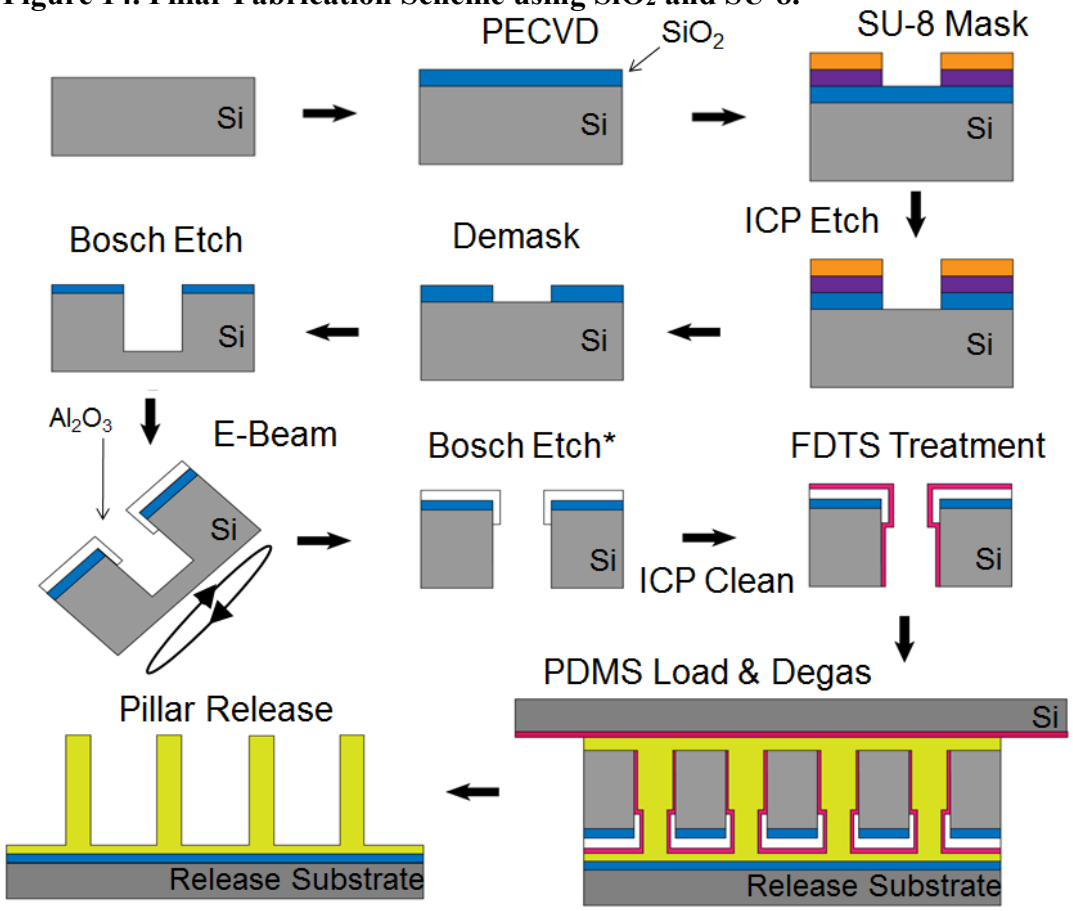

Figure 15. Pillar Fabrication Scheme using Al2O3 wherever possible.

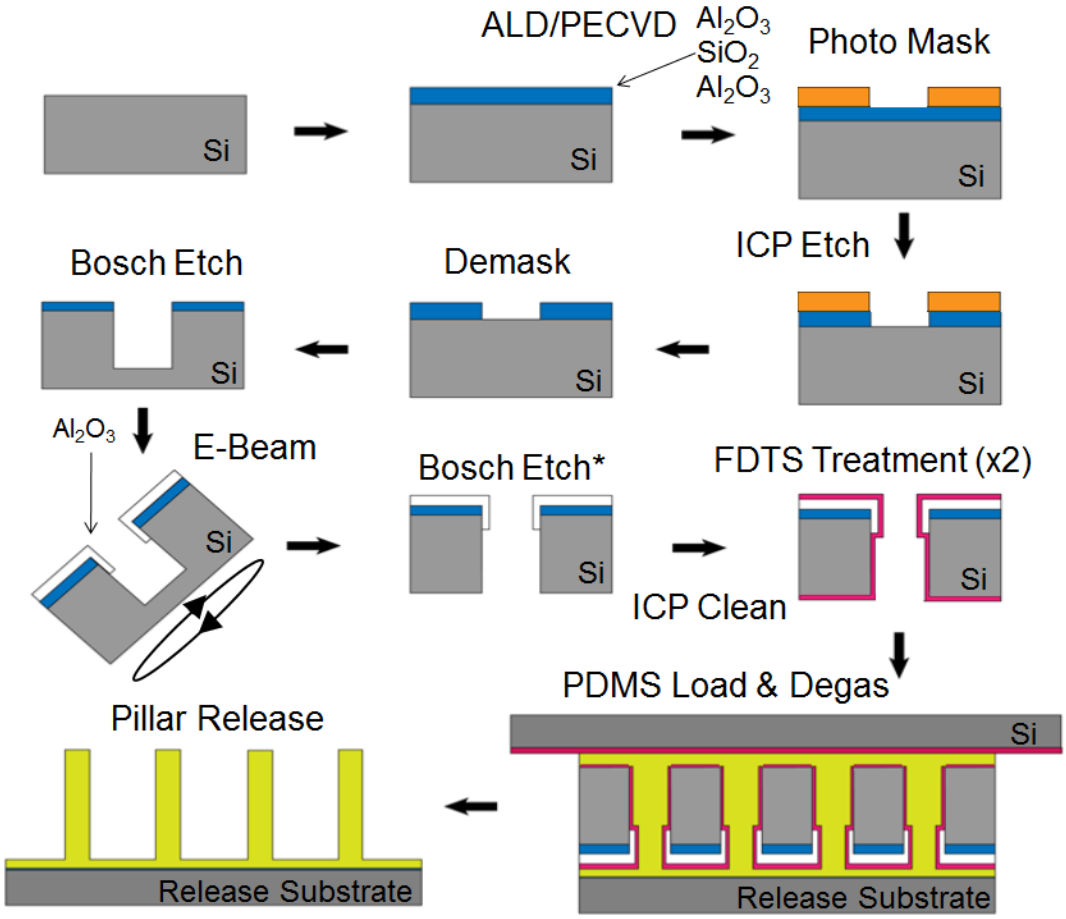

6. Bosch Etch Completion and Debris Removal

Using the techniques described above, including customized etch process recipes during Bosch silicon deep reactive ion etching, patterned hard mask stacks containing alumina, and the reapplication of a second hard mask onto the surface and sidewalls of the patterned partially etched wafer before continued etching, complete etches through 1mm silicon wafers in 100 micron diameter mold voids can be made (see Figure 16, Figure 17 and Figure 18). As debris or over passivation can cause the etch rate of some features being etched to slow, even when employing pre-cleans on

the etch chamber, it is necessary to over-etch beyond the point that a few mold voids open all the way through the wafer thickness. In order for complete arrays to be etched, it is necessary to etch until almost all arrays on the wafer have completed etching. As additional over-etching can begin to rapidly expand the bottom on the etch at the interface of the silicon mold wafer and the carrier substrate, it is useful to minimize over-etching to only the amount necessary. For this reason and others discussed earlier, the use of a glass substrate is preferred. This provides a stable carrier which can be left attached to the silicon mold wafer while continuing to etch, as well as when using transmission microscopy to inspect the mold for complete, incomplete, or debris containing features as the etch is finished.

Figure 16. Diced cross section of fully Bosch etched 1mm pillar mold.

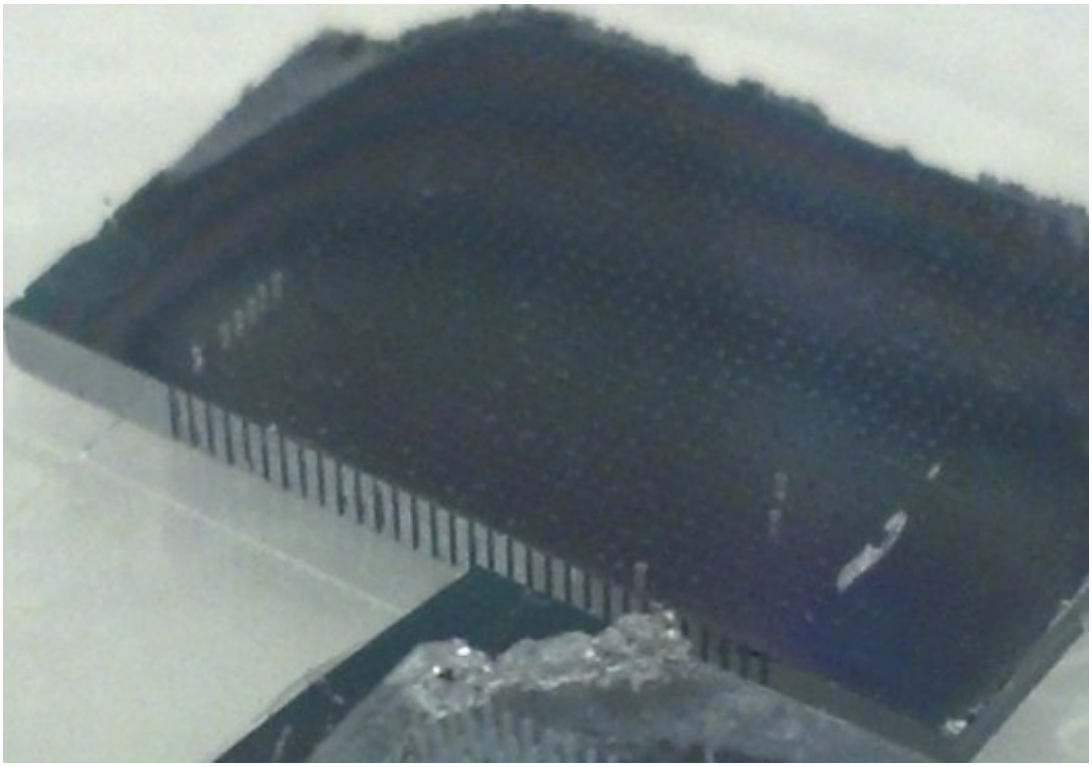

Figure 17. Diced cross section of partial Bosch etched pillar mold.

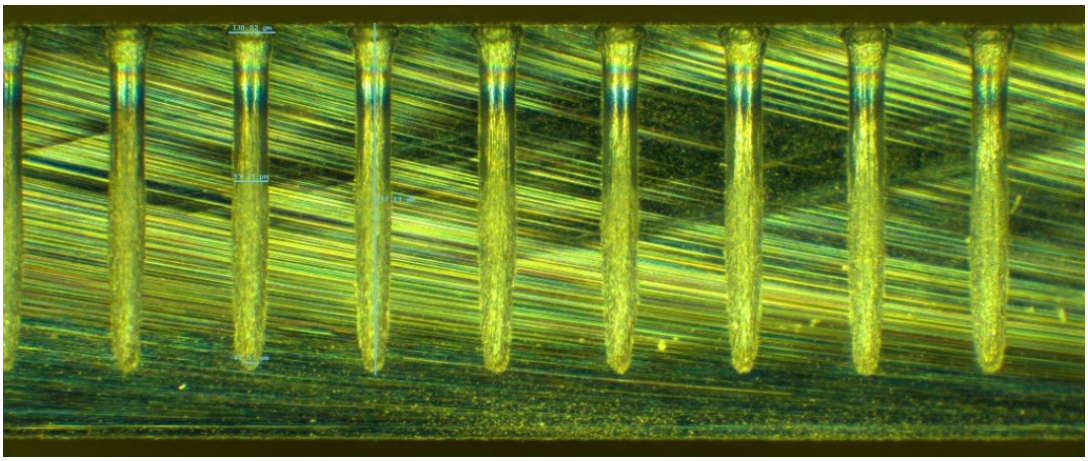

Figure 18. SEM cross section of pillar mold showing necking and footing.

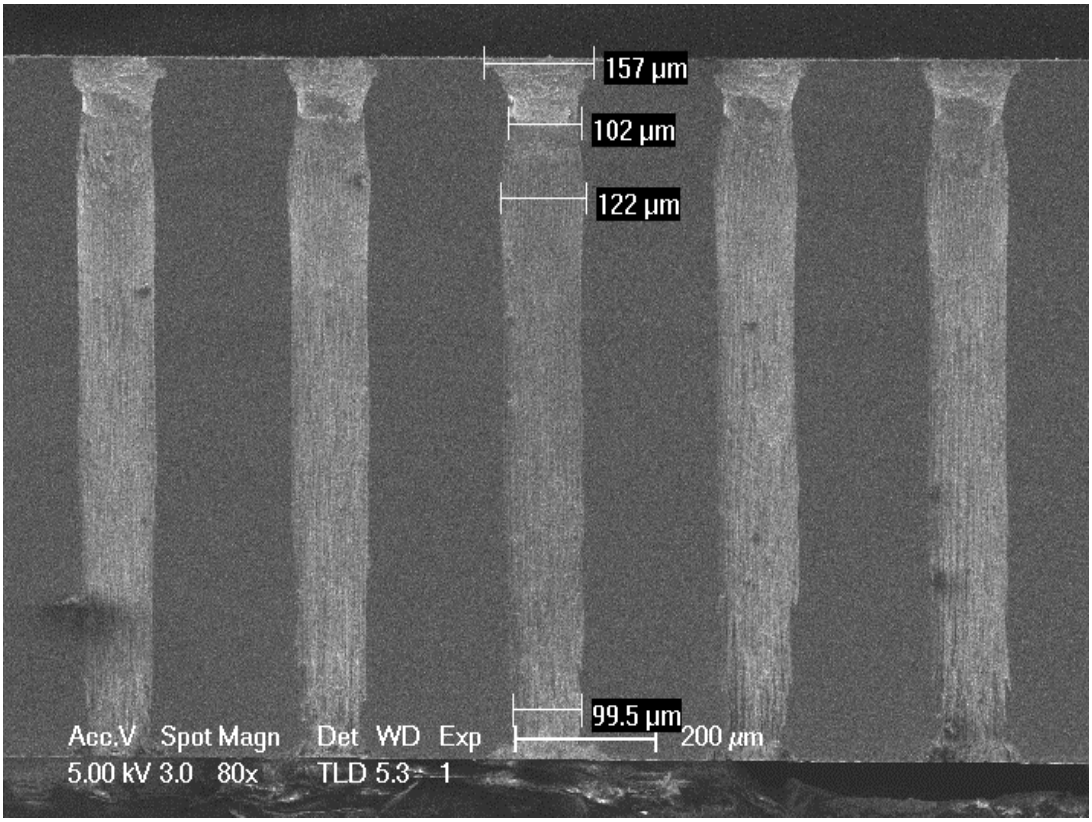

Unlike the fabrication scheme for nanoporous alumina membranes, the etch used in this case does not need to stop on a thin delicate membrane. However, excess

over-etching will cause expansions, or feet, to form at the bottom of the etched features. These feet will make it impossible to extract cast pillars from the mold in one direction, as they will act as anchoring structures causing the pillars to neck and break rather than release. In the case that a single side-polished wafer has been used, the rough bottom surface will then necessarily become the only interface that can be released from and will be imprinted and transferred during the release of cast pillars. Ideally, narrowing pillars are best for insertion and implantation into tissues. Thus, eliminating footing and ending with a narrowing etch is preferred and also allows the polished side of a single side-polished wafer to be used as the interface for the cast pillar release minimizing film at the interface.

7. Mold Sidewall Preparation and Release Layer Deposition

A successful release between the surfaces of the silicon mold and the cast polymer is critical to producing a complete array of full height pillars. Adhesion between the silicon mold and the pillars can cause the pillars to narrow and break at the base of the mold while in the release process. This occurs because the surface area of the interface between the cast pillars and the silicon mold is very large compared to the narrow cross section where the force releasing the pillars from the mold is applied. For instance a 100um diameter, 1mm deep silicon pillar mold would have a surface area of 314000 square microns while the cross sectional area that the releasing force is being applied to would only be 7850 square microns, a factor of 40 times smaller. If the adhesion between the silicon molds is anywhere near the

strength of the bulk cast polymer film, the pillars will always neck and tear at the base being pulled on rather than releasing.

When cured against silicon or silicon dioxide, PDMS forms very stable bonds such that in some cases, bulk PDMS can be torn apart rather than delaminating from a silicon or silicon dioxide substrate it has been cured against. To minimize adhesion at the interfaces between the cast pillars and the silicon mold, a form of passivation is needed. The already existing thin fluorocarbon passivation layers deposited during the Bosch silicon deep reactive ion etching process, while helping to diminish adhesion forces, are not sufficient.

A Teflon like fluorocarbon passivation layer is required to diminish unwanted adhesion between the cast polymer and the silicon mold surfaces and improve the release process. While many possible candidate molecules exist that could reduce adhesion and stiction (the static friction that must be overcome to have relative motion between objects), fluorocarbon molecules that can be chemically attached to the sidewalls of the silicon mold as a monolayer are used. Given the need to coat the vertical and horizontal surfaces of the mold and ensure that the chemical attachment occurs along the internal surfaces of the molds, MVD (molecular vapor phase deposition) is used to coat the molds. The chemical selected to reduce adhesion and stiction is FDTS (Perfluorodecyltrichlorosilane), which contains a long fluorocarbon tail that hosts 17 fluorine atoms and a chlorosilane head that is very reactive and can attach to silicon surfaces.

To prepare the silicon molds, the molds are separated from the glass carrier and from the areas of the processed wafer that do not contain molds. These molds are then solvent cleaned with acetone isopropanol and deionized water to remove vacuum grease and debris that might be attached to or inside the molds. To remove the fluorocarbons left by the mold fabrication process and prepare the silicon surface for the vapor deposition of FDTS, the molds are subjected to a long O_2 plasma ashing process burning away all the carbon based materials on the molds and activating surface bonds on the silicon. The ashing process is repeated twice in succession, and in between the molds are inverted so that all surfaces are exposed to the ashing process. In addition to this, an inductively coupled plasma reactive ion etch using oxygen can also be employed before the solvent cleans. However, this is generally not necessary and requires vacuum grease to keep the molds mounted during the etch, potentially further contaminating the mounted side of the molds while cleaning the top surfaces of passivation molecules.

Given the limited time that the O_2 plasma ashed silicon mold's surface remains reactive, it is preferable to immediately transfer the molds to the MVD chamber and start the FDTS deposition process with haste. In the event that a whole wafer full of molds is being prepared, placing the molds on one or two clean carrier wafers without any vacuum grease or adhesive can substantially increase the speed of the transfer between the ashing chamber and the MVD by decreasing the number of items that need to be individually transported from dozens to two easily transported carrier wafers. It is also useful at this stage of the fabrication process to separate

clean high yielding molds and dirty damaged molds so that sets of known good molds can be prepared and stored together in preparation for polymer film casting.

MVD provides a low pressure environment where heated FDTS can be released as a vapor which can then deposit itself on the surface of the silicon mold and the chamber's interior. While the adsorption of the molecular monolayer is initially a physical phenomenon, the reactivity of the chlorosilane group ensures that chemical attachments occur. After a 20 minute deposition process, the samples are exposed to a 110C bake to increase the amount of chemical bonding and are inverted and returned to the MVD for a second exposure which coats the previously unexposed surface. One final bake is applied to react the bonds from the second vapor deposition, and the silicon molds are then ready to use or store for future molding use. The FDTS coating on the finished silicon molds has proven very stable under standard storage conditions provided containers are sealed from dust.

D. Casting and Releasing Pillars from Molds

Once the silicon molds have been fabricated, flexible polymer pillars can be cast and released (see Figure 19, Figure 20 and Figure 21). The following section describes different casting and releasing strategies that have been investigated using PDMS as starting material, and ultimately describes the creation of biologically compatible conductive pillars using PDMS. Other polymers that could be similarly cast are not discussed.

Figure 19. Optical image of released 1024 pillar PDMS array.

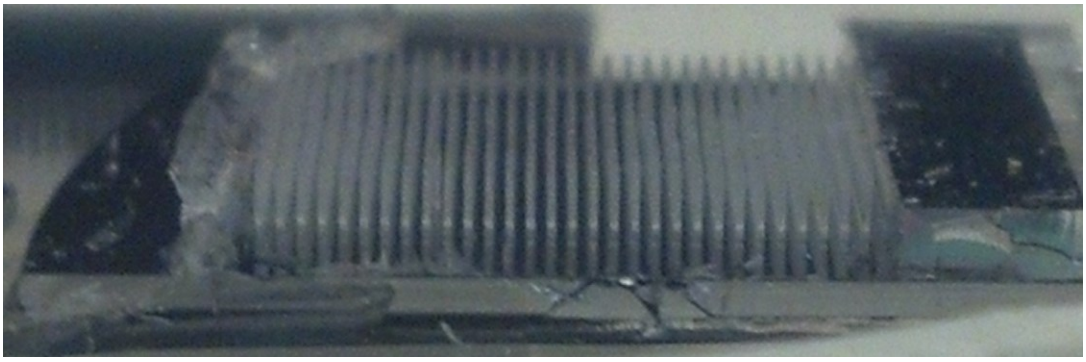

Figure 20. SEM image of released PDMS pillars illustrating array uniformity.

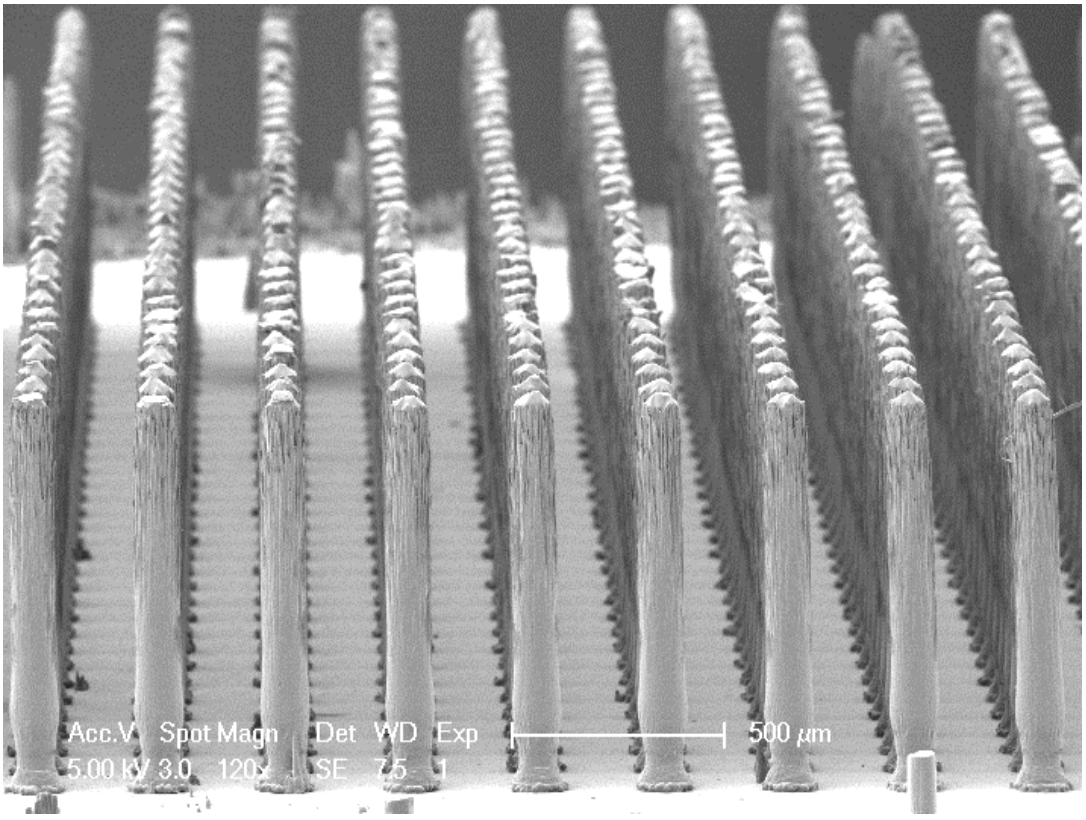

Figure 21. SEM image of pillar highlighting necking and remasking region.

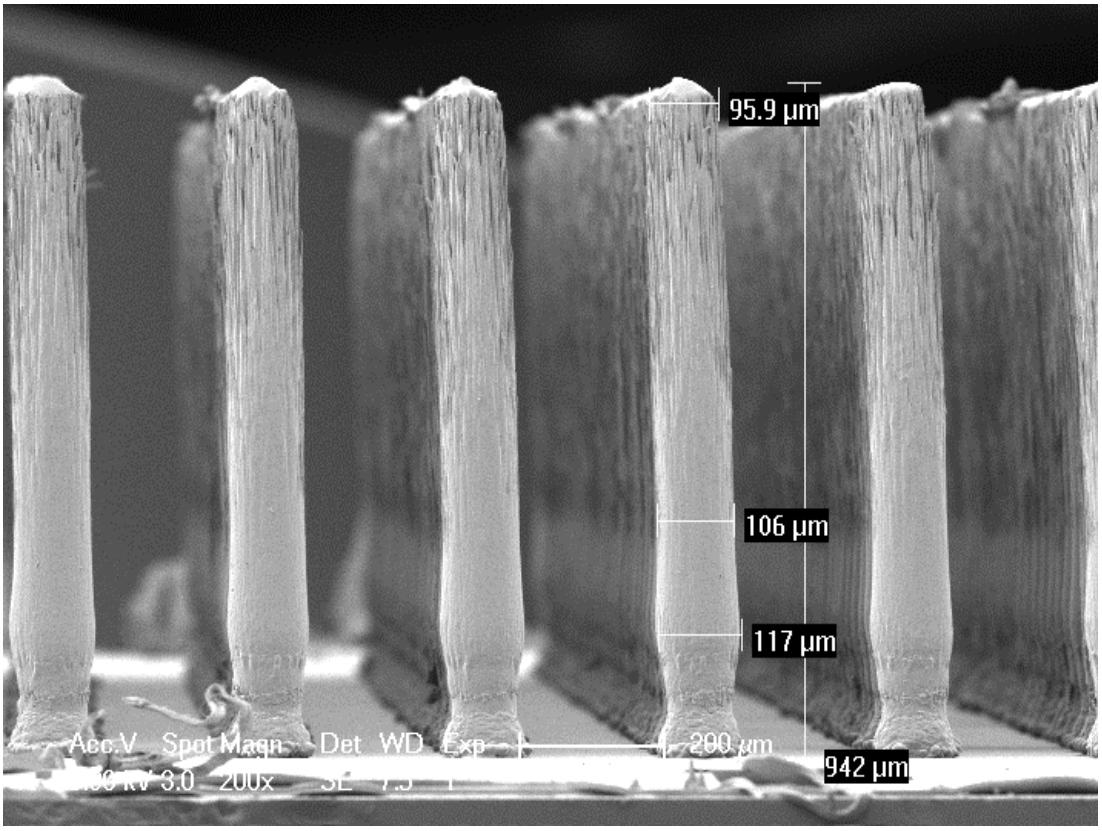

1. Casting Pure PDMS Mold

This casting process calls for the preparation of PDMS. First, the Sylgard 184 base component is measured out and then 10% by weight of the activator component is added. The two component system is vigorously mixed in a plastic cup or metal weighing dish, preferably with flat sidewalls that don't trap material. The mixing process is meant to distribute the activator component homogenously throughout the viscous solution but will also trap air bubbles. These are removed with a vacuum desiccation of at least 20 minutes. One continuous desiccation can be employed, or alternating periods of vacuum and re-pressurization can be used. In the case of mixing a large volume of PDMS, it is best to observe the vacuum desiccation as the

expanding solution being degassed can run over the container. Similarly, small containers being degassed also need to be watched when being pressurized as these may be thrown around the desiccator by the pressure change.

If molded pillars are desired which are backed by a bulk of PDMS, a mold can be placed in the container with a second flat and preferably polished FDTS treated piece of silicon below it. Then the PDMS can be degassed and re-pressurized repeatedly until bubbles stop appearing from within the mold voids. The FDTS treated silicon substrate allows the top of the polymer pillars to easily be separated from the thin film between the two pieces using a razor blade at a low angle shearing the tops of the pillars along the film interface. Without this substrate it would be necessary to remove the bulk of PDMS under the mold before releasing the pillars and this process could easily cause the tops of the pillars to be torn off when removing the bulk.

Once the mold no longer contains trapped air bubbles, the silicon mold voids are completely filled with PDMS. If a backing of silicon is desired it can be placed on top of the mold after being activated in O_2 plasma. The rough side of a single side-polished piece of silicon wafer is preferred as the increased surface area improves adhesion between the cured PDMS and the substrate. The further down into the PDMS the pillar backing piece is pressed, the thinner the film at the base of the pillars will be. Pressing the pillars all the way into the mold will result in a very thin film, which may not be continuous, so adhesion may be limited by the area of the pillars attached to the substrate.

The PDMS must be cured before it can be released. In order to induce strain into the pillars to make the release process more reliable, the mold and PDMS can be cured at 150C for at least 10 minutes such that it will contract at room temperature. Additionally, freezing the mold and PDMS after baking them can further help separate the pillars from the sidewalls of the silicon mold. After curing and freezing the PDMS and silicon mold, the two or three pieces of silicon along with the PDMS between them can be cut away from the rest of the cured PDMS. The FTDS treated piece is then cut free of additional PDMS at the edges and a razor blade or scalpel is used to pry up the piece free. The thin interface layer of PDMS is removed by using a blade at a low angle, shearing the tops of the pillars along the film interface as previously described.

Releasing the independent pillars from the silicon mold requires cutting all PDMS from the edges of the mold and working a thin blade around the edges until the PDMS film begins to separate from the mold on all sides. This is much easier in cases where a thick film exists between the mold and releasing substrate or that when there is no releasing substrate and the pillars are connected to a bulk of PDMS. In the event that a very thin to non-existent layer of PDMS is between the mold and releasing substrate, this can be a very delicate and difficult process. Too much force, and a blade may slip all the way in between the mold and the releasing substrate and cut the pillars from the releasing substrate, rendering them useless inside the silicon mold. When the mold is loose, two thin blades can be introduced to either side of the mold and slightly inserted into the juncture. The two blades can then be pried up

together to cause the mold to lift away from the releasing substrate vertically. Prying with a single blade on a single edge or corner of the mold can cause the mold to lift at an angle catching the pillars inside and causing them to be torn from the releasing substrate.

It is worth noting that while PDMS is capable of being drawn and narrowing without being torn apart, it is always advised that the wider side of the mold face the releasing substrate and the narrowing side face the FTDS treated silicon substrate in case the mold is not entirely vertical or either end of the mold has been expanded by footing or widening under the hard mask during the Bosch silicon deep reactive ion etching process.

2. Casting Metal Loaded Molds

As the goal of this process is the creation of conductive flexible polymer pillars for use as neural recording electrodes, development of a conducting polymer or hybrid material was required. In most cases where siloxane based rubbers that conduct are required, such as for flexible electronics applications, metal particles or carbon black have been blended into the mixture homogenously before curing. These materials become very viscous and easily trap gases when they are being mixed. Often, use of such materials requires a press to extrude the material into the desired shape before curing as well as a static mixer to combine the PDMS and the particles without introducing trapped bubbles. Without such machinery or a way to combine the developed molding technique with them, working with metallic particle filled PDMS mixtures is very difficult.

Commercial carbon black filled siloxane elastomers as well as silver particle filled blends found in literature were investigated. Both were very difficult to mix by mechanical stirring, and also extremely difficult to degas and load into the silicon molds. Resulting pillars that were successfully released would only conduct partially, (see Figure 22) while others would be cast with areas missing conductive filler or contained trapped air bubbles or other forms of insulating voids. As a result, neither path of investigation resulted in particularly conductive pillars or bulk films. In the case of filling with silver particles, the particles would tend to fall out of suspension or at least away from cast interfaces leaving an insulating surface. The use of solvents to mix the PDMS and fill particles without introducing bubbles was also not successful as degassing the solvent after mixing never resulted in a product that would successfully cure. It is assumed that part of the compounds involved in crosslinking the polymer were vacuumed off before the solvents. These issues might be overcome with static mixing techniques and injection press molding methods, but those are not applicable in a lab setting. Given the techniques available, casting particle filled mixes of PDMS proved unmanageable due to viscosity and trapped gases.

Figure 22. SEM of partially and fully conductive fill loaded PDMS pillars.

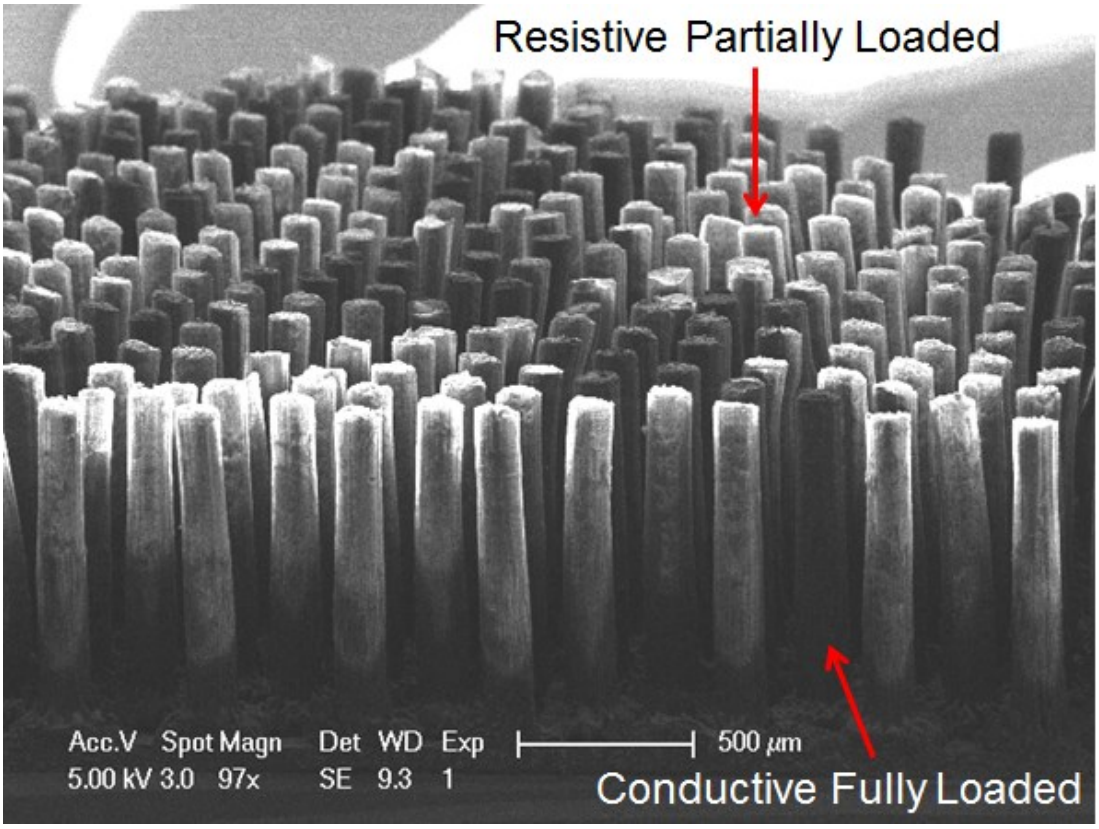

3. Casting Magnetically Loaded Molds

Magnetic guidance of ferromagnetic particles, and in particular nickel particles, has proven incredibly useful in overcoming difficulties related to casting PDMS containing conductive fill particles. The application of a strong magnetic field can be used to draw nickel particles contained within PDMS into a silicon mold. This effect can also be used to increase the local density of nickel particles within and near the silicon mold while helping to displace gas bubbles and volumes of PDMS without nickel.

Magnetic guidance has been investigated for loading wires directly into through silicon vias[4]. While this initially appeared directly applicable to these investigations,

wire segments of the dimensions required to be loaded into the center of pillar voids in the silicon molds were not able to be directed into the position. It was only when migrating to magnetic particles instead of magnetic rods that magnetic guidance worked with the molds.

Several different PDMS nickel formulations were investigated including different loadings of nickel particles as well as different sizes of particles. These included both 50 micron as well as 5 micron powders of nickel and ~45 micron sliver coated nickel powders. Loadings of 33% and 50% metal powder by weight were also investigated. Experimentally, it was determined that the finer powder of nickel combined with the higher fill percentage provided the most conductive resulting pillars. This finding is due to the higher densities of particles overcoming the percolation threshold for conduction. While not investigated, it is likely that even denser loadings of smaller particles of nickel would provide greater conduction. Loadings above 50% nickel in PDMS have not been extensively examined as they can be difficult to mix and magnetic guidance already tends to increase the effective loading in the pillars.

As the magnetic guidance process is rather complex and differs from the standard pillar casting process, a complete description is provided at the end of this work. Key differences are stated and explained below.

The FTDS treated silicon substrate is taped down at the center of an alumina dish with the polished side up using double-sided Kapton polyimide tape. This keeps the substrate in place so that it is easier to maintain the alignment and position of the mold and correctly position the releasing substrate. The PDMS mixture is first mixed

and degassed, then nickel powder is added and mixed in and again degassed before being applied to the mold. Whenever the mixture of PDMS and nickel is added to the silicon mold, a neodymium magnet is applied to the underside of the alumina dish and moved back and forth across the mold area driving additional nickel into the mold. The magnetic particles in the PMDS cause the mixture to act as a ferrofluid, (see Figure 23) and each movement of the magnet guides the particles into the mold voids. The PDMS-nickel is deposited on the FDTS coated substrate and prior to the mold being placed, then PDMS-nickel is applied to the top of the mold after it is positioned. Because of the high viscosity of the PDMS-nickel after each application of PDMS-nickel and magnetic guidance, the mold is then degassed with the magnet directly underneath the aluminum dish aligned with the mold's location. This process of adding PDMS-nickel followed by magnetic guidance and degassing is repeated four times which helps overcome the viscosity of the mixture, remove trapped bubbles, and completely fill the pillar voids in the mold. As the PDMS-nickel is guided across the surface of the mold, it is drawn into the mold and PDMS free of nickel accumulates at the edges of the expanding PDMS-nickel pool in the alumina dish. Over these repeated magnetic guidance movements, the nickel in the mold voids becomes locally densified. As the motion of the magnet guiding the nickel drags the PDMS as well, the silicon mold can slip off the FDTS coated substrate. The mold must be realigned while being kept in plane to avoid introducing bubbles or displacing compacted nickel in the mold. After the final degassing step, a

releasing substrate that has been activated with O_2 plasma can be aligned and placed directly over the filled mold.

Figure 23. PDMS-Nickel acting as a ferrofluid while under magnetic guidance.

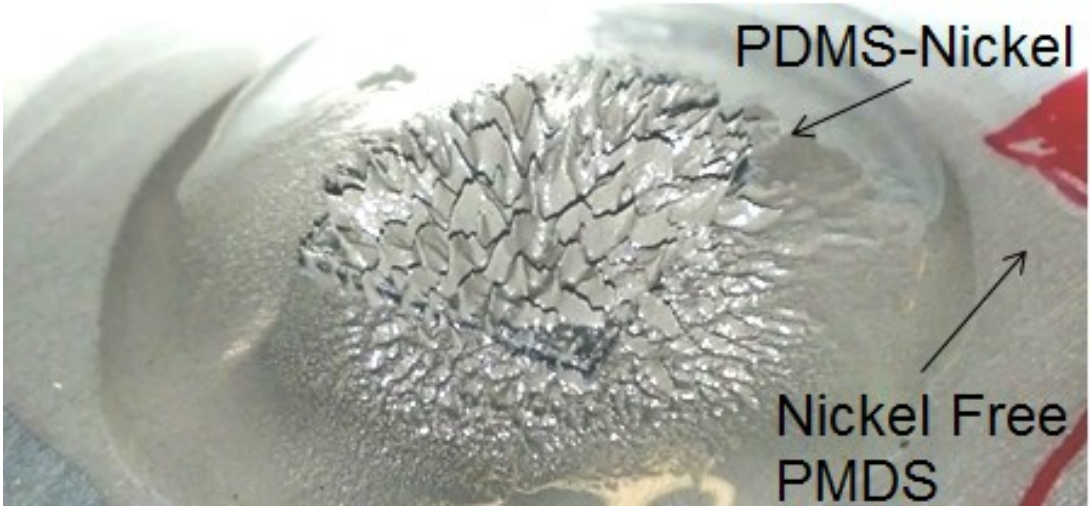

Magnetic guidance of dry nickel powders into a prepared mold without PDMS followed by the addition of PDMS or PDMS-nickel have not resulted in releasable pillars. This is because only an insufficient amount of siloxane elastomer is able to get into the pillar voids in the mold to facilitate the release as the nickel particles are unable to deform when they are tightly packed together.

4. Removal of Excess Cast Film

The PDMS-nickel film within and above the mold can be conductive, therefore it is important that individual pillars be isolated from each other so that they can be used as independent neural recording electrodes. As the PDMS-nickel film is gray and does not transmit light, the cast film layer above the pillars can make the pillar impossible to locate on the surface of the mold, which makes alignment of the pillars

to a particular position on a releasing substrate difficult. Both of these difficulties are overcome by blading off the PDMS-nickel film on top of the mold once the magnet has been withdrawn. Finally, to ensure good contact is made between the releasing substrate and the bare mold surface, pressure can be applied downward onto the mold to extrude small hills of dense nickel filled PDMS just above the pillar voids in the mold. These bumps ensure good contact with the releasing substrate when it is contacted against the mold and minimize the chance of air gaps between pillars and releasing substrate that could hinder the full release of the pillar array. The complete mold casting scheme, (see Figure 24) while complex, is quite novel and overcomes the many challenges discussed. After the blading process, some PDMS-nickel can remain as a film on the surface of the mold but it will not contain enough nickel to cause shorting between the released pillars even if the surface of the mold being used in the release is unpolished (see Figure 25).

Figure 24. Magnetically guided mold casting scheme.

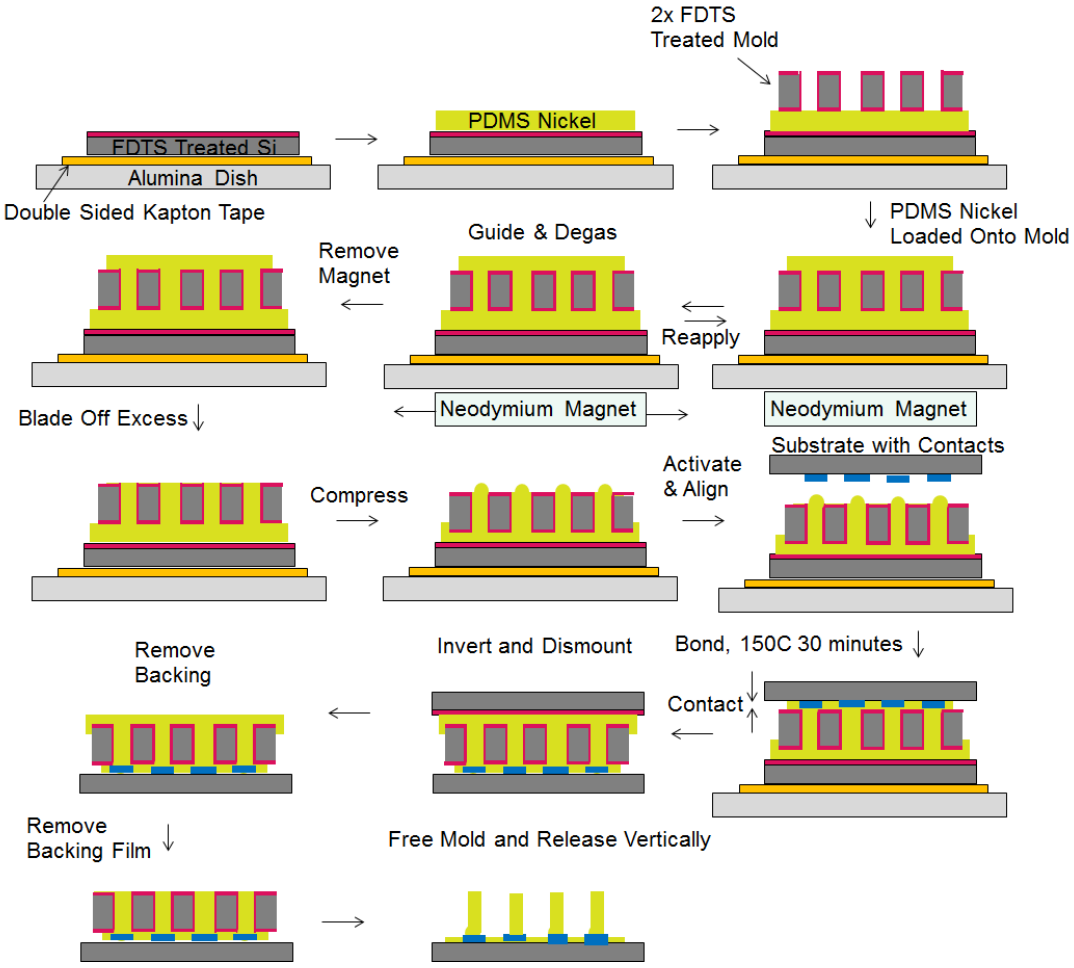

Figure 25. Nickel loaded flexible conductive pillar electrodes.

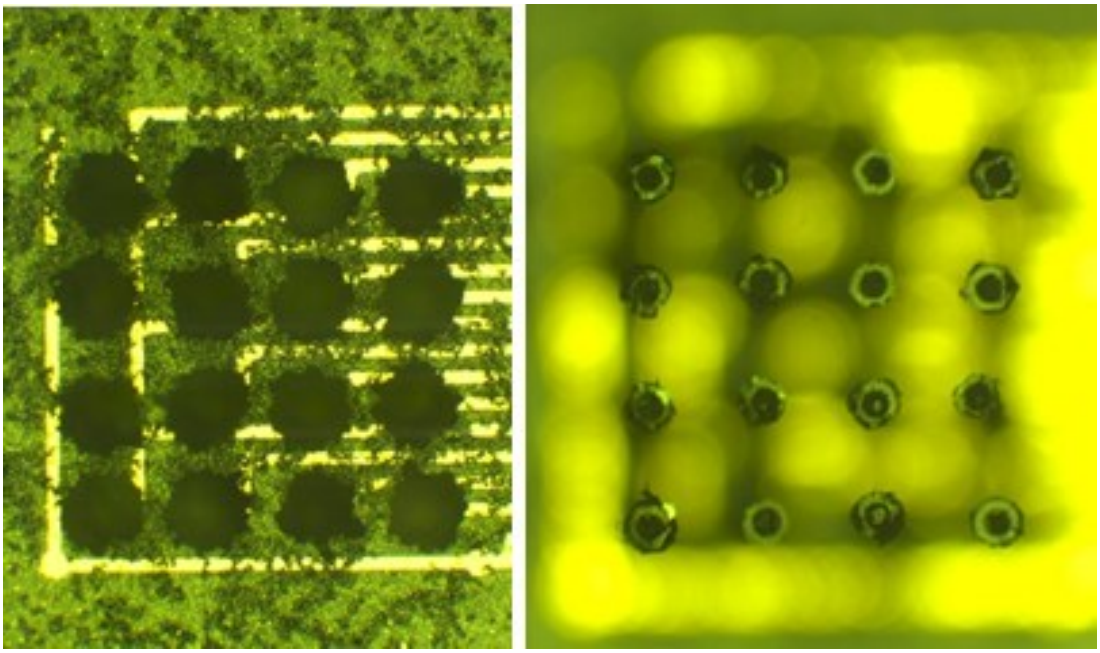

5. Deposition of Biologically Compatible Conductive Gold Layer

Nickel is cytotoxic and not biologically compatible, and this is unacceptable when considering the proposed use of this pillar molding technique. Platinum, gold, silver, and titanium would all be far more biologically compatible materials but they cannot be guided magnetically. By plating nickel in a more compatible material such as silver or gold, the biocompatibility of the electrodes can be greatly improved. This process of plating can either occur before the powder is used or after the pillars are cast and released. In the event that individual particles are plated, a chemical formulation is preferred while with the completed pillars electroplating is also an option. In the case of the devices shown here an electroless cyanide free gold deposition solution is applied to a released pillar array that has been ashed in O_2

plasma. The nickel that is directly exposed at the surface of the pillar is plated in a fine layer of gold improving the biocompatibility of the pillar array.

E. Alignment and Electrical Contact with Wireouts

To make use of the flexible conductive polymer pillars as neural recording electrodes, it is necessary to connect them to a conductive interconnect or a wireout or directly place them on open pads on a CMOS chip. These wireouts can then run to contact pads that can be connected to recording systems. This section briefly describes alignment methods and different types of wireouts that have been aligned to fabricated pillars for demonstration purposes.

While 1mm tall molds with up to 1024 pillars have been fabricated on silicon substrates using methods already described, demonstration of conducting neural recording pillars has focused on easier to align 16 pillar systems. These slightly smaller and lower density arrays still maintain the prerequisite 1mm recording height required for implantable devices. Additionally, a 16 pillar 4x4 array with a 400 micron pitch is the same size, count, and density as those Utah recording electrode arrays most often used in simple animal based studies.

1. Fabrication of Small Gold Wireouts

Wireouts designed to be compatible with dual hemisphere animal studies were designed after consultation with Ray Rui Ma and the Neural Interaction Lab directed by Todd P. Coleman at UCSD. These featured contacts for two 16 pillar arrays, with one per hemisphere as well as contact pads to mount a 34 pin interface that could be

mated to the recording head stage used in their animal studies. This design was used to produce conducting wireouts of titanium and gold on glass. These were used to verify pillar to contact pad conductivity (see figure 26) as well as to verify that the pillars and wireouts did not contain shorts.

Figure 26. Flexible conductive pillar electrodes on gold wireouts for testing.

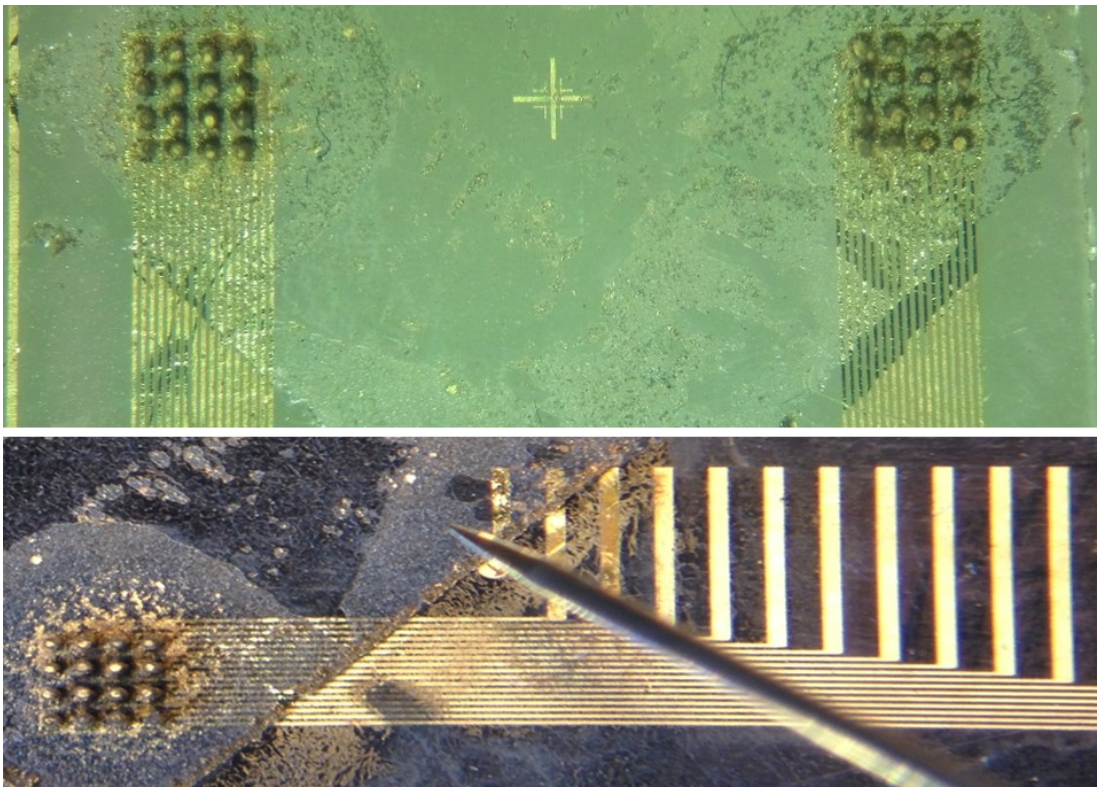

2. Alignment of Small Gold Wireouts

Alignment between the pillars and these wireouts were carried out with two different mechanisms. The first was a custom built assembly that hosted spring clips attached to a frame that would hold glass slides of 75mm length over a three axis mechanical alignment stage. The wireout was taped to a 35mm x 75mm glass slide with a small amount of double-sided Kapton at either end, and then activated with O_2

plasma being mounted in the assembly facing downward. A prepared mold and FDTS treated substrate not adhered to the aluminum dish was made. After excess PDMS-nickel was bladed off and the mold was depressed so that a slight bump of PDMS-nickel extended from the pillar voids in the silicon mold, it was placed on the alignment surface. While under a microscope, the stage was then quickly manipulated into alignment with the matching contact locations and driven up into hard contact. Continuing to use the microscope, good alignment and contact was verified and the stage was slowly brought down. The PDMS-nickel left on the surface is sufficient to keep the mold in place while the alignment stage is lowered and the aligned stack of mold and wireout are extracted and inverted. The bake and release process then proceeds normally with the caveat that the extraction process be carried out with great care so as not to cut the metal lines on the wireout surface.

The second method for alignment of the mold to the gold wireout required a flip chip bonder. The Finetech Fineplacer Lambda was used for this alignment. The standard PDMS-nickel mold preparation process was used including taping the FDTS treated substrate to the aluminum dish. The gold wireout was picked up by the placing arm of the Fineplacer after being activated with O_2 plasma and inverted. Due to size restrictions, the aluminum dish holding the mold was cut down to a size just larger than the substrate and then placed under the Fineplacer. The mold was aligned on the Fineplacer stage to match the positioning of the wireout held on the arm and the two were bonded. In the bonding process, the arm lowered the wireout onto the mold and then applied pressure as well as heat from both under the substrate as well

as above the wireout. The cure at 150C occurs on the Fineplacer, providing no opportunity for the alignment to slip before the cure starts unlike the previously described method using a custom assembly. Once cured, the arm is released and the pillars can be released from the mold following the standard process while being careful not to damage the conductors on the wireout.

3. Fabrication of Multi-Electrode Arrays

To further demonstrate the use of the fabricated pillars as neural recording arrays, they needed to be integrated with a head stage designed for neural recording. A Multi-Channel Systems MEA2100-System recording system was chosen as a platform. This particular system included a 120 channel head stage and pin interface. After examining several 120 electrode multi-electrode arrays produced by MCS and receiving a technical drawing of the contact pads in their 120 electrode arrays, compatible multi-electrode arrays were designed and fabricated (see Figure 27). These used 100 micron electrode contacts which are equivalent in size to the fabricated pillars, as well as a 400 micron pitch matching the 16 pillar molds and arrays.

Figure 27. Custom 2 layer MEA (multi-electrode array) design.

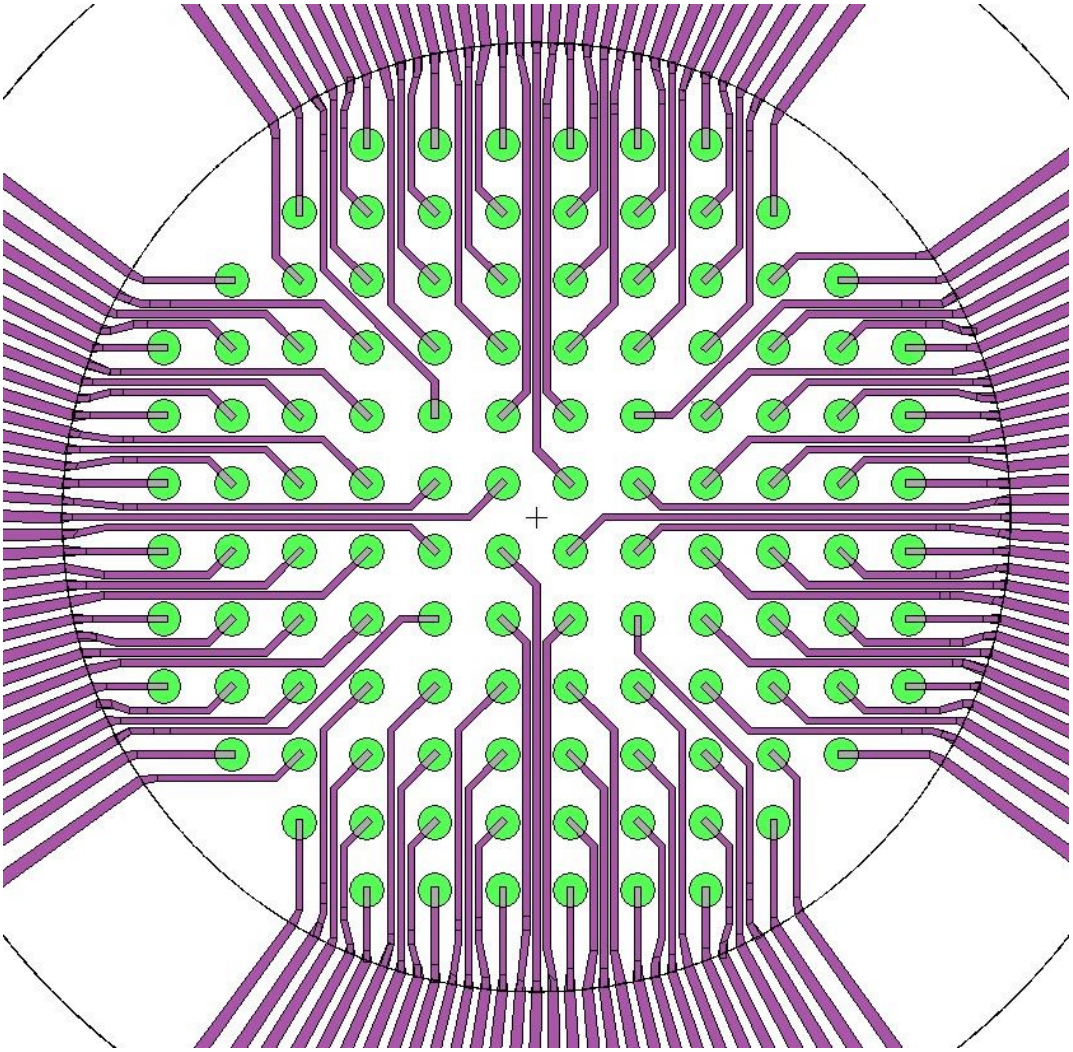

The fabricated multi-electrode arrays were made using electron beam deposited titanium and platinum and a liftoff process using nLOF 2020 or nLOF 2070 photoresist and standard processing recipes. Liftoff was carried out using heated stripper (Microposit 1165) at 70 degrees for several hours and low intensity sonication in a heated bath was also employed in cases where liftoff was problematic.

To make the most economical multi-electrode arrays possible two different possible dielectrics were investigated. Similar materials to both of these are used in different MCS multi-electrode arrays. Due to its ability to be directly patterned and used as a dielectric, SU-8 was initially investigated. This avoided the deposition and etching process usually required when putting down and opening contacts through a dielectric layer. SU-8 2025 was spun to a thickness of 20 microns and patterned to provide openings to the electrode contact array as well as the pad ring.

Following this process, a cylindrical well like those found in MCS multi-electrode arrays was fabricated. Standard media wells are composed of glass, but wells produced for these arrays were fabricated from PMMA (Poly(methyl methacrylate)) resin using a FormLabs Form 1 3D printer. To attach the PMMA rings to the multi-electrode array already patterned with SU-8, the ring was partially dipped into additional SU-8 and then flood exposed and hard baked to seal the ring in place.

Delamination of the SU-8 layer from the multi-electrode array eventually occurred when the wells were left filled with aqueous biological buffer and maintained under incubation conditions for one week. Even with the addition of Omnicoat and slowly ramped hard bakes, the SU-8 patterning process employed was not compatible with the conditions required to culture neurons.

While more costly, low stress silicon nitride was used to replace patterned SU-8 as the dielectric layer in the multi-electrode arrays. 860nm of silicon nitride was deposited using a dual frequency PECVD produced by Advanced Vacuum. This was

patterned using nLOF 2020 or nLOF 2070 and a standard processing recipe. A 10 minute, CHF_3/O_2 ICP RIE plasma etch was then used to open the pattern in the silicon nitride layer and the photoresist was stripped off with stripper (Microposit 1165).

Given the delamination issues already experienced with SU-8, unpatterned PMMA resin was investigated to bond the silicon nitride dielectric to the printed PMMA ring. The bottom half of the ring was dipped into PMMA resin and then mounted to the silicon nitride layer. The PMMA resin was then exposed to a low power 350nm UV source for 24 hours to crosslink the resin.

The PMMA resin attachment bond held for longer than the SU-8 bond previously employed, however some of these devices also delaminated from the silicon nitride. Ultimately, commercial Loctite marine epoxy was used to replace SU-8 or PMMA resin to form a stable, biologically friendly, and watertight bond between the PMMA ring and the silicon nitride substrate.

4. Alignment on Multi-Electrode Arrays

As the prepared PDMS-nickel filled mold has to be directly contacted to the electrodes of the multi-electrode array, the alignment, bonding, and release of the pillars from the silicon mold onto the multi-electrode array must precede the attachment of the PMMA ring. The previously described alignment methods are not compatible with the fabricated multi-electrode array. This is because the multi-electrode array is 50mm x 50mm in size. This is beyond the dimensions the custom assembly can accommodate as well as larger than the Fineplacer can safely pickup

while its optics are centered on the electrode contact area that needs to be aligned. A SUSS MJB3 contact aligner was used in place of these two methods. This takes advantage of the 50mm x 50mm size of the multi-electrode array. The multi-electrode array is vacuum sealed to a small mask vacuum plate and set in the system after being activated by O_2 plasma. The prepared mold stack on the bottom of a cutout aluminum dish is set on a 50.8mm x 75mm glass slide for easy handling and transport to an oven after contact alignment is complete. The contact aligner is used to align the bladed mold surface with the multi-electrode array looking down through the glass and silicon nitride. The mold is brought up into hard contact with the electrodes at the center of the multi-electrode array. Once good contact is visible in the optics of the aligner (see Figure 28), the vacuum holding the multi-electrode array is cut and the multi-electrode array left resting on the mold. The whole stack can then be lowered away from the vacuum plate, extracted from the aligner, and carefully transported to a waiting oven at 150C for the 30 minute cure. Care must be taken while releasing the cured mold both to make sure the release is vertical and to avoid damaged to the wireout. Once cured, the cylindrical well can be manufactured and attached, resulting in a completed demonstrative conductive flexible polymer electrode array integrated into the custom MEA (see Figure 29) that is ready for biological testing and recording.

Figure 28. Custom MEA aligned to prepared mold and ready to bond.

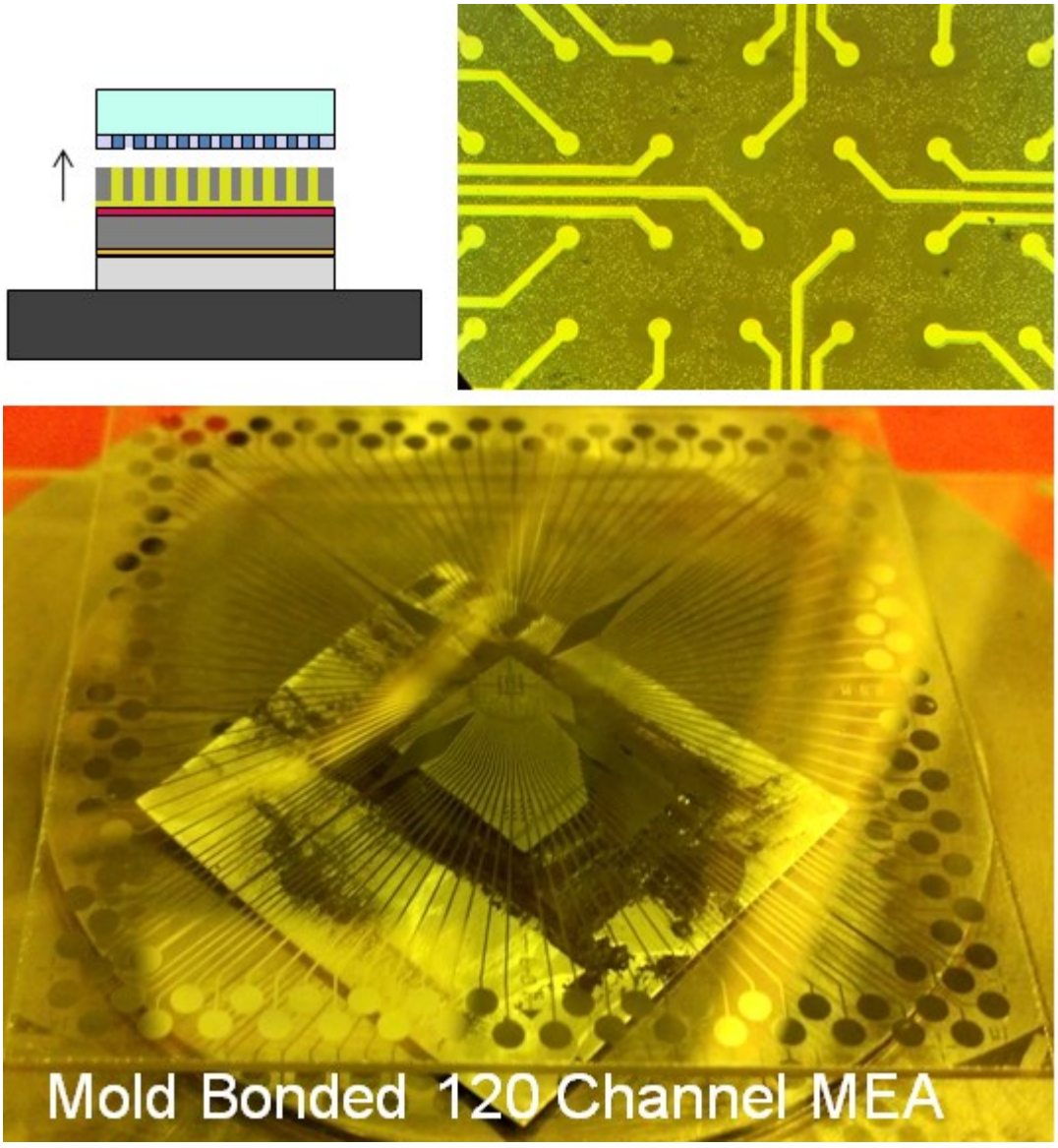

Figure 29. Completed custom MEA with flexible conductive pillar electrodes.

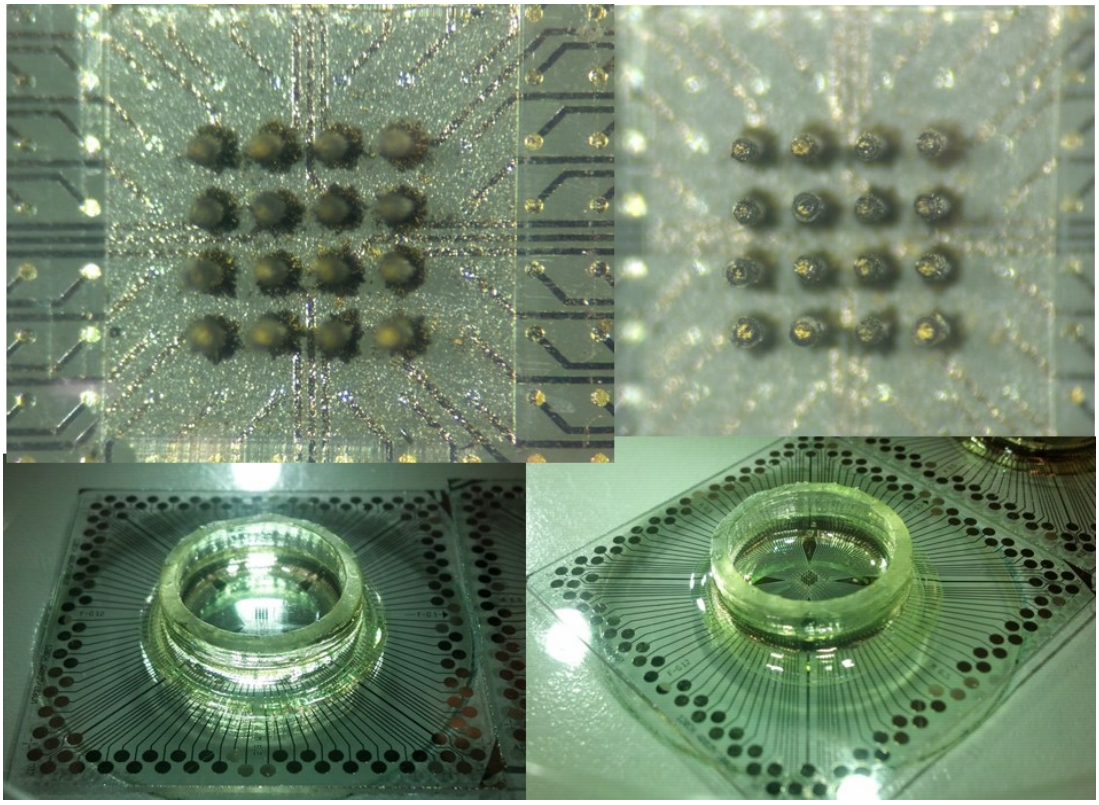

IV. Testing and Experimental Demonstration of Fabricated Alumina Nanoporous Membranes

The following chapter covers experimental investigations associated with ion pumps as well as selective ion pumps and selective chemistries. Both planar devices as well as through plane devices are discussed. Alumina nanoporous membranes fabricated using the scheme discussed earlier are demonstrated as research instruments for experimental studies. Limited selectivity between the biologically meaningful cations potassium and sodium are shown using alumina nanoporous membranes fabricated as a stable scaffold to host deposited selective chemistries.

A. Investigations with Planar Devices

Following the work of Joakim Isaksson first published in Nature Materials[2], similar planar PEDOT:PSS devices were fabricated. Eventually, these initial investigations were followed by lithographically defined devices featuring both PEDOT:PSS and SU-8 layers that were patterned. These could be modified to feature gaps free of PEDOT:PSS and were capable of supporting potentially ion selective transport materials rather than regions of over- oxidized PEDOT:PSS.

The stability of these devices, and particularly the delamination associated with the interfaces of the PEDOT:PSS layer greatly limited their use. A number of different formulations of PEDOT:PSS and reactive saline terminated molecules designed to improve adhesion were investigated including formulations with DMSO (Dimethyl sulfoxide) to provide extra doping. Momentive Silquest A187, a polyepoxysilane, was found to improve adhesion when spun down before PEDOT:PSS or when co-mixed and spun. Immediate activation of a glass or silicon surface in O_2 plasma just before application of PEDOT:PSS was also found to improve adhesion and limit delamination over time due to hydration. This did not require the use of reactive polyepoxysilanes.

1. Testing of First Generation Planar PEDOT:PSS Devices

The first generation of these devices had wells 5.5mm away from the over-oxidized or selective regions (see Figure 30). When testing these with a potential applied between the two bodies of PEDOT:PSS and over-oxidized PEDOT:PSS in the ion transport region, currents for salts such as one molar KCl in the wells were

equivalent with currents when deionized water was in the wells. This led to the finding that diffusion of ions through the PEDOT:PSS was very slow. This could be overcome with additional potential applied to the wells to cause field driven transport of ion into the PEDOT:PSS layer, but this is not ideal for a device pumping into or out of intercellular fluids.

Figure 30. First generation long channel PEDOT:PSS planer pump.

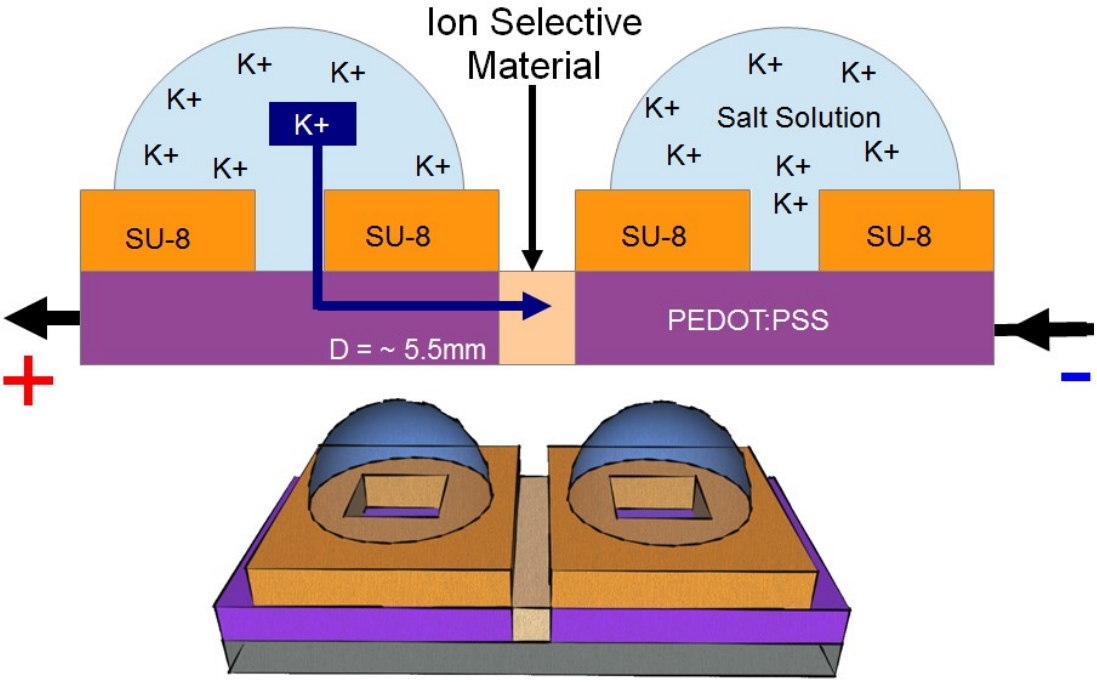

2. Testing of Second Generation Planar PEDOT:PSS Devices

As diffusion of ions across the PEDOT:PSS limited ion transport across the junction, a second generation of devices was designed and fabricated with the wells nearly adjacent to the transport region (see Figure 31). These devices displayed currents with 1M salt solutions two orders of magnitude larger than with deionized water. Testing the ion transport selectivity of materials using these planar devices

proved difficult as the SU-8 tended to delaminate from the PEDOT:PSS that became hydrated over time. Additionally, the narrow spacing between the wells that was necessary to avoid the diffusion limitations of the PEDOT:PSS made loading of potential ion selective transport chemistries difficult. Any time these materials come into direct contact with a salt solution, transport currents may become very high and irregular as leakage paths formed under, over, or through the material.

Figure 31. Second generation short channel PEDOT:PSS planer pump.

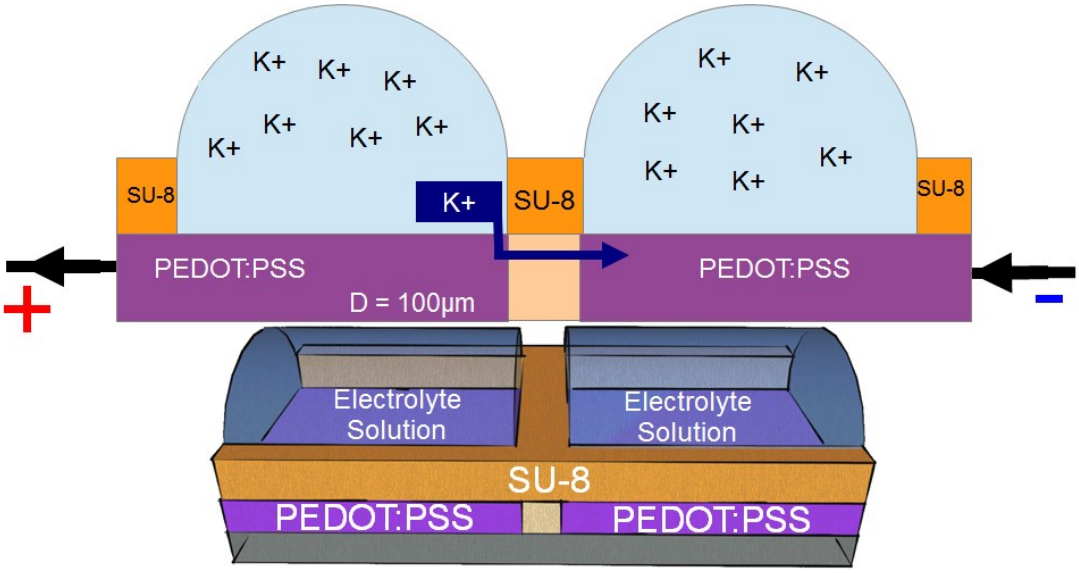

Several other materials polymers were also investigated to replace PEDOT:PSS such as TCNQ (Tetracyanoquinodimethane) and Polyaniline. These materials did not produce reversible oxidation reduction curves in salt solutions, making them impossible to use repeatedly in a biphasic device without further refinement.

B. Investigations with Non-Alumina Membranes

As planar devices had numerous issues related to delimitation and leakage paths, due to the devices construction that was in plane with the direction of ion transport and applied field, devices that transport ions through plane were considered. These have several benefits compared to planar devices. First, they can be made very thin, so less applied potential is needed to generate the same electrical field across the device. Second, material interfaces are perpendicular to and not in line with the ion conduction path, limiting the risk of delamination. Third, arrays of devices may be built using a single plane of stacked materials and lithographic patterning techniques.

While the alumina nanoporous membrane fabrication scheme was being developed, other porous membranes were investigated for their potential use in an ion transport device. These included porous polycarbonate membranes as well as silicon nitride membranes with 1 micron holes.

1. Holey Silicon Nitride Membrane Windows

The silicon nitride membranes were purchased from Norcada's selection of holey nitride membrane windows for TEM use. These windows were 500 microns by 500 microns in a silicon handle and contained an array of 1 micron holes at a 10 micron pitch. PEDOT:PSS was spun across the membranes and characterized to ensure that spun PEDOT:PSS films could form over small openings of one micron or less (see Figure 32 and Figure 33). This characterization included SEM (scanning electron microscopy) imaging using an FEI Sirion SEM as well as a FEI FIB (focused ion beam) milling system. The SEM was used to capture top down images of the surface

texture and uniformity of the cured PEDOT:PSS film while the FIB was used to mill away half of a film covered hole in the window region to determine the thickness of the bridging film, and to determine if the hole had been filled. This analysis indicated that the spun PEDOT:PSS films did not fill the holes in the membrane, but rather bridged the surface. This is important as it indicates that conductive cores of PEDOT:PSS do not form when spun over porous membranes, ensuring that ions rather than electrons will be transported between two spun layers of PEDOT:PSS sandwiching a porous membrane. Given the fragile nature of these porous nitride membranes meant for TEM studies, transport experiments with them were not investigated.

Figure 32. SEM of 40nm thick PEDOT:PSS layer spun across 1µm pores.

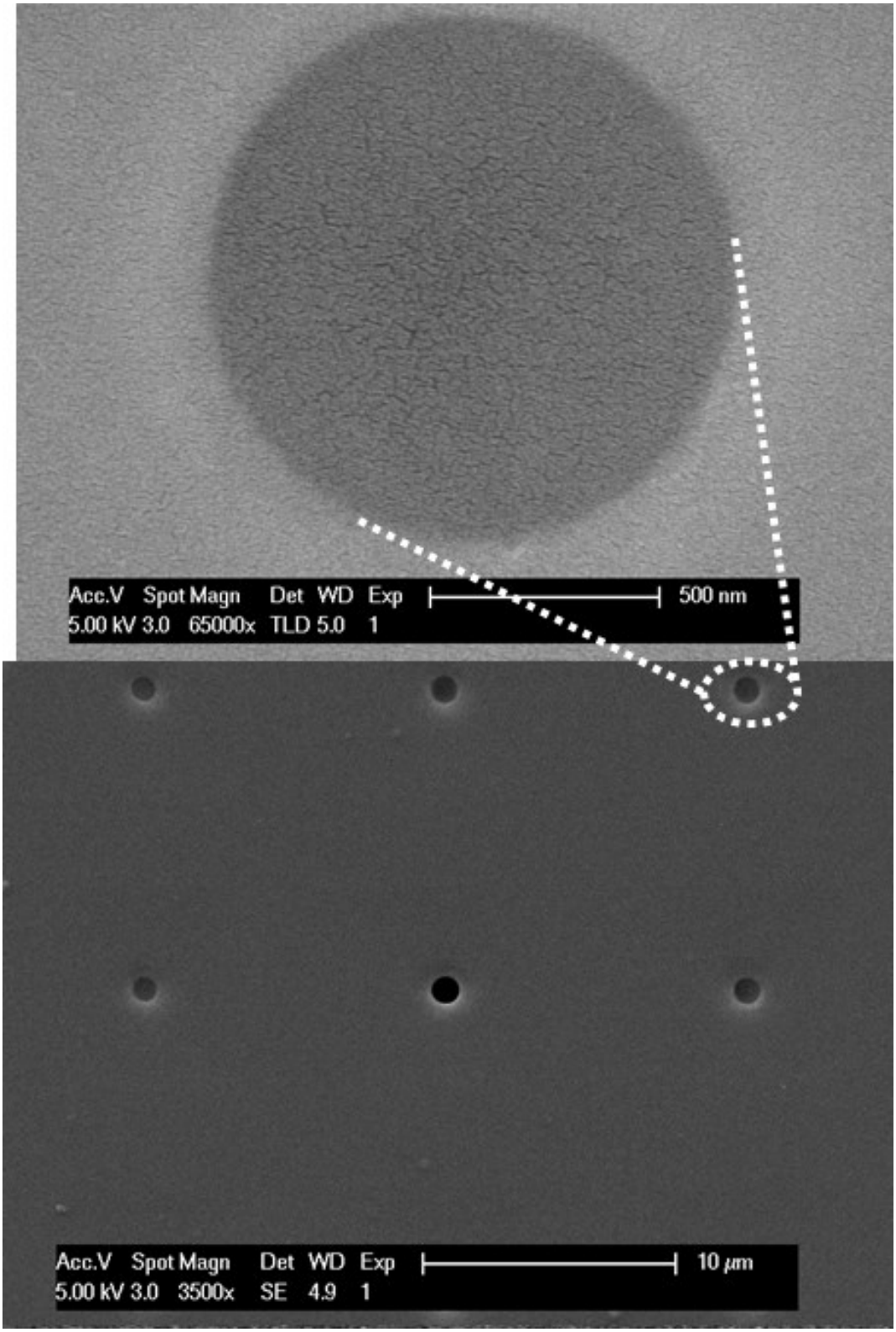

Figure 33. FIB / SEM image of 40nm cross-section of PEDOT:PSS film.

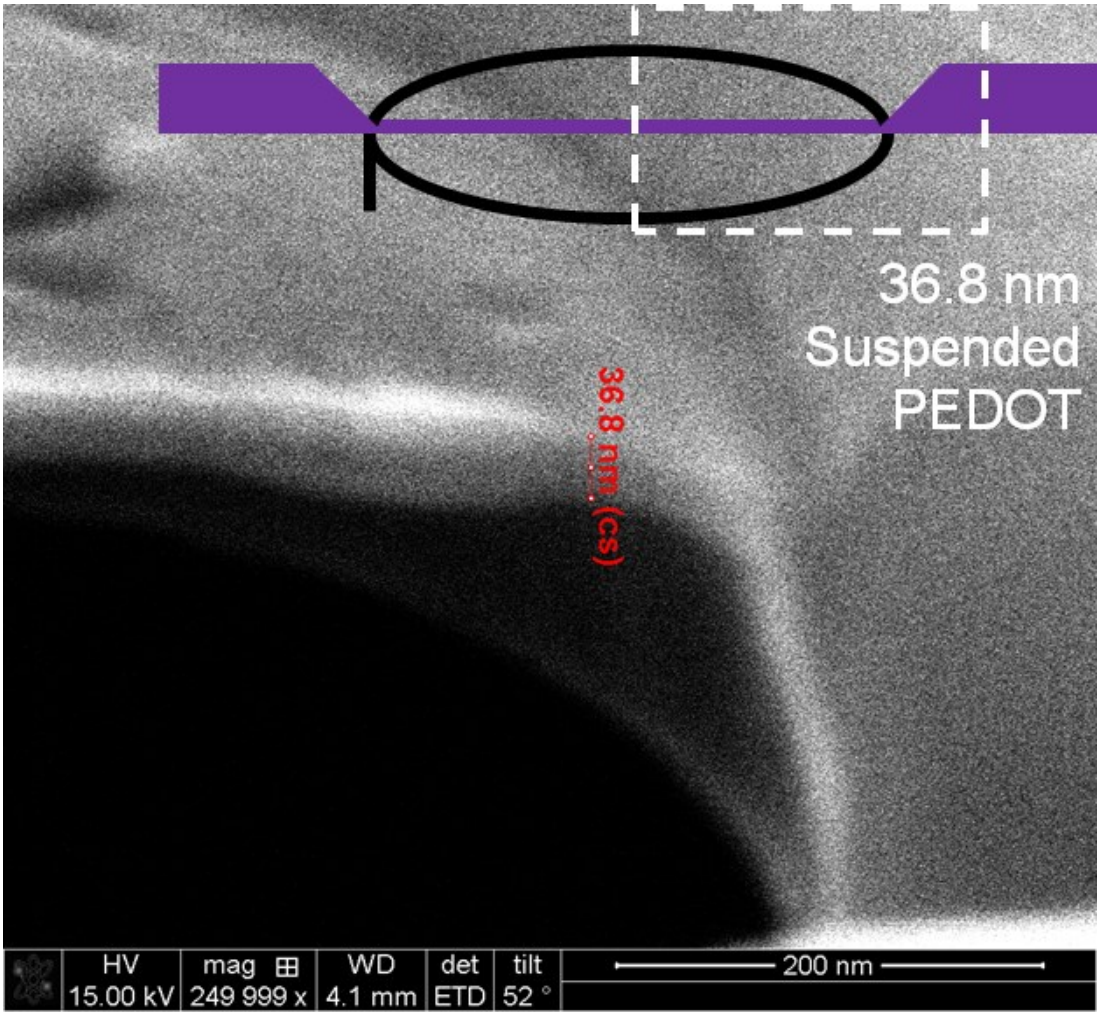

2. Track-Etched Polycarbonate Membranes

Track-etched membranes of polycarbonate 13mm in diameter and 12um in thickness with 15nm pores were purchased from Whatman (Nuclepore Polycarbonate 110401) for these experiments. The membranes were either treated with a crown ether (18-c-6) which was attached within the track-etch pores, or 40nm thick layers of PEDOT:PSS polymer electrodes were fabricated on both faces of the polycarbonate membrane.

3. Polycarbonate Membranes with PEDOT:PSS

In the case of the PEDOT:PSS prepared devices, single sided Kapton tape with a 8mm hole punch through it was applied to both sides of the polycarbonate membrane before the PEDOT:PSS was applied and spun. Each side of the membrane was spun and then baked at 115C for 20 minutes. Following the final bake, the outer edge of the tape frame around the membrane was cut to remove PEDOT:PSS that would connect both sides together. These electrodes were made accessible for cell transport studies by the application of silver paint (silver in iso-butyl methyl ketone) (Electrodag 1415M), followed by the attachment of cut strips of aluminum tape as lead wires. The membrane was sealed in a two-well solution cell by two 1mm thick PDMS gaskets made using Sylgard 184. The gasket was laser cut, and window size was a diameter of 5mm for each gasket. The cell (see Figure 34 and Figure 35) was made of two milled Teflon blocks containing the solution wells. This cell and similar cells sharing the same PDMS gasket assembly stack and operating principles were also used for demonstrative investigations of the fabricated anodized alumina nanoporous membranes discussed in Chapter II and later in this chapter.

Figure 34. Two chamber Teflon testing cell.

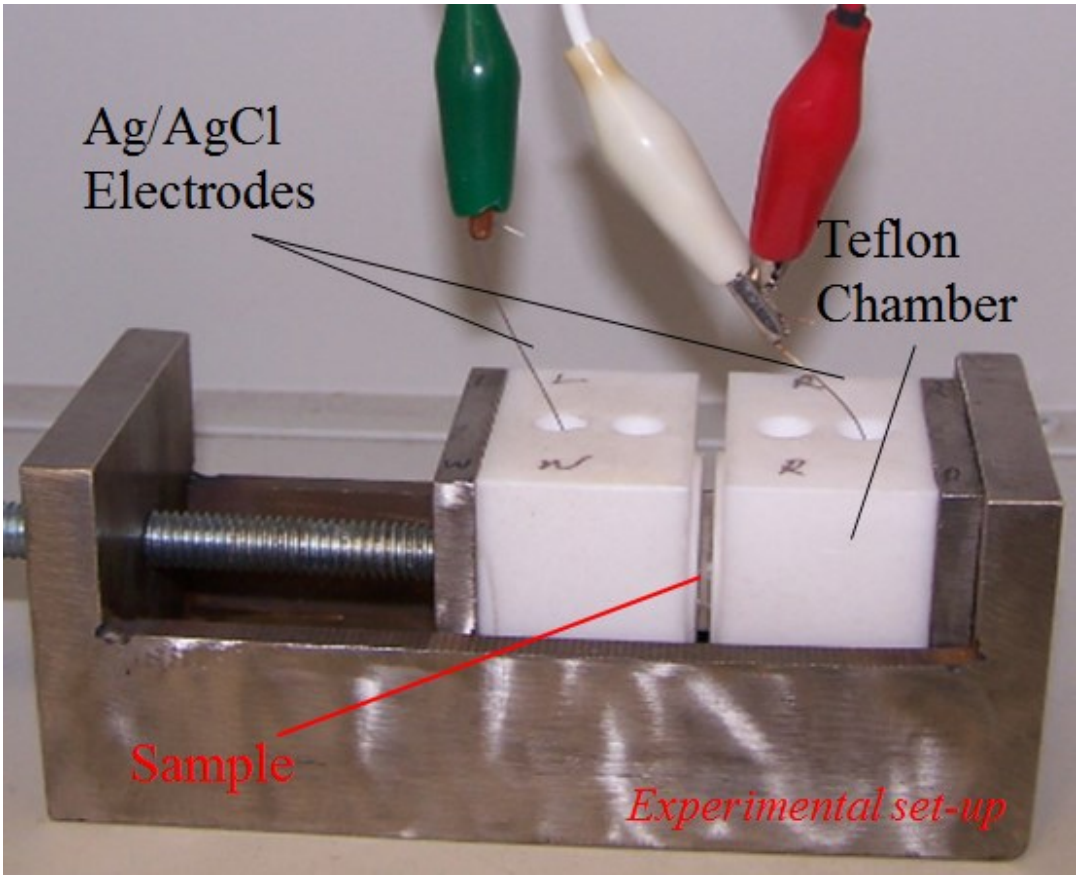

Figure 35. Disassembled Teflon chamber with gaskets and nanoporous sample.

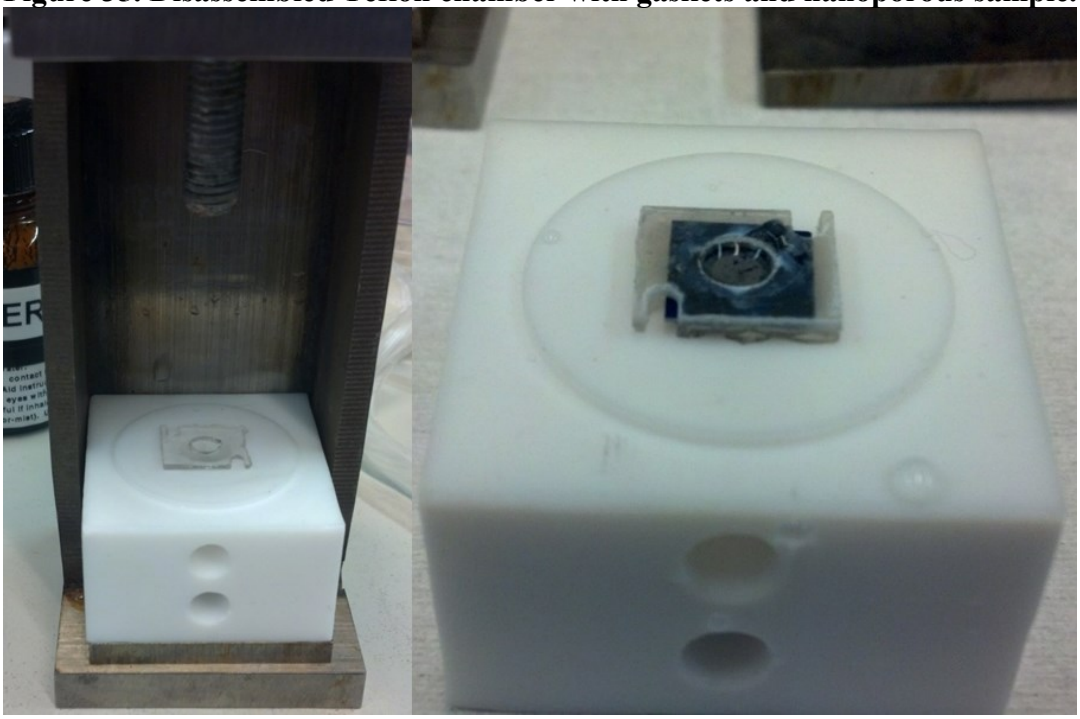

0.01M solutions of KCl, NaCl, and $CaCl_2$ solutions were transported across the membrane stack using both a fixed potential (I*t) and a cyclic potential (CV). These potentials were applied either from directly across the two PEDOT:PSS PH1000 layers on either side of the polycarbonate membrane (see Figure 36) or from Ag/AgCl electrodes 1.5mm from the membrane residing in each well (see Figure 37). The experiment was run at 2 volts as well as 4 volts. CV times were 300 seconds per cycle and fixed potential times (see Figure 38) were 400 seconds.

Figure 36. CV plots of double-sided PEDOT-PC-PEDOT pump with potential applied to the PEDOT layers.

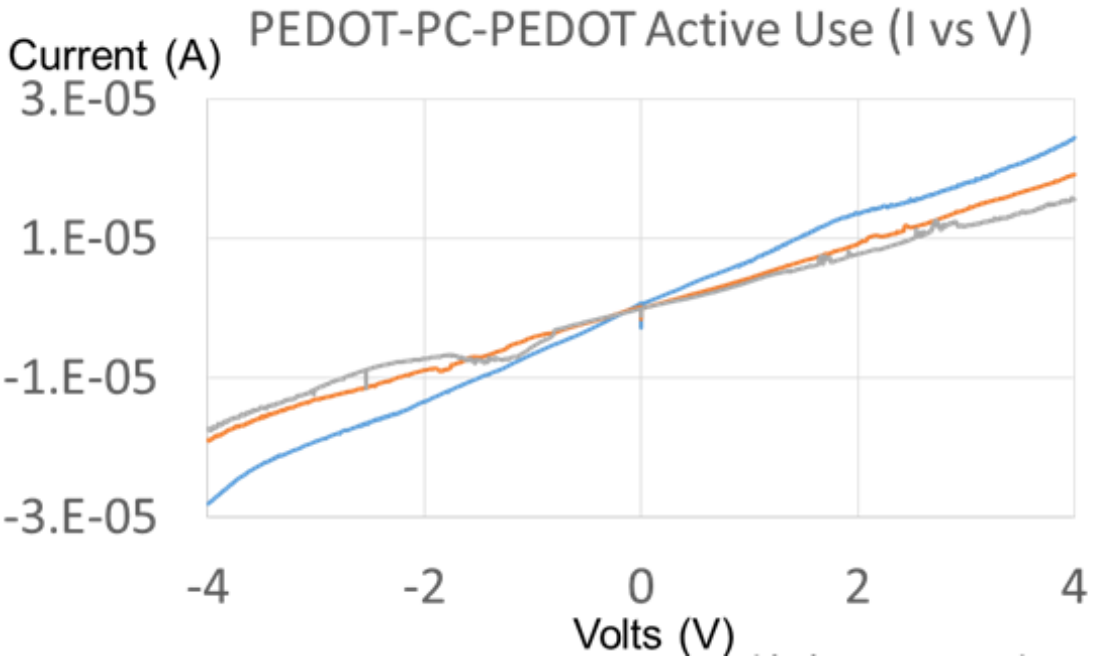

Figure 37. CV plots of double-sided PEDOT-PC-PEDOT pump with potential applied to the salt solution in the chambers via Ag/AgCl electrode.

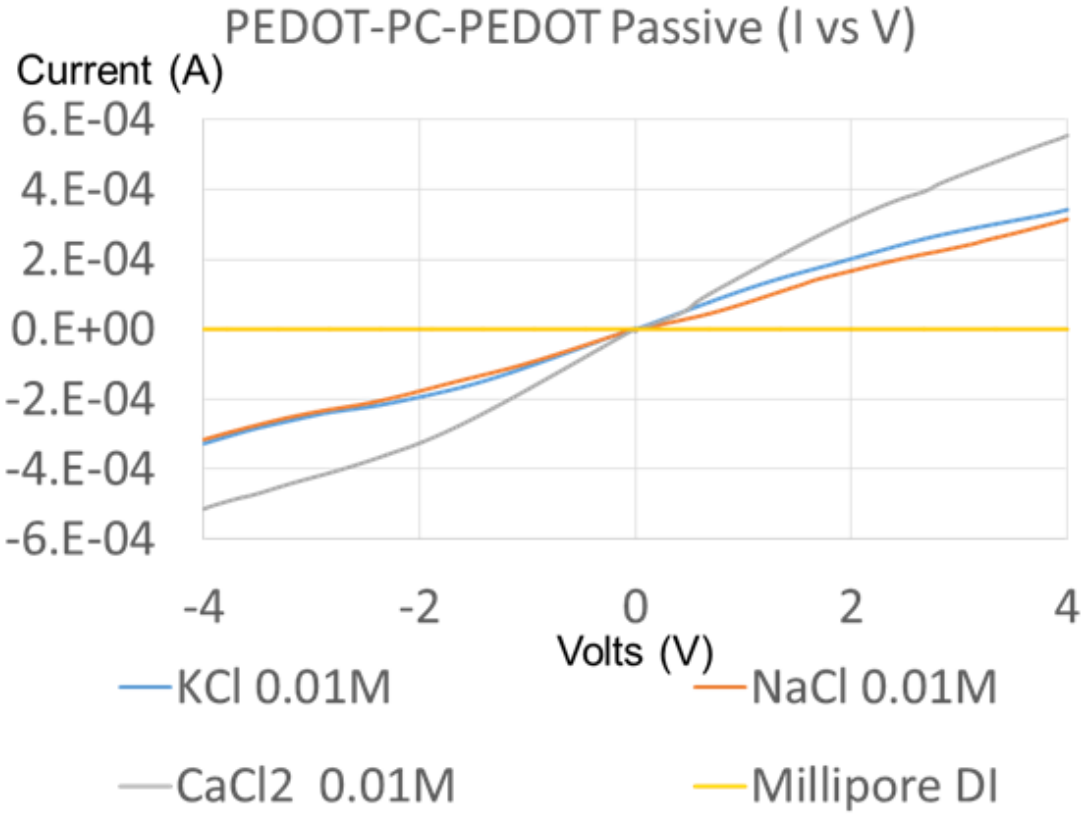

Figure 38. I(t) plots of double-sided PEDOT-PC-PEDOT pump with potential applied to the PEDOT layers.

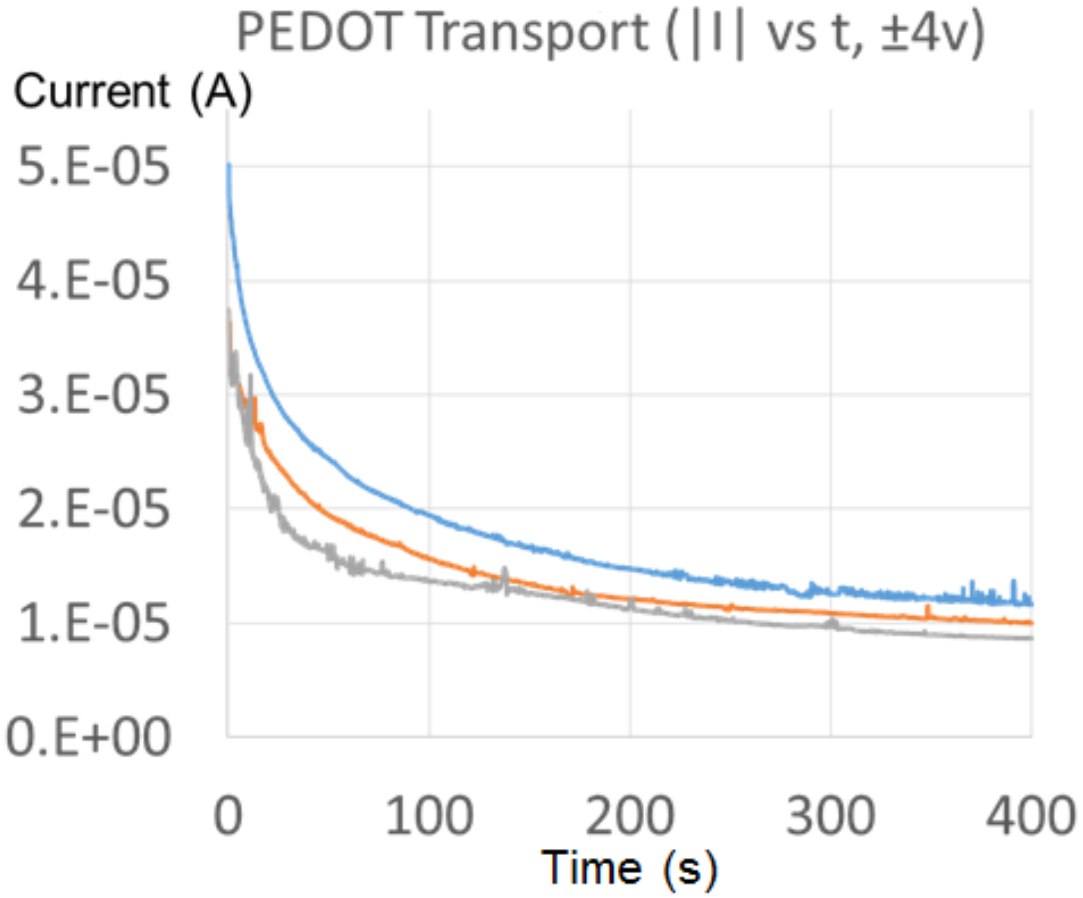

The CV measurements taken across the PEDOT:PSS layers indicate that the PEDOT layers are functioning in their transport of ions under applied voltage conditions. Additionally, these measurements show that the PEDOT:PSS on its own is not selective to NaCl, KCl, or $CaCl_2$. When voltage is applied across the PEDOT:PSS and the oxidation-reduction reaction drives transport, KCl is slightly enhanced in line with its higher mobility in water while $CaCl_2$ does not show a doubled current despite its two electron charge. This is likely because the transport is limited by the rate of the oxidation-reduction reaction within the PEDOT:PSS layers.

Under passive operation, when voltage is applied to electrodes within the wells the carriers must drift across both the PEDOT layers and internal gaps within the polycarbonate nanopores. In this case, the current is higher as the applied voltage is not diminished by contact resistance to the PEDOT:PSS layers and $CaCl_2$ has double the current of NaCl and KCl reflecting its two electron charge. If the PEDOT:PSS was not oxidizing and reducing to transport carriers in the first plot, it would mirror the curves in the second plot.

As stability with planar PEDOT:PSS devices was a major early challenge, extended timed current plots at a fixed voltage were taken. To maintain the PEDOT:PSS in a neural and non-depleted state, these measurements were taken at alternating fixed negative and positive voltages for 400 seconds in each direction per salt solution being investigated. The data was then converted to an absolute current value and the runs for each salt were averaged. These repeated measurements all show an initial decay before settling at a fixed current level. This implies that while there is an immediate impulse potentially associated with PEDOT:PSS directly over the nanopores, the transport rate eventually stabilizes. Furthermore, this repetitive extended experiment at 4 volts does not cause degradation, delamination, or hydration as these would have resulted in increasing curves rather than stable curves.

From these results, it is clear that nanometer thick layers of PEDOT:PSS can be spun on the fronts and backs of nanoporous membranes to produce double-sided ion pumps. Given this finding, the other component of a selective electrically gated ion pump, namely selectivity between cations, is the focus of the remainder of this

chapter. Additionally, due to the ease of processing PEDOT:PSS to make an electrically gated ion pump as described, the demonstrative investigations carried out using the anodized alumina nanoporous membranes produced using the developed fabrication scheme primarily focus on investigating chemistries for cation selectivity.

4. Polycarbonate Membranes with Crown Ether Functionality

Hydroxymethyl-18-crown-6 and hydroxymethyl-15-crown-5 were both functionalized onto track-etched polycarbonate membranes working from the carboxylic group available for attachment.

Once the functionalization was complete, the membrane was rinsed in ethanol to remove crowns that were not attached, then rinsed in deionized water. The membrane was carefully extracted from the solution and rolled flat between two PDMS gaskets with 5mm diameter openings as described earlier and placed in the two-well Teflon testing cell. Ag/AgCl electrodes were placed in each well as described earlier to apply voltage and record current measurements.

Both hydroxymethyl-18-crown-6 and hydroxymethyl-15-crown-5 were attached to track-etched polycarbonate porous membranes following the same functionalization method described above. Neither functionalization produced stable results that differed significantly from control samples of track-etched polycarbonate porous membranes. Additionally, subsequent investigations of the samples tested after different intermediate steps in the functionalization process, such as O2 plasma treatment and heating, showed temporary changes from the control similar to those that the functionalized membranes exhibited. From these investigations, the

conclusion is drawn that these monolayer functionalizations are either unsuccessful, unstable, or do not block a significant enough portion of the pores to produce a stable noticeable effect. These results limit the potential for further investigations of selective chemistries using polycarbonate track-etch pores.

Due to the fragile nature of the polycarbonate membranes, as well as the low compatibility with many solvents, these membranes are less useful than alumina based membranes. Additionally, it is not possible to easily lithographically pattern tracked etched polycarbonate membranes, making feasible multi-channel devices difficult to envision.

C. Investigations with Fabricated Nanoporous Membranes

Due to the stability of alumina as well as the nanoporous nature of the membranes developed, the alumina nanoporous membranes are an excellent tool for investigation of ion transport properties through materials under applied electrical fields. The silicon support structure makes these devices easy to handle, functionalize, and experiment with. Additionally, these nanoporous alumina membranes may also be useful as a scaffold for investigations of biological or biologically inspired organic membranes.

1. Attaching Chemistries to Nanoporous Alumina

In order to investigate ion transport using nanoporous alumina membranes, chemistries of interest needed to be integrated into the pores' volume, along the sides of the pores, or as a film across the surface of the membrane. Direct attachment to

the nanoporous membrane can occur immediately after fabrication or after post-fabrication treatment with ALD to grow alumina to narrow the diameter of the nanopores. If attached chemistries are significantly shorter than the radius of nanopores, hydration paths can exist that will present a considerable contribution to observed currents and will effectively diminish signals presented by the chemical under test.

2. Surface Functionalization of Nanoporous Alumina

Two primary routes have been used to attach molecules of interest to the alumina pore surface. The first of these methods is the direct attachment of molecules that contain triethoxysilane or trimethoxysilane terminations. As methoxy groups are slightly more reactive than ethoxy groups, trimethoxysilanes are preferred. However, both terminations are sufficient for the needed reaction. A variety of means exist to react a target molecule of interest with these termination groups, but these are outside the scope of this work. The other method is to terminate a molecule of interest with an OH bond and prepare the alumina surface with a molecule containing both an isocyanate group and a triethoxysilane or trimethoxysilane termination group. In this case, the attachment points off of the silane react with the alumina surface while the isocyanate reacts with the OH bond of the target molecule.

As both of these routes rely on the same ethoxysilane or methoxysilane terminations in order to react, the alumina surface can be prepared in the same manner for either route of functionalization. The nanoporous alumina array is activated using O_2 plasma for 5 minutes (100mW, 300mTorr O_2) and is then placed

in 30% reagent grade hydrogen peroxide for 30 minutes. Following this step, the nanoporous alumina array is dried on a hotplate or in a heated vacuum oven to remove all water content from the array before proceeding with the reaction. The plasma activation is used to clean the surface of organic material as well as break surface bonds, this in turn promotes the attachment of OH groups onto the surface of alumina when exposed to hydrogen peroxide. As ethoxysilane, methxoysilane, and isocyanate bonds are reactive to water, the drying step is necessary anytime an aqueous solution, such as hydrogen peroxide, is employed before functionalization. However, this is not required if the hydrogen peroxide step is skipped and the sample is plasma activated and immediately functionalized.

For other forms of alumina as well as some other oxide materials, this sort of preparation activity could be carried out using sulfuric peroxide, also known as Nanostrip (buffered form), or Piranha. However, the alumina phase and porosity generated by the anodization process make it an ill-advised process as membranes being prepared in this manner tend to be significantly degraded.

3. EthoxySilane- MethoxySilane- Direct Attachment

In the case of direct attachment, the terminated molecules of interest are generally too large to deposit and attach as a vapor. Therefore solution phase functionalization is the only possible route. Depending on one's intent, solutions anywhere from pure or neat material to micro-molar concentrations can be prepared. Hydrophobic or flexible linker molecules with single or double ended attachment points can be added to solutions to increase the hydrophobic nature of the product material, as they will

be co-deposited. Additionally, diluted HCl can be added to solutions to enhance the rate of the reaction, but this can lead to materials reacting in the solution phase rather than on the nonporous alumina surface.

Single monolayers of molecules can be attached using micro-molar concentrations in dry solvents that will not react with methoxy or ethoxy groups such as dry ethanol, dry methanol, dry DCM (dichlorometane), or Hexafluoroisopropanol. Samples should be placed in degassed vials of such solutions and the reaction must be allowed to proceed overnight without heating. After the reaction is completed, unattached molecules can be rinsed off by application of additional fresh, non-reactive solvents. Using ALD shrunken pores, this method can form pores with molecules of interest across the remaining pore diameter.

Thicker, non-monolayer films can be formed using higher concentrations of molecules of interest in solutions that are allowed to condense on the surface and into the nanopores or the alumina array. Using a vacuum oven, the solution is slowly heated up to 110C while under no more than 25 inHg vacuum pressure. Solvents under these low pressure conditions tend to easily wet the alumina nanopores facilitating the transport of the molecules for functionalization. As the solvent is removed by evaporation, thermal energy reacts with the ethoxysilane or methoxysilane bonds, calcinating them and forming a network from the alumina surface outward within the pore diameter and also across the alumina membrane surface. The formation of films, as well as monolayers, is possible as the ethoxysilane and methoxysilane bonds can react with themselves given proper

conditions. Ideally, the surface is reacted and additional molecules bond with the initial layer until the whole network is indirectly attached to the surface. The addition of H_2O can promote the formation of bonds between ethoysilane or methoxysilane groups similarly to the application of HCl to the prepared solution.

4. Isocyanate Linker Based Two Part Attachment

Using an isocyanate based linker molecule which contains ethoxysilane or methoxysilane bonds, such as (3-Isocyanatopropyl)triethoxysilane, is ideal for attachment of monolayers. This is because the OH bonds required to attach to isocyanate are not reactive with each other and because this reaction can be catalyzed. While the initial reaction of the isocyanate containing molecule could be carried out in a solution phase, the preferred method is to run the reaction in the vapor phase. Due to the small size of the linker molecules involved, vapor deposition is easily realized with a vacuum oven. As the transport and reaction kinetics are more favorable for the reaction than in the solution phase, this is particularly preferred to densely react linkers with the internal surfaces of the alumina nanopores. The use of these linkers has the additional benefit that OH terminated forms of molecules of interest will generally be smaller than triethoxysilane or trimethoxysilane terminated forms such that the solution phase transport of these into nanopores should be enhanced.

To vapor deposit and react isocyanate containing ethoxysilanes and methoxysilanes, it is ideal that a small volume container with a chimney be used with a vacuum oven. This maximizes the vapor that is transported to the alumina

nanoporous film being functionalized. The samples that are to be functionalized are placed in a jig that suspends them above the bottom of the closed container. Critical to the design of the jig is the concept that the window which contains the nanoporous membrane is exposed from both sides and that the jig only provide support through contact with surfaces away from the membrane and window. Several generations of increasingly refined jigs have been produced, with the latest of these a custom 3D printed jig (see Figure 39) made from photo-patternable PMMA resin using a Formlabs Form 1 printer.

Figure 39. Model of 3D printed jig developed to assist in vapor deposition.

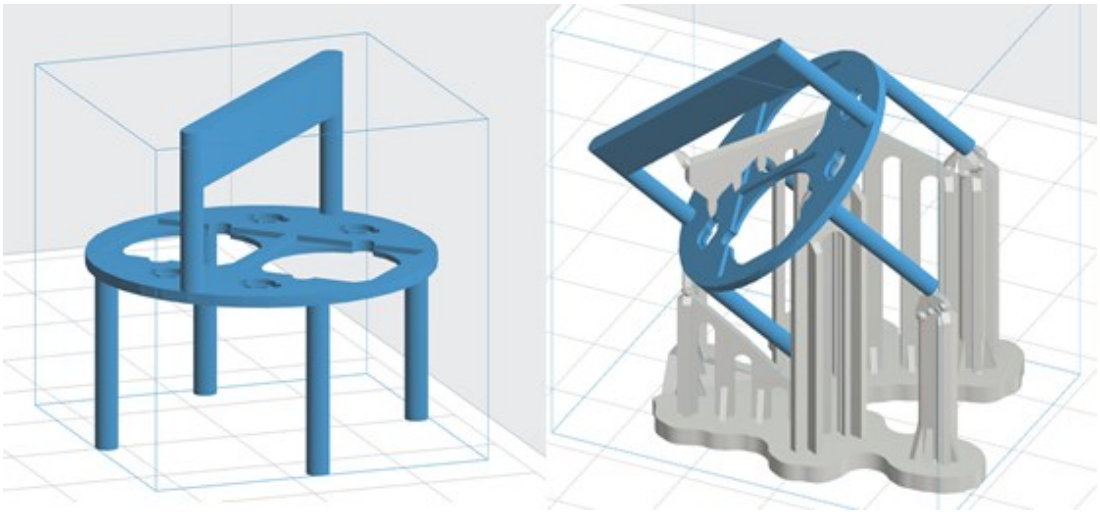

In order to vapor functionalize a linker molecule to samples using this method, a 100 uL to 200 uL volume of the linker molecule is added to the bottom of the 50 ml jar just after the jig with a prepared sample loaded on it is placed in the jar. The jar is immediately closed, except for the chimney, and placed in the vacuum oven. The oven is pumped and purged with N2 twice and is left pumping down at 50C for at least 30 minutes, while the vapor is physically adsorbed on the surfaces of the

nanoporous alumina. The oven is then ramped to 110C and left at this temperature for one hour to drive the chemical calcination reaction of the bond on the surface of the alumina, and then ramped back down to room temperate. Before extraction of the reaction container and the samples, the system is again pumped and purged twice with N2 to clear remaining unbound excess linker molecules.

After the attachment of the linker molecule, the OH terminated molecule of interest should quickly be attached. Due to the reactivity of the isocyanate group with water, leaving these samples in anything other than a completely dry environment will lead to the loss of reactive groups capable of bonding to the target OH terminated molecule of interest. Before the second reaction, the samples should be washed in dry solvent not containing OH bonds such as DCM. Following this, the samples can be transported into a prepared solution generally containing millimolar concentrations of the OH terminated molecule of interest in a dry solvent free of OH bonds. The second reaction should be allowed to proceed for 24 hours and can be enhanced with the addition of a catalytic amount of tributyltin. The attachment chemistries for both the direct one step method as well as the vapor deposition based two step method are shown (see Figure 40).

Figure 40. Ethoxysilane based methods for crown ether attachment.

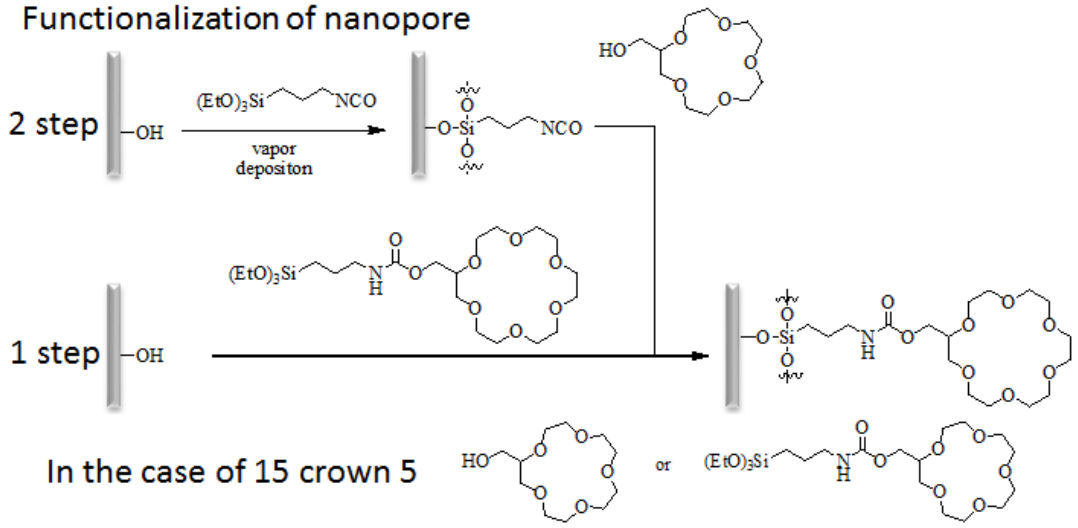

5. Atom-Transfer Radical-Polymerization Based Attachment

One additional method that was examined for crown ether attachment to alumina nanoporous membranes was ATRP (atom-transfer radical-polymerization) based crown polymer attachment (see Figure 41). In this method, a repeated monomer containing a desired crown can be polymerized from the attachment surface inward toward the center of the nanopore. This technique relies on the same basic ethoxysilane attachment mechanism, but attaches an aminopropyl group which is then reacted to have a bromine termination. This termination can then be used in a copper based radical-polymerization reaction where the bromine is transferred to the end of each new crown ether monomer that attaches. This reaction is continued until either the monomer is depleted or the pores are filled.

Figure 41. Atom-transfer radical-polymerization based crown ether

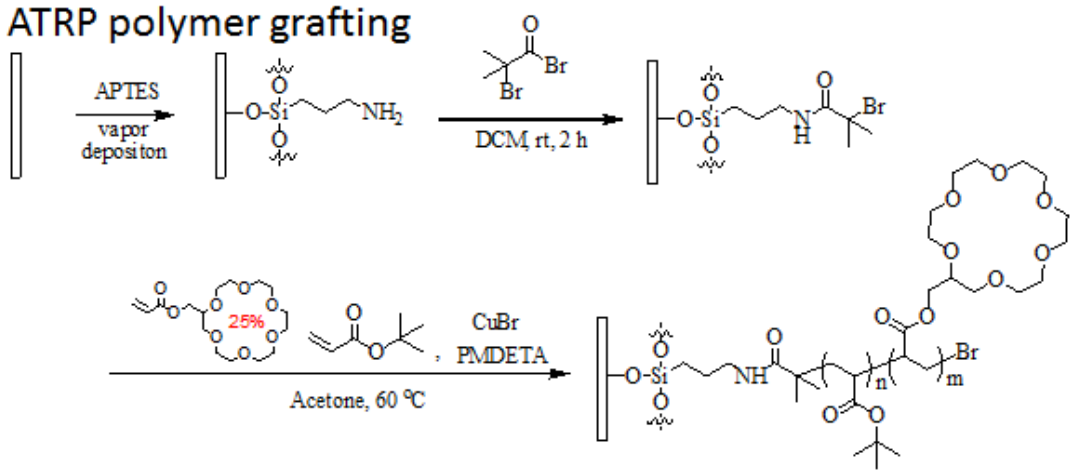

6. Characterization of Ethoxysilane and Methoxysilane Attachments

To ensure that attachment methods using ethoxysilane and methoxysilane terminated molecules did a good job of functionalizing the alumina surfaces in the nanoporous alumina arrays, a characterization experiment was carried out on a number of different types of materials using the same protocols. PDMS, alumina, silicon dioxide, and silicon nitride films were reacted following the above described vapor functionalization method, then properly rinsed and characterized. To provide further evidence of successful functionalization, as well as the intact functionality of the isocyanate groups, an OH and chlorine containing molecule was also reacted with some samples before the final rinse to provide an additional signal. XPS (X-ray photoelectron spectroscopy) was used to probe the surface of the films and determine elemental content as well as the presence of bonds associated with the attached isocyanate. This technique excites electrons using a focused beam of X-rays of known energy and then collects and analyzes the energies of emitted photos,

allowing the binding energies of the source electrons in the surface material to be determined. This includes those valence electrons contributing to bonds between atoms. As a result, both elemental information as well as bond information can be extracted using XPS.

XPS measurement scans on alumina samples as well as glass and silicon nitride all provide low carbon signals. Additionally, alumina and glass both also featured control measurements with low nitrogen peaks. By vapor functionalizing 3-isocyanatepropyltriethoxysilane on these three materials, the ethoxysilane attachment routes for both the direct and two step vapor phase attachment chemistries were confirmed. Lower carbon content, as well as fewer C-O, C-N, and N=C=O peaks in the cases of glass and silicon nitride samples suggest that alumina is better able to react with and attach to using ethoxysilane chemistry. In the case of vapor functionalized alumina, (see Figure 42) significant carbon and nitrogen peaks are present which were not visible in the alumina control sample. Additionally, after fitting the bond energies that form the broadened C1s peak, (see Figure 43) the characteristic N=C=O peak from the now attached isocyanate is visible. Solution reactions of OH terminated chlorine containing molecules that were carried out after functionalization provided evidence that the attached isocyanates were able to react with hydroxides. This reaction effectively attached the chlorines to the sidewall via the attached ethoxysilane linker molecules and provided a good marker to confirm attachment as no other traces of chlorine were present in any samples. The results provide evidence that both functionalization routes are compatible with alumina

surfaces.

Figure 42. Wide scan of 3-isocyanatepropyltriethoxysilane functionalized

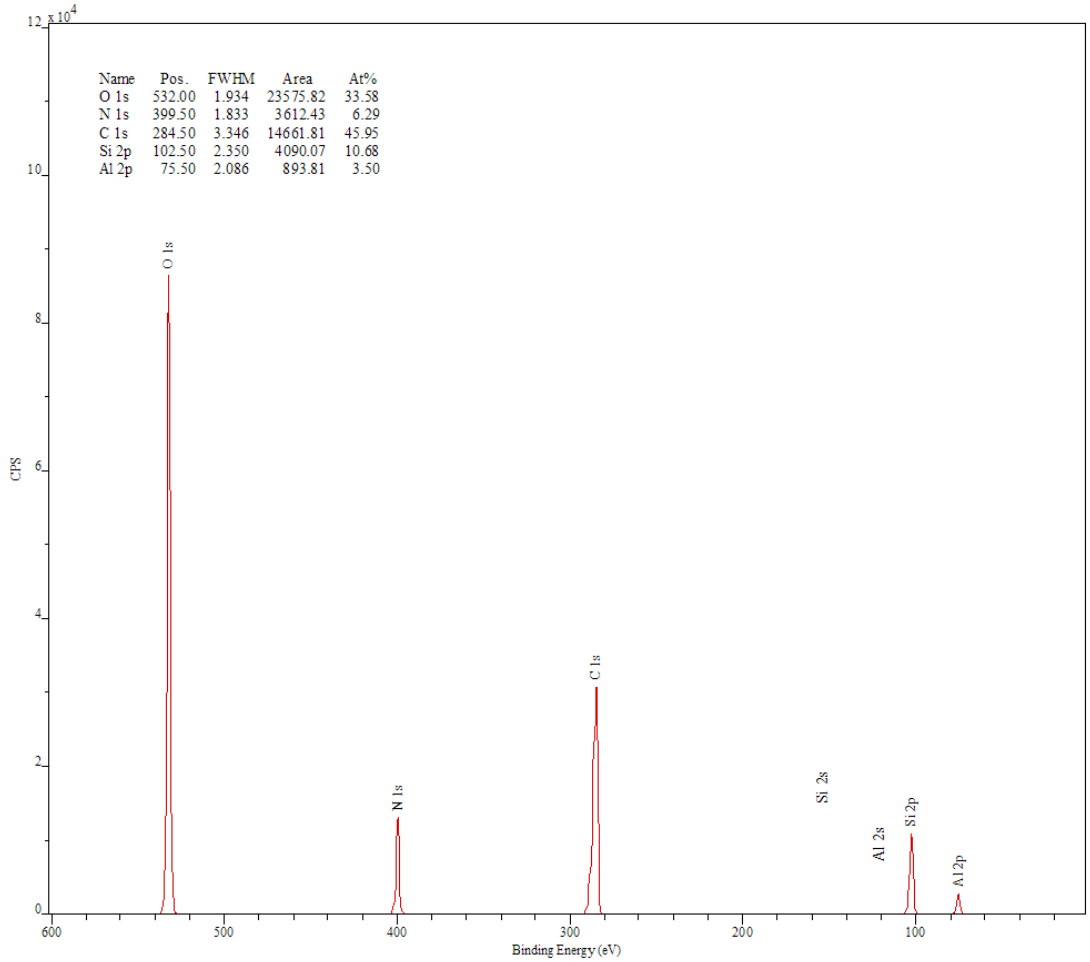

Figure 43. Narrow C 1s scan of 3-isocyanatepropyltriethoxysilane on alumina.

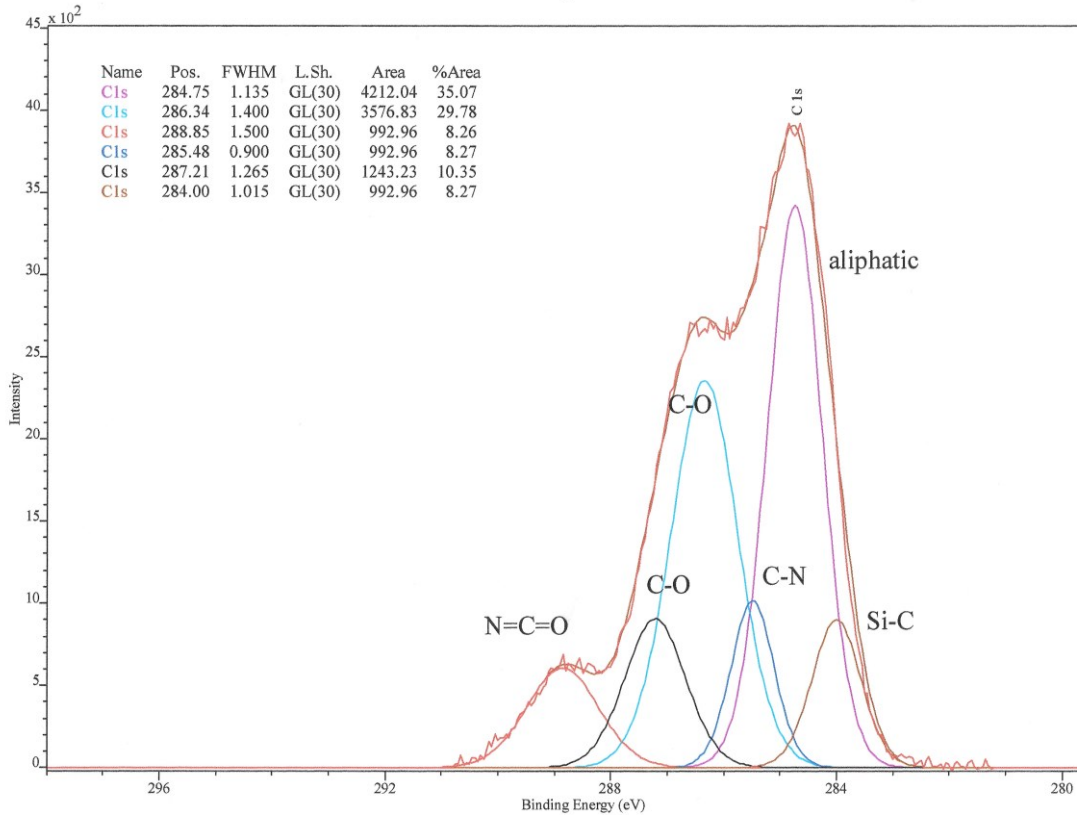

7. Trichlorosilane Attachment Chemistry

Chlorosilane attachment chemistry is often used in literature for attachment of molecules to silica or alumina surfaces. Chlorosilane based chemistry is at the heart of the reaction that attaches FDTS to silicon in order to reduce adhesion and stiction as mentioned in regard to the preparation of pillar molds. Unfortunately, the same strong reactivity which renders chlorosilanes useful also makes it difficult to prepare and maintain in an unreacted state. As the molecules used in this work were reacted to form desired terminations or entirely synthesized from obtained commercial precursors, the lab facilities available did not support the stable preparation, storage, or use of chlorosilanes. The use of chlorosilane based attachments would be a

potential area for future work in demonstrating and improving the utility of nanoporous alumina arrays.

8. Chemical Modification via Attachment Chemistries

Using the attachment methodology described, the robust alumina nanopore membrane can be reacted to host many different kinds of functionality to produce desired hydrophobicity, pH sensitivity, or selective chemical binding. The possible functionality that can be added is only limited by the range of molecules that can be modified to work with one of the above attachment mechanisms.

9. Anodized Alumina Pore Constrained Templated Meso-Silica

While most often examined for its highly porous structure when produced as powder, templated meso-silica compounds can be combined with the nanoporous alumina membranes to add additional levels of functionality[5-7]. Meso-silica refers to a series of compounds primarily produced by reacting TEOS (Tetraethyl orthosilicate) with deionized water, a solvent such as ethanol, HCl, and a surfactant. Based on the evaporation rates of the solution, condensation of silica occurs slowly and in a templated fashion due to interaction with the surfactant molecules. Depending on the concentrations and surfactants used, a large and interesting array of ordered porous films can be produced. Porosity is developed after film is condensed, and the surfactant is generally removed by combustion under 500C+ conditions. Like nanoporous alumina films, these meso-porous silica materials have large internal surface areas and can be functionalized using methods similar to those

already discussed for alumina. Additionally, as meso-silica is condensed from a solution, it is possible to directly incorporate different types of functional groups by adding them to the solution before it is condensed.

Commercially produced porous anodized alumina disks with pore diameters of 60 microns to 200 nm have been used to constrain condensing solutions forming meso-silica. The sidewall constraints have shown significant effects on the self-assembly of surfactant and silica molecules, leading to the formation of ordered vertical nano pores within the condensed meso-silica.

To investigate the possible combination of meso-silica within and across the fabricated nonporous alumina membranes produced, several meso-silica experiments were made focusing on co-condensation of functional groups. These included comparisons with commercial anodized alumina porous products known as Whatman Anodisc.

To form the silica–surfactant nanocomposite precursor solution, a mixture of ethanol (0.16 mL), TEOS (0.24 g), and 21 uL of HCl aqueous solution (2.8 mM) was refluxed at 60 °C for 90 min. After this step was completed, ethanol (0.33 mL), 84 ul of HCl solution (55 mM), and CTAB (30 g) were added to the refluxed solution, which was stirred for 30 min. This process produced the precursor solution, which was then used immediately due to the reactive species present.

Trimethoxysilane terminated 18-Crown-6 was produced and added to a meso-silica precursor solution, which was prepared such that the mole fraction of the crown was 5% of the TEOS in the solution. The solution was made with TEOS,

ethanol, DI, HCl, and the cationic surfactant CTAB (Cetrimonium bromide). After the solution was prepared, it was applied to the nonporous alumina membranes and the other samples via their top surfaces while very light vacuum was applied to the region below the sample. This was done to ensure that the meso-silica precursor solution was drawn into the nanopore and that they were wetted. After 4 25 uL drops of precursor were deposited, the vacuum was cut and 4 more drops were added to the top surface. The samples were left to condense in enclosed environments with additional vials of ethanol to slow the evaporation and condensation process.

To test different preparation and condensation conditions, a soluble potassium salt was employed to potentially assist with scaffolding arrangement of the crowns and solution. These were condensed both at standard ambient conditions with a supply of excess ethanol and under light vacuum (10 inHg) at an elevated temperature of 60C with a supply of excess ethanol. After the samples were allowed to condense for 15 hours, the samples were heated to remove the CTAB. Unfortunately, as the crown functionality was already condensed, it was impossible to expose the devices to 500C+ temperatures, as this would degrade the crown. Instead, the samples were baked under vacuum at 150C for 6 hours and then thoroughly rinsed in fresh ethanol to help remove the CTAB.

Commercial anodized alumina porous membranes are structurally fragile and face difficulties being lithographically processed. Anodized alumina integrated into a silicon platform, such as in the fabrication scheme discussed, could be manufactured to specific pore sizes to best couple with the addition of functionally enhanced meso-

silica to produce specialized functionalities that could then be lithographically processed.

D. Demonstration of Fabricated Nanoporous Membranes as Investigative Instruments

Using the nanoporous alumina membrane fabrication scheme, significant numbers of nanoporous arrays were manufactured. These were prepared with a variety of chemistries to demonstrate the investigative uses of the fabricated devices. In particular, these nanoporous arrays were treated with crown ether containing molecules and investigations relating to the enhancement of the selectivity of specific cations were carried out. A few of these are presented here showing clear cation selectivity across the nanoporous membranes while under an applied electric field. Each of these investigations used 0.01M buffered salt solutions and centered Ag/AgCl electrodes as discussed earlier.

1. Investigation of Triethoxysilane Terminated 15-Crown-5

While many different experiments with crowns were investigated, the most significant series entailed the use of triethoxysilane terminated crown eithers. These materials were deposited in a neat condition and allowed to penetrate the prepared alumina surface. The triethoxysilane groups allowed the crowns to both attach to the nonporous alumina sidewalls, and also react with each other to form a network. The first investigation of such a film that was both in the nanopores and covering the surface focused on 15-Crown-5 which was expected to be selective towards sodium.

By recording reparative cyclic voltammetry measurements for both KCl and NaCl, (see Figure 44) a strong variation in selectivity was noted with respect to applied potential. With the backside well held 1 volt above the front side well, sodium is selectivity preferential transported. In this case, sodium cations are driven through the crown filled nanopores and out the crown film. However, when the voltage is applied in the opposite direction so that cations are driven into the film and then into the nanopores below, the current ratio approaches the expected ratio for diffusion in water. Additionally, for some small voltages around 500mV in this direction, current ratios are preferentially selective to potassium cations. While only preliminary, these results suggest that there is a mechanism at work directing the way in which the population of 15-crown-5 molecules interact in the nanopores and within the thin film above them.

Figure 44. Current ratio of KCl to NaCl showing selectivity versus voltage.

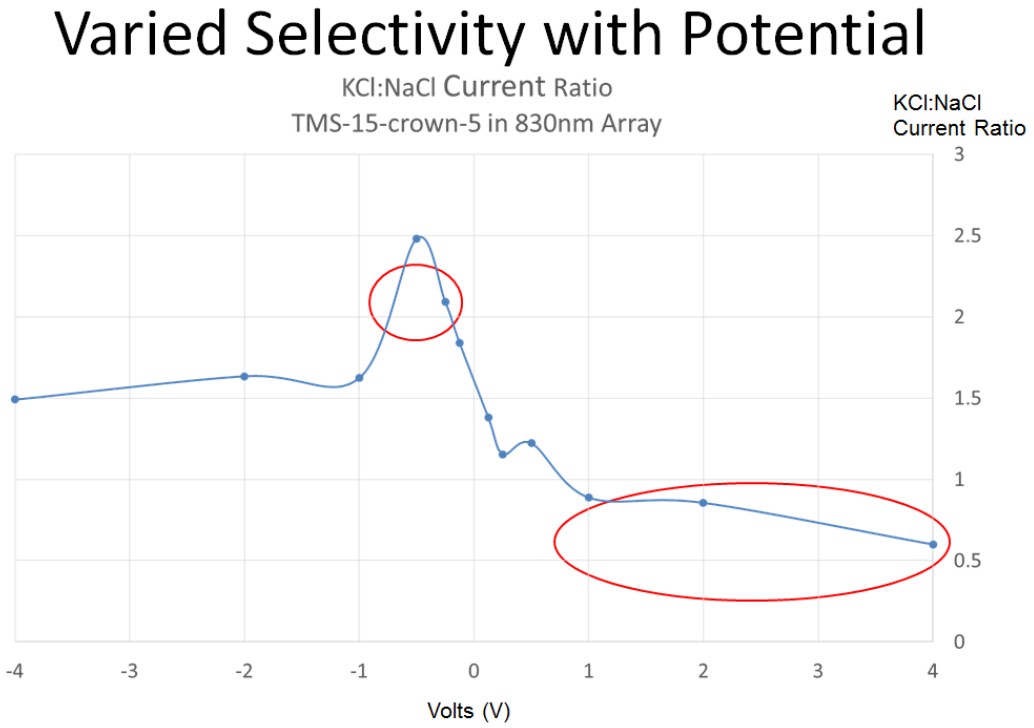

2. Investigation of Triethoxysilane Terminated 18-Crown-6

Following the interesting results of the neat triethoxysilane terminated 15-crown-5 experiments, the same procedure was used with 18-crown-6 molecules. In this case, positive voltages applied to the backside of the array with respect to the front side result in almost one to one current transport, (see Figure 45) which does not reflect the difference in mobility between potassium and sodium. In this direction, the cations should be transported from the backside into the nanopores and then out through the thin crown film layer. This makes the transport area that contains crowns and which can potentially interact with cations go from a small area in the nanopores to a large area in the film. Conversely, when the field is applied so that cations are driven into the film, through the crown containing nanpores, and then out the

backside of the array, the device becomes highly selective towards the preferential selective transport of sodium. Upon further analysis, it appears that rather than facilitating potassium transport under these applied field conditions, the 18-crown-6 molecules inhibit potassium while allowing the normal current of sodium to be transported. It appears that in this configuration perhaps some form of partial hydration facilitates one to one transport when the field is applied in one direction, but a conformation change occurs which traps and slows potassium when the polarity of the field is reversed. As only a unidirectional selectivity would be required for the envisioned gated selective ion pump motivating this work, a behavior such as this one but which was significantly inhibitory towards sodium rather than potassium would be completely functional for the design.

Figure 45. Unidirectional selectivity between KCl and NaCl with 18-crown-6

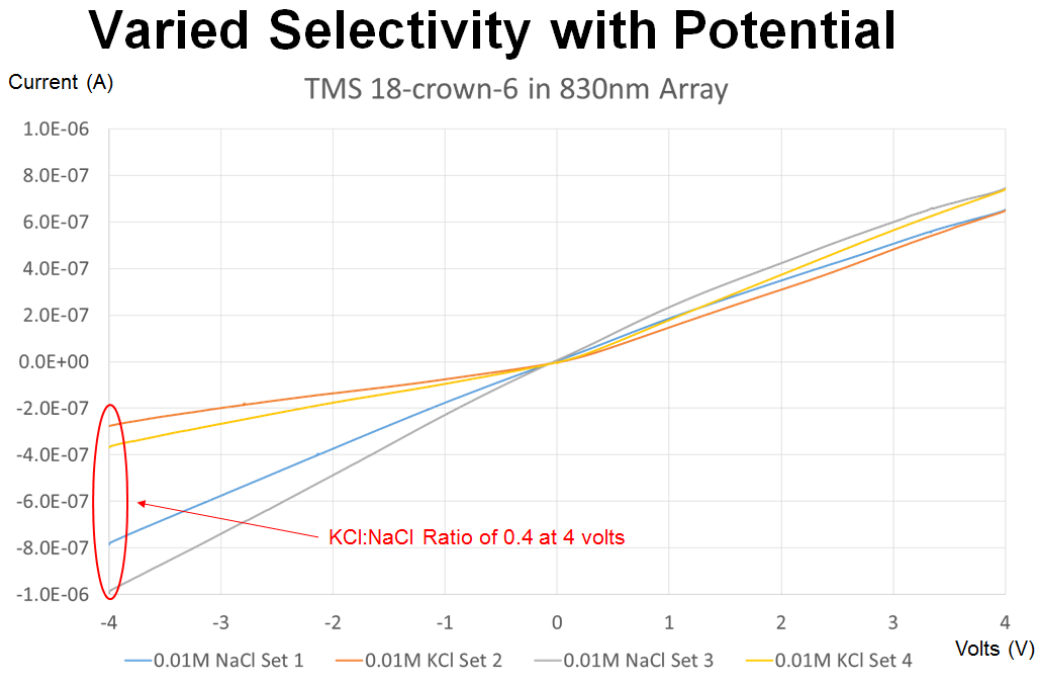

3. Selective Hydration Effects of Triethoxysilane Terminated 18-Crown-6

Following the observation of unidirectional selectivity favoring sodium transport in the triethoxysilane terminated 18-crown-6 experiment, additional investigations were carried out on the same sample. A series of current plots with fixed voltage steps was measured (see Figure 46). This time consuming testing method was used to attempt to determine exactly what the observed unidirectional selective behavior was and what it could be caused by. Using this method, voltages were fixed for hundreds of seconds at -0.5v, -1v, -2v, 0.5v, 1v, 2v, allowing a better view of the steady state behavior at each applied voltage. The whole experiment, which already included four repetitions in each measurement sequence, was then run multiple times for both KCl and NaCl in order to check stability. While the current stayed very stable and non-selective when the voltages were positive, with cations moving towards the front side of the array from the backside, the results in the other direction varied significantly. The potassium measurements in the negative direction, with cations heading towards the backside of the device, remained at a constant current level. Meanwhile the three NaCl measurements trended towards higher and higher currents. Disassembly of the sample initially revealed a pristine film of crown material across the surface. However, as soon as the small amount of moisture remaining on the array surface evaporated, the whole area which had been exposed by the PDMS gasket to solution during the testing regime immediately began to pull away from itself and crack (see Figure 47). This occurrence further validates the hypothesis that hydration as well as voltage-directed realignment of the crown material is playing a major role in the

observed selective behaviors. It is worth noting that before conducting these experiments, the functionalized and reacted film was crystal clear without any sign of stress or defects. Thus, the application of voltage, salts, and hydration must be directing the movements of the crown molecules enough that the reorganized material pulls itself apart when slightly dehydrated.

Figure 46. Multi step potential measurements of KCl and NaCl.

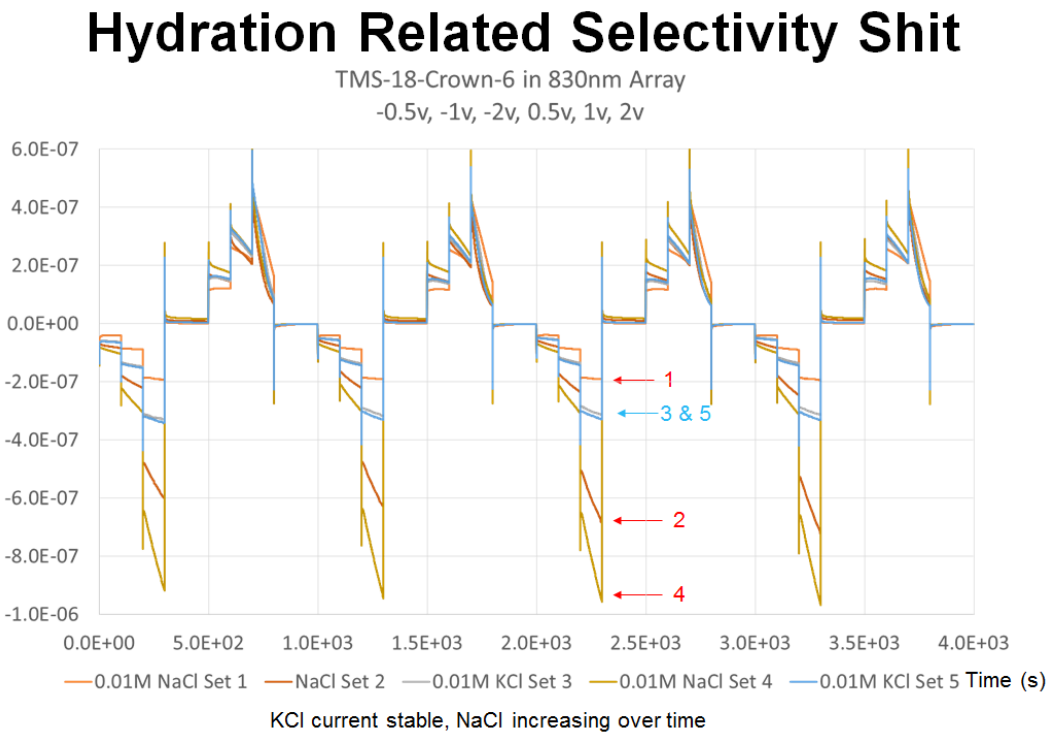

Figure 47. Cracking in TMS-18-c-6 surface film upon re-exposure to air.

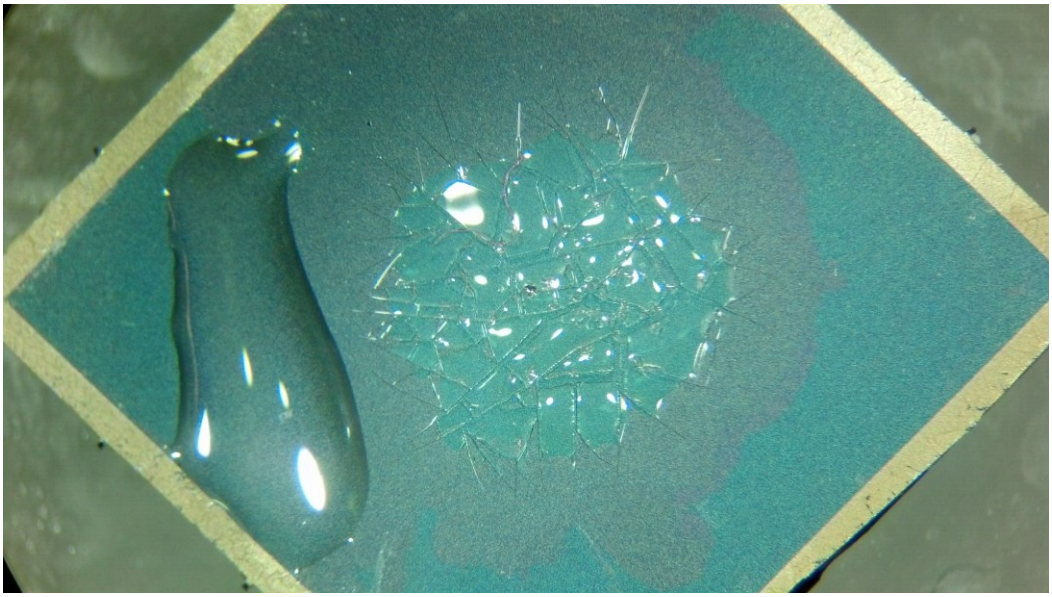

4. Anodized Alumina Pore Constrained Templated Meso-Silica 18-Crown-6 Experiment

Following the protocol described earlier, a co-mixed meso-silica precursor solution was condensed in and across a prepared nanoporous alumina membrane to demonstrate the functionality of the combination of the two techniques. The resulting device showed a similar one to one and unidirectional selectivity result to those in the previous case. However, the voltage polarity under which these two phenomena occurred was reversed and the selective region was preferentially selective to potassium instead of inhibitory towards it (see Figure 48). Additionally, the inhibitory selectivity towards sodium at positive voltages (see Figure 49) and specifically at 500 mV produces the largest preferential selective ratio towards potassium of any among all the stable experiments that were measured.

Figure 48. Cracking in TMS-18-c-6 surface film upon re-exposure to air.

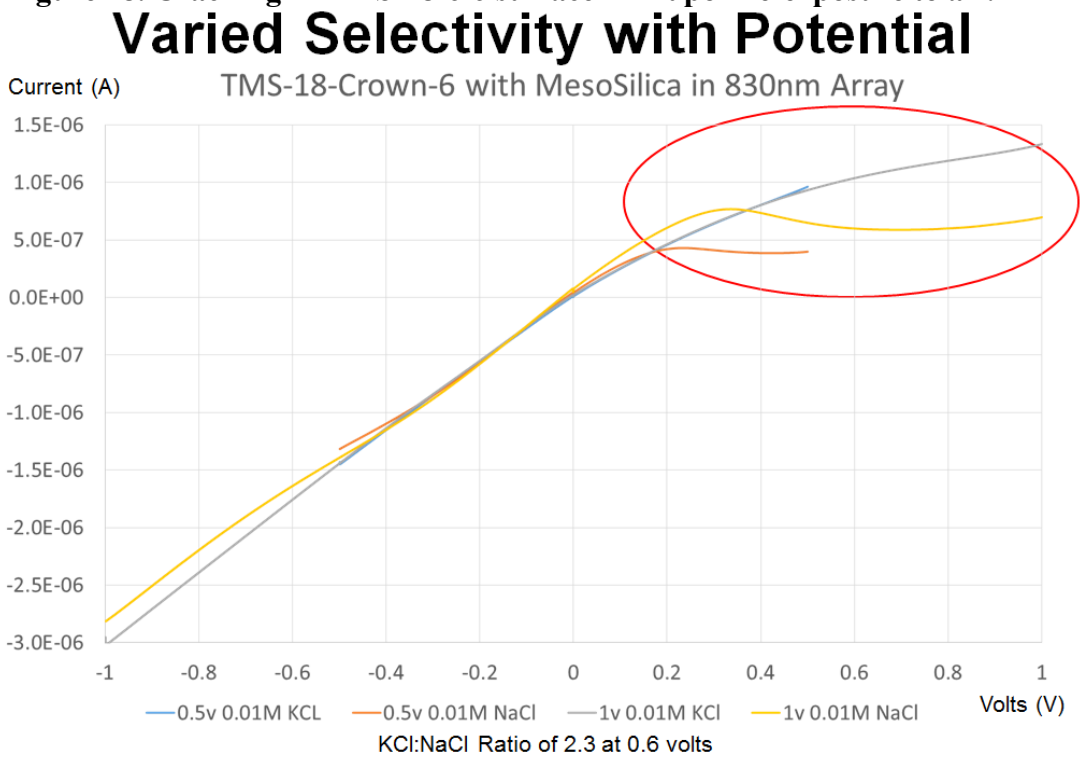

Figure 49. Cracking in TMS-18-c-6 surface film upon re-exposure to air.

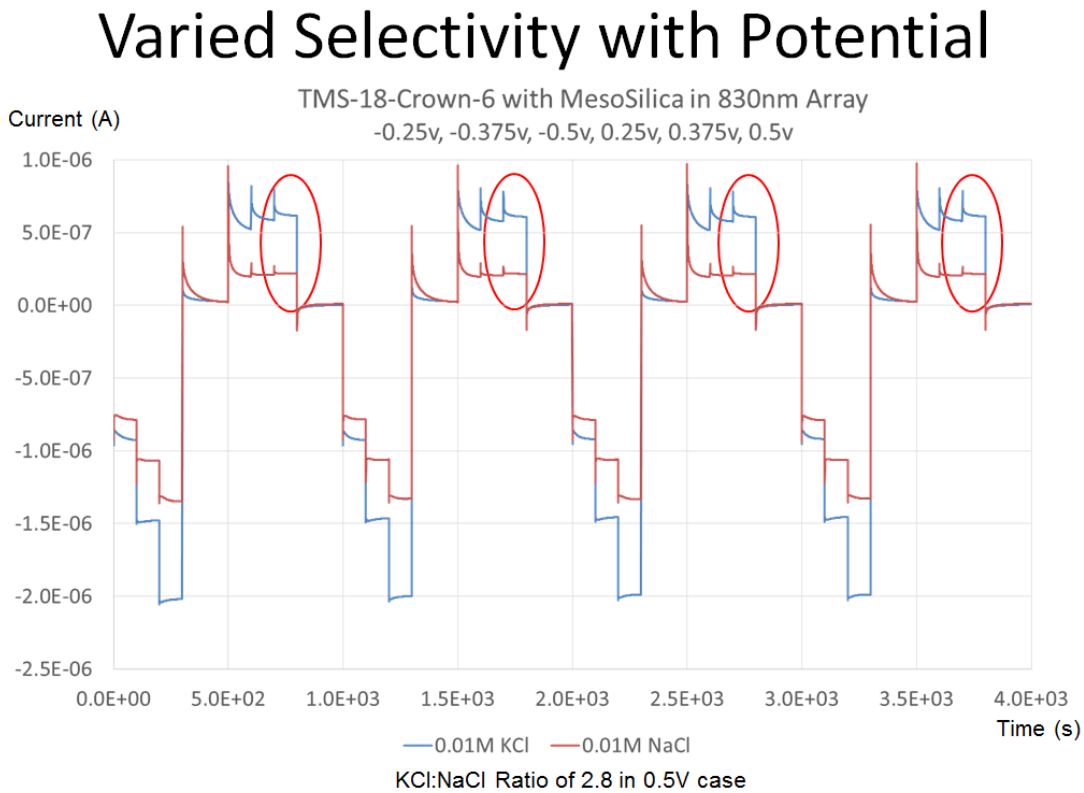

The difference between the behavior of the pure triethoxysilane terminated crown material and the 5% triethoxysilane terminated crown material in meso-silica is assumed to originate in the structural differences between the two materials. Hydration should not be impactful to the structurally stable meso-silica. Additionally, the change in behaviors may be contributed to by the self-ordering process that forms the meso-silica pores. These pores may be capable of templating along the alumina nanopores to form their own linear channels within the alumina nanopore film, but the material that reacts and forms meso-silica on the surface of the nanoporous alumina film may be very disordered. This could mean that it would be significantly easier for cations to travel into the bottom of the nanoporous alumina film rather than traveling in through the top disordered meso-silica surface.

5. Trends in Triethoxysilane Terminated Crown Ethers

The nanoscopic geometry of the alumina nanopores produced using the nanoporous alumina fabrication scheme enables some interesting field dependent selective transport behaviors. These behaviors are very different from the standard models of crown cation interactions that do not involve applied fields. As selectivity has been shown to vary with applied potential amplitude as well as direction with respect to the pore and crown film geometry, many different selective cation transport schemes could be developed to transport or concentrate a particular cation using only changes to the applied potential. Often devices with much simpler selective behaviors have to rely on conformational changes that occur by switching

pH, a condition that is not nearly as easy to change as voltage supplied across a pair of electrodes.

E. Single Nanopore Studies

Studies of single nanopores can also be used in transport investigations. While many methods of forming single nanopores, such as TEM milling, are expensive they can provide benefits complimentary to the benefits of nanoporous alumina membranes. While nonporous arrays can transport and provide similar functionality to nanopores, the huge population of nanopores in the case of a nanoprous film makes it much better at recording at low concentrations of species. Whereas a single nanopore might require a mole solution of a salt to attain measurable currents, a nanoporous film could operate at much lower salt molarities due to the parallel transport across the population of nanopores involved. For the most sensitive of studies, single nanopores are excellent tools for gating or translocation events that would be impossible to distinguish among a population of parallel pores, but that can be observed in a single nanopore.

1. Single Nanopore Investigation of Triethoxysilane Terminated 15-Crown-5

An investigation was carried out using triethoxysilane terminated 15-crown-5 and a TEM drilled nanopore in a silicon nitride / alumina / silicon nitride / alumina membrane. The exact membrane thicknesses were 15nm Si_3N_4 / 15nm Al_2O_3 / 15nm Si_3N_4 / 10nm Al_2O_3. As the membrane was formed using a Bosch etch, the bottom

alumina layer was used as a hard stop for the etch as it was completed. By burying the alumina, the top surface of the etch was left less reactive to ethoxysilane attachment. The drilled membrane was treated in Nanostrip (buffered sulfuric peroxide) for 15 minutes at 60C and then moved into a deionized water bath to remove the Nanostrip. Following this, the membrane dried and was mounted to aligned PDMS gaskets and placed in a Teflon jig. The sample was wetted in ethanol for 10 minutes while under vacuum desiccation. The jig was then set on top of a reservoir of dry ethanol that formed the bottom solution well, and the void inside the top of the jig was filled with dry ethanol to form the top solution well. The assembly was transported to an oven and heated to 50C with the top well sealed with PDMS to prevent evaporation. Once the solutions came to temperature, the jig was quickly extracted and a 5m molar solution of triethoxysilane terminated 15-crown-5 in dry ethanol was used to replace almost the entire volume of the upper well. It was then re-covered with PDMS and returned to the oven. Diffusion, as well as the concentration gradient, drove the crown through the nanopore and into the larger bottom well, while the silicon nitride on the top surface did not readily allow attachment of the crown. In combination, these two effects ensured that a significant amount of crown was transported across the membrane and had the opportunity to react with the exposed and activated internal alumina surface of the nanopore. The low concentration of crown involved ensured that the film that attached would only consist of a single monolayer and that a bulk film could not form. After 1 hour, the

jig was extracted and the solution in the wells was exchanged for fresh ethanol and then re-exchanged for deionized water.

In order to examine the transport properties of the crown 1 Molar Tris-buffered salt solutions of KCl, NaCl, and $CaCl_2$ at 7.6pH were employed. Measurements of 5 minutes each were taken at 50 mV increments from 600 mV to -600 mV and then the recording process repeated 3 times each. While translocation or gating events appeared in all the data plots (see Figure 50, Figure 51 and Figure 52) that would not easily be observed individually in a many-pore system, no other trends appeared that are absent in the many-pore system. Similarly, the shape of data seen in nanoporous alumina experiments corresponded to the events and non-linear conductivities that are observed to occur after several hundred mV are applied in either direction.

Figure 50. Single nanopore with 1M $CaCl_2$ with 600 to -600 mV fixed scans.

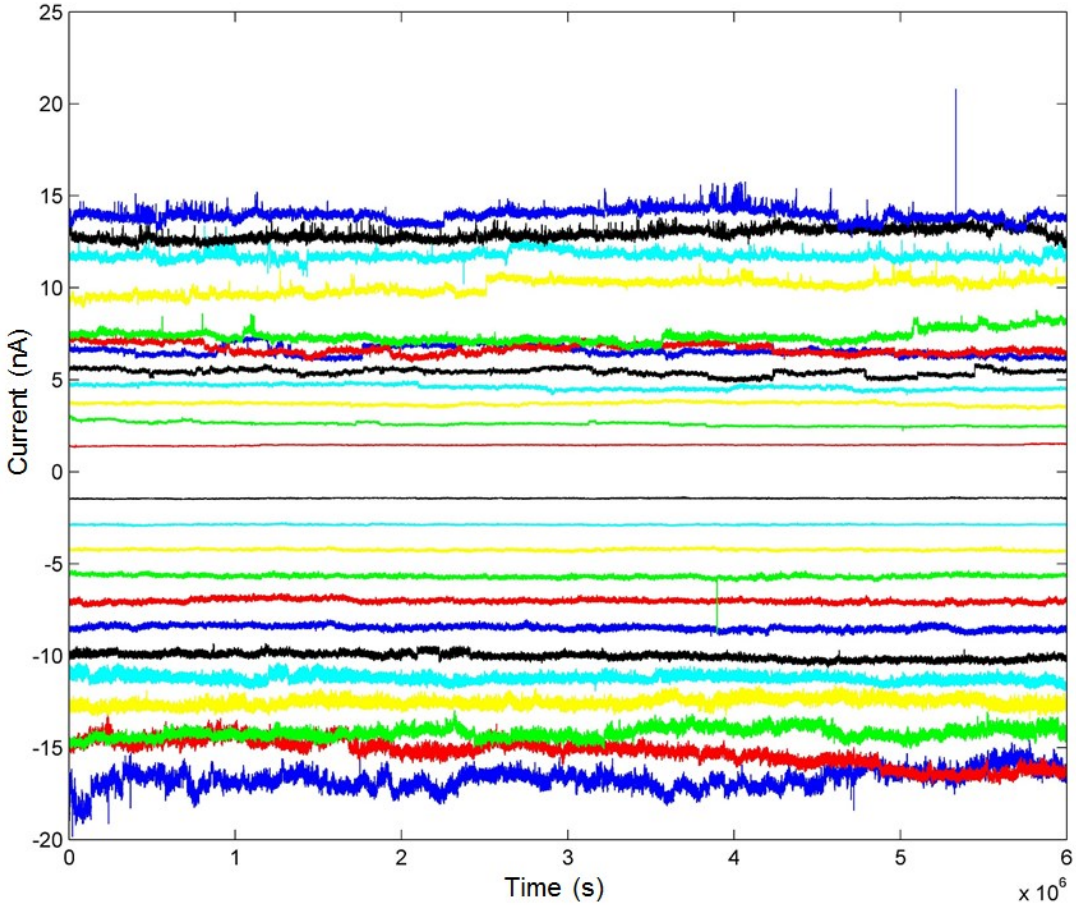

Figure 51. Single nanopore with 1M KCl with 600 to -600 mV fixed scans.

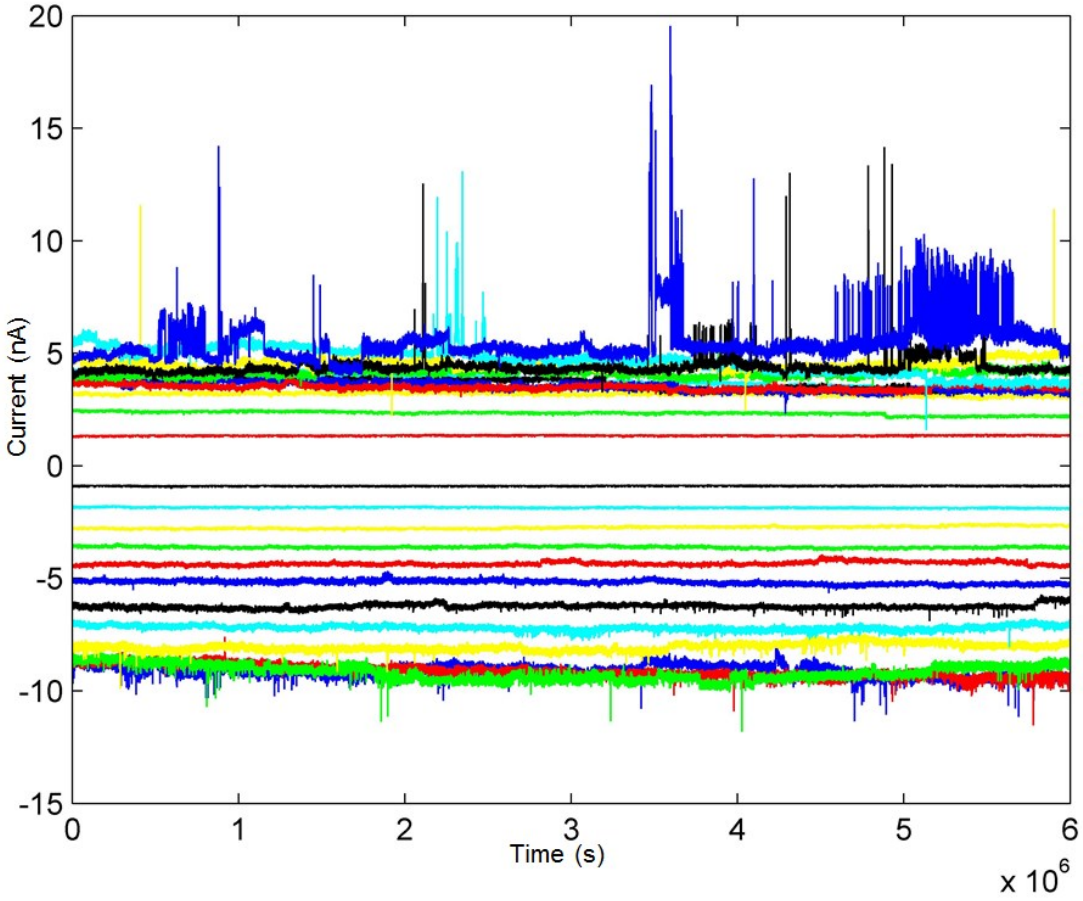

Figure 52. Single nanopore with 1M NaCl with 600 to -600 mV fixed scans.

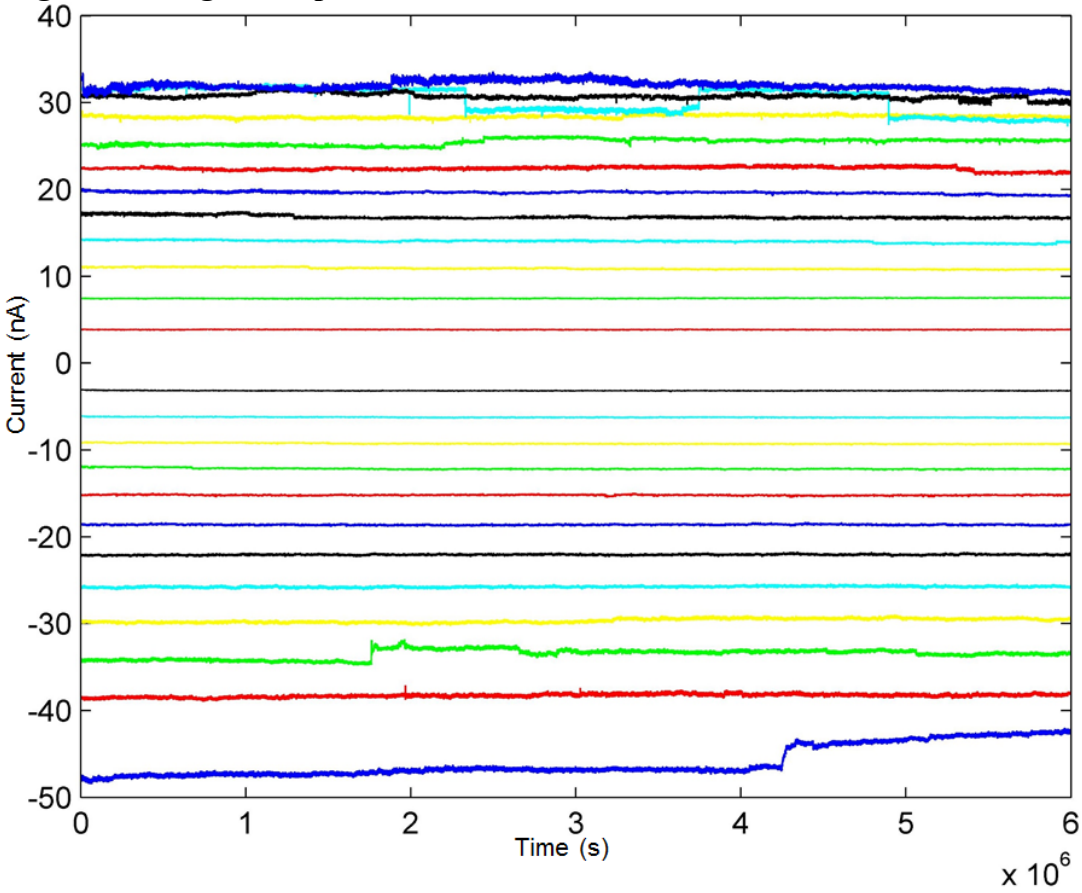

V. Testing and Experimental Demonstration of Fabricated Recording Electrode Pillars

The following chapter covers experimental investigations associated with neural recording electrodes and similar pillar structures fabricated using the fabrication scheme and methods discussed earlier. This chapter's investigations of the mechanical, electrical, and biocompatibility of the neural recording electrodes are also explored. Finally, a recording from living neurons taken using the produced electrodes integrated into a custom multi-electrode array and a MCS MEA2100

recording system is detailed. These investigations highlight the utility of the fabricated devices and demonstrate their potential for future neural recording studies.

A. Mechanical Properties of the Neural Recording Pillars

One motivation behind the creation of flexible polymer neural recording electrodes is that softer electrode pillars will cause a lessor immediate and long-term inflammatory response. Additionally, with a modulus closer to neural tissues, brain micro motion will not result in the trauma and death of immediately surrounding tissues. Both of these effects should lead to improved long-term recordings in implanted arrays. Therefore, the mechanical properties involved are investigated.

1. Flexibility of Fabricated Neural Recording Pillars

Because of the inherent elasticity of PDMS, the neural recording electrodes' starting material, the pillars are extremely flexible. Once released from the mold in which they were cast, the pillars can be bent to 90 degrees and will return to their original shape and position without permanent deformation even when magnetically packed nickel content exceeds 50% of the weight of the pillars.

2. Ideal Mechanical Behavior

An ideal neural recording pillar would be ridged like silicon (Modulus of 200 Giga Pascal) up to the point of being inserted through the Pia-arachnoid layer tissue membrane protecting the brain. Upon breaching the last protective membrane, it would then immediately become much softer as it displaces the brain tissue it is being inserted into. Finally the pillar, after the completion of the insertion and once

the pillar had come to rest, would approach a modulus near 100 Kilo Pascal, which is the upper end of neural tissue modulus. While this is ideal, such a material would need to be able to significantly alter its mechanical properties over time, a difficult task given the triggering events entailed and the environment in which such a pillar would need to maintain its biocompatibility and conductivity.

The proposed solution is the creation of a flexible pillar, which is tough enough to be inserted but not significantly more so than that. This solution leaves the pillar as soft as it can be while still being able to be inserted.

3. Mechanical Behavior of PDMS Pillars and PDMS-Nickel Pillars

Using a Hysitron Triboindenter Nanoindenter, the Young's Modulus for the prepared standard PDMS used as a starting point for all pillar experiments was approximately 3 MPa. This value matches well with figures provided by Dow Corning for the standard composition of PDMS employed. As a follow up to this investigation, additional testing was carried out using a tensile testing cell and a linked laser micrometer. Strips of material were prepared containing different levels of linker as well as loadings of nickel particles. While all measurements (see Figure 53) were similar, there was enhancement of the mechanical stiffness of the materials containing additional PDMS cross linker (activator). This is reasonable as additional cross linker provides the mechanism by which the polymer forms the extended network that provides its mechanical properties. Interestingly, loading of nickel shows a slight negative impact on mechanical stiffness. While this appears counterintuitive initially, this is reasonable given the testing conditions. Nickel which

replaces a given fraction of cross linked PDMS polymer acts as an inelastic solid. Under compression, this solid fill will clearly provide additional structure support. However, if this same material is provided a tensile rather than compressive loading force, the adhesion between nickel and the PDMS polymer rather than the inelastic mechanical properties of the nickel become prevalent. Essentially, the PDMS may overcome the adhesive force between itself and the engulfed nickel filled particles, pulling away from the otherwise mechanically solid elements within the volume. Given the nature of the test that was conducted, which drew upon strips of PDMS / cross linker / nickel composites and then measured their displacement versus force as they were unloaded back towards their initial length at zero displacement, it is understandable how this small deficit in mechanical stiffness results. Additionally, as the measurements were taken in larger volumes of composite PDMS, no simple mechanism to densify the mixed nickel to the same levels found in the magnetically densified pillar mold voids exists.

Figure 53. Tensile Young's Modulus testing for different PDMS composites.

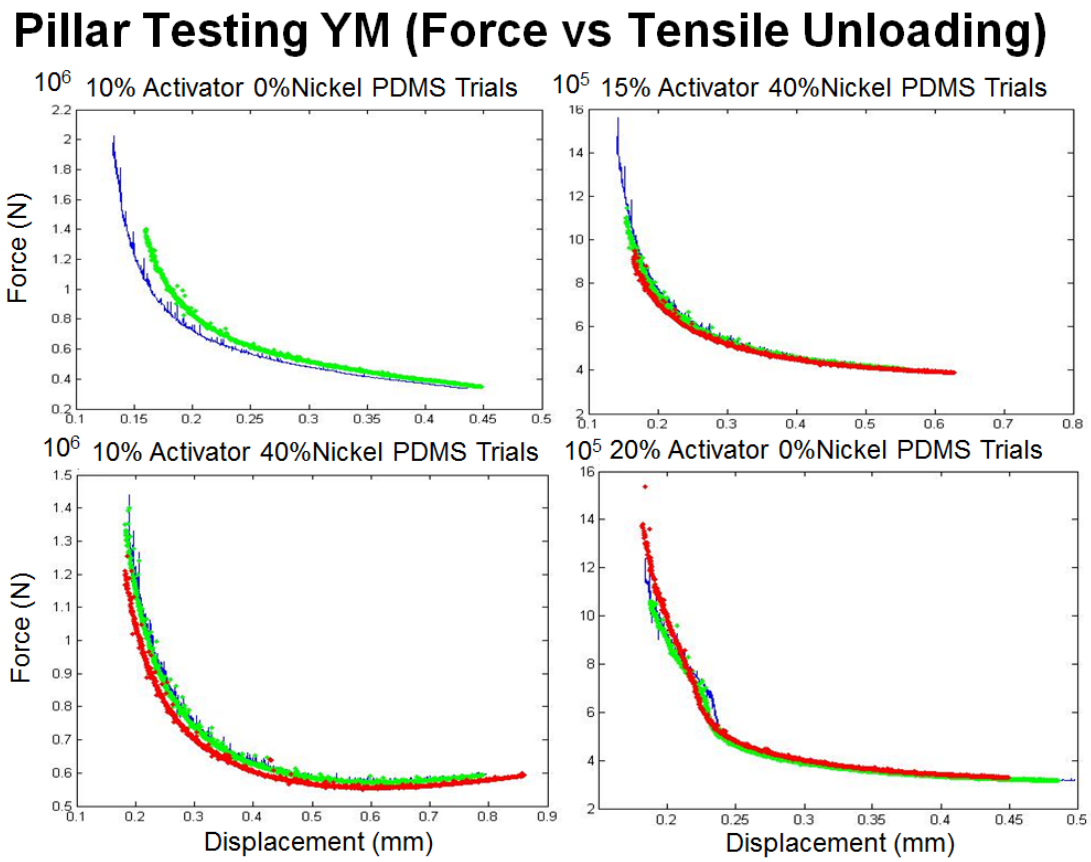

4. Possible Improvements to Mechanical Behavior of PDMS-Nickel Pillars

The stiffness of the fabricated PDMS-nickel pillars may be improved with the application of permanent or temporary coatings to assist with insertion into the brain and Pia-arachnoid membrane.

Permanent coatings such as SU-8, and particularly aerosol spray based formulations of SU-8 (Microchem SU-8 MicroSpray Photoresist Aerosol), are one possible route for increasing pillar stiffness. In this case, pillar tips could be left unexposed while the sides and substrate are exposed to a UV dose and developed to support neural recordings from the tips of the arrays while leaving a stiff support

shell. Alternatively, UV light could be directed horizontally through a mask at a pillar array while the array was rotated to expose and crosslink a series of support cylinders, leaving exposed areas along the pillars' sidewalls.

Temporary coatings could also be used, and these provide the potential for some gradual decreases in overall stiffness as the coating dissipates. One particularly interesting option is the use of sucrose as mentioned in Chapter I, which can be dissolved by intercellular fluid over time. In this case, the pillars can be inverted and dipped up to their bases in a solution of supersaturated sucrose, and then drawn out vertically. The resulting coating of solution hardens as it cools while still inverted, and can also assist in forming a sharp tip for improved insertion characteristics. By no means is this the only possible option for temporary coatings. Many other options can be formulated, but they must remain biocompatible even after dissolving or dissipating.

B. Electrical Testing

Electrical testing of individual PDMS-nickel pillars integrated with gold wireouts has shown resistances as low as 200 ohms when measured from pillar tip to wireout contact point.

1. Direct Electrical Testing

Initial electrical testing was completed by casting conductive flexible polymer pillar electrodes from 1024 pillar molds (see Figure 54). These pillar electrodes were cast without the later developed pre-bonding excess film removal technique, and as a

result featured a continuous conductive film connecting all pillars together. These pillars were not gold plated. Even with this base fill, the produced conductive pillar arrays were sufficient to SEM and examine for areas of charging, highlighting any pillars that might not be properly conducting. Additionally, measurements were made by connecting a conductor across the top of the pillar array and a second probe to the conductive film perimeter. Ideally, this measure could be divided by the number of pillars to provide an approximation of the pillars' conduction. Pillar geometry could then be used to calculate resistivity. However, this was not possible. Small amounts of PDMS at the top surfaces of the pillars partially blocked contact, forming intermittent and non-ohmic connections which made measurements across the whole pillar population unreliable.

Figure 54. Conductive 1024 pillar array initially used for electrical testing.

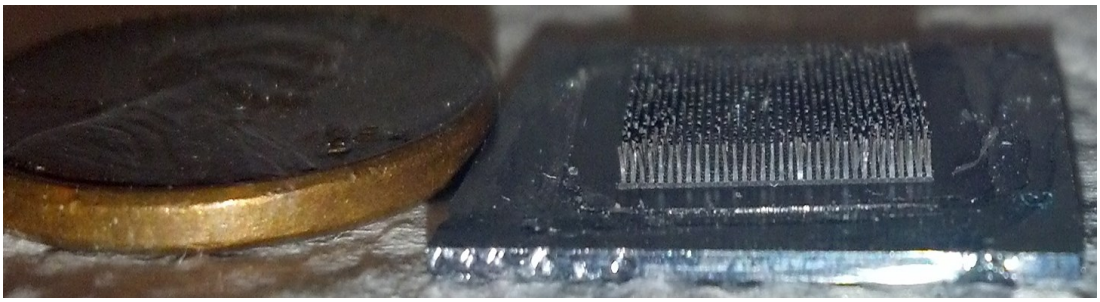

By probing local pairs of pillars with a probe station of 60 micron probes tips and dividing the resistance between the two pillars forming the conducting pair, clear measurements could be produced. Measurements using this method were clearer and pillar resistance was observed in hundreds of ohms per pillar. Using this method, it also became clear that dry physical contact between the probes, the pillars, and the network of conductive particles provides a non-ohmic resistivity that can be sensitive

to mechanical pressure changes. Given the continuous contact that is entailed when pillars are in an electrolyte or intercellular fluid, these effects are not expected to be present.

2. Electrical Testing of Individual Pillars

Once pillars were formed using the developed molding and bonding techniques previously discussed, individual independent pillar electrodes were able to be probed with the other point of contact made to the wireout on dielectric. Pillar electrodes aligned and bonded to gold wireouts provided clear information about the conductivity of the electrodes produced at different initial nickel fill loadings, and additionally verified that the pillar interconnect interface was conducting while the pillar to pillar conductivity was negligible. Accounting for pillar geometry, resistivity values of 830 Ω·cm at a 30% weight loading of nickel and 140 Ω·cm at 50% weight loading of nickel were found following the magnetic guidance and densification procedures discussed previously.

C. Demonstration of Biocompatibility and Neuro Spike Recording

In order to determine the biological compatibility of the conductive flexible polymer pillar electrodes developed, they were integrated into a custom designed and fabricated planar multi-electrode array that was compatible with a Multi-Channel Systems MEA2100-System in order to be able to record neural activity in vitro. This recording method was chosen as it was an ideal initial step to both investigate biocompatibility and also begin to demonstrate the recording functionality of the

conductive flexible polymer pillar electrodes. Additionally, the accessibility of line animal implantations at the University of California Santa Barbara is limited, making in vitro records the best option before extending collaborative efforts to other institutions.

Due to the possible interaction between neurons and nickel, which is known to be cytotoxic, the pillars were plated in an electroless gold plating solution prior to experimentation. The treatment resulted in microscopic conformal layers of gold plating on all exposed nickel that would otherwise be directly interacting with cell buffer solution. To demonstrate initial biocompatibility, neurons were plated onto the fabricated custom MEAs with conductive flexible pillar electrode arrays. The neurons were incubated for up to two weeks and cell adhesion to the multi-electrode array surfaces was maintained, indicating the continued viability of the attached cells (see Figure 55). Activity from these incubated neurons was then recorded using the MEA2100-System. The recorded signals (see Figure 56) show activity in a number of the 2D and pillar recording sites. Inhibition of these signals (see Figure 57) via the application of Tetrodotoxin (TTX), a neurotoxin that inhibits the firing of action potentials, confirms that the signals observed are the result of neural active occurring near the pillars electrodes.

Further measurements and investigations are ongoing while the biological protocol required to form robust populations of neurons in virto on these devices is being developed. Depending on if enhancements are found by altering the biological protocol involved, other routes of enhancement may include pre-plating the nickel

particles with gold, migrating to more biocompatible fill particles, or additionally modifying the chemistry found at the surface of the PDMS to better facilitate growth of neuronal cultures. Pre-plating the nickel fill particles with electroless gold prior to mixing the PDMS-nickel compound would ensure that all the nickel that is used to form the conductive flexible polymer pillar electrodes is biologically safe. Similarly, moving towards a biologically compatible magnetic particle could also completely remove the possibility of cytotoxicity. PDMS can be particularly non-ideal for in vitro neural growth, so a modification of the standard surface chemistry towards something more stiff and glass-like might drastically improve the growth and activity of the plated neurons.

Figure 55. Transmission images of living neurons attached to pillar MEA.

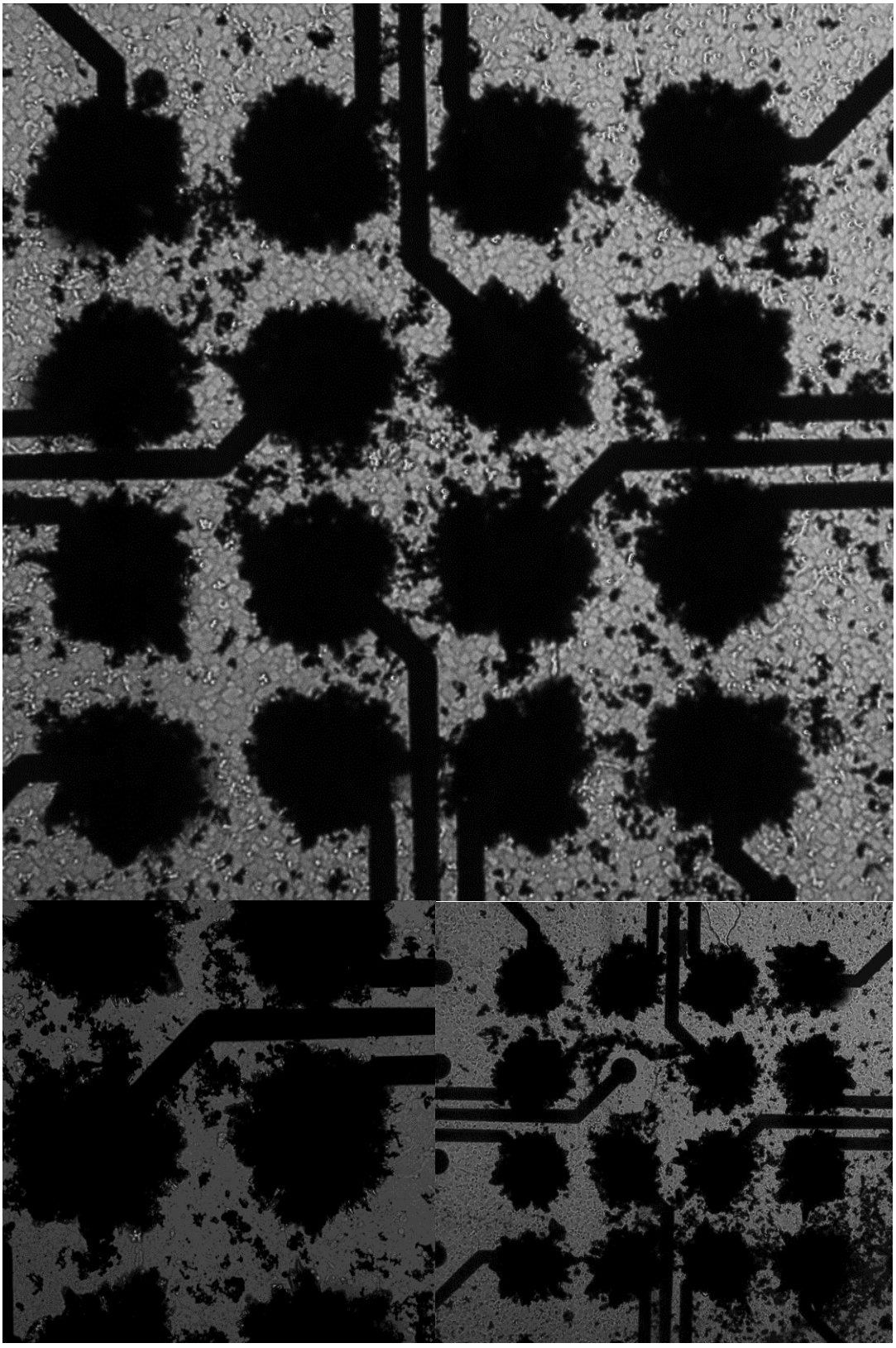

Figure 56. Recorded electrical measurements from 120 channel pillar MEA.

Figure 57. Recorded neural signals before and after applying tetrodotoxin (TTX)

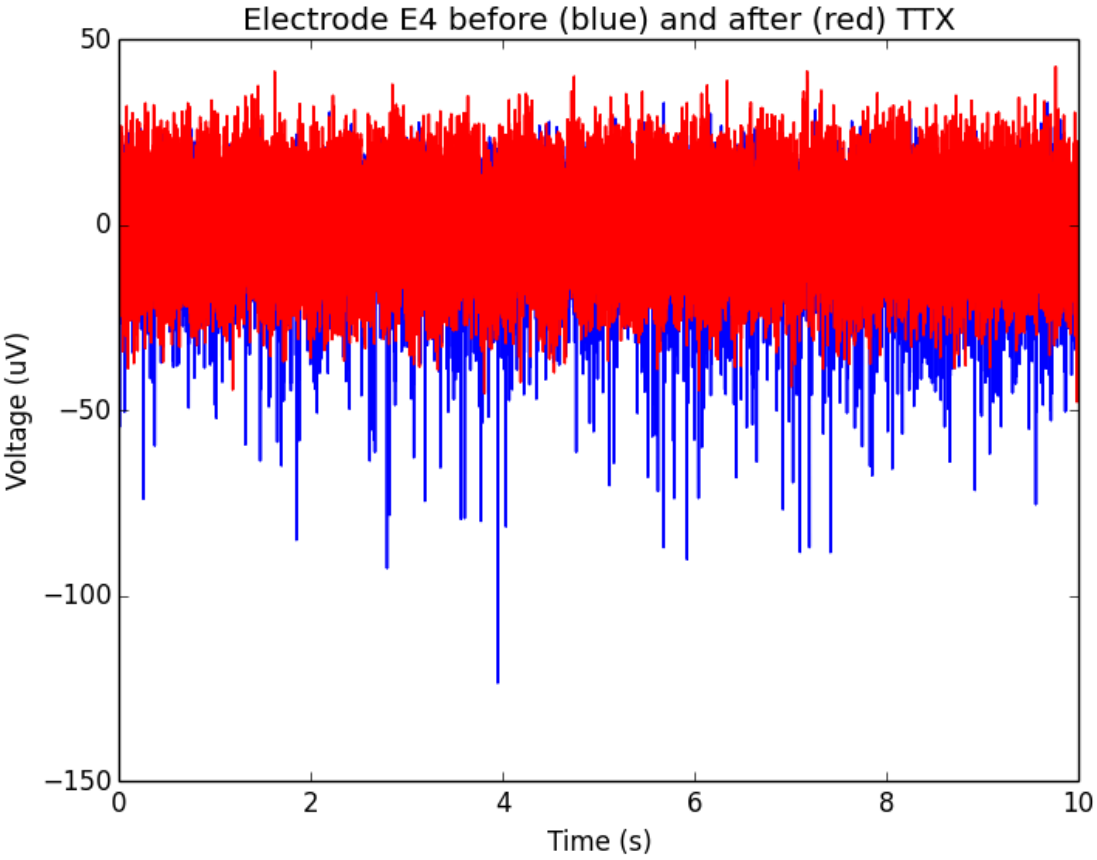

VI. Conclusions and Future Avenues

In general, motivation for this research stemmed from the desire to gain a greater understanding of the neuronal circuitry driving the human brain to enhance the lives of patients suffering from conditions such as debilitating diseases of the peripheral nervous system and sensory organ failure. From these motivations, two novel biomimetically inspired schemes to improve the lives of patients and provide enhanced methods for interfacing with neural systems were envisioned. From these schemes, the critical interfacing elements and their associated requirements were determined and these requirements were transformed into two microfabrication

development programs. These programs resulted in fabrication schemes that produced the envisioned critical neural interfacing components. Additionally, investigative demonstrations using devices produced via these fabrication schemes have highlighted the utility and functionality of the neural interfacing structure developed.

A. Flexible Polymer Neural Recording Pillar Electrodes

The conductive flexible polymer pillar electrodes produced are extremely flexible and quite conductive. The fabrication scheme developed has yielded a product which meets the required criteria. While the road to beneficial chronic human medical implants is very long for such a radically new device structure, in vitro experimentation is the first step towards potentially one day directly improving the lives of patients with diseases of the peripheral nervous system.

1. Recoding 3D Neuronal Networks (“Mini Brains”)

Beyond simple two dimensional cultures of neurons, which could easily be recorded with planar recording arrays such as a standard multi-electrode array, recording from three dimensional volumes of neurons may be the first research activity in which these novel structures begin to shine. Three dimensional neuronal networks suspended in supporting gel have the possibility of growing with far more diverse and interesting levels of connectivity, and require the ability to record across a volume. Additionally, the soft nature of the conductive flexible polymer pillar

electrodes would provide a much better environment when the in vitro experiment is being transport around the lab and experiencing acceleration akin to micro motion.

2. Spatially Localized Neural Recording using Planar and Pillar Recording Electrodes

By recording from both two dimensional planar electrodes on a recording array surface as well as conductive flexible polymer pillar electrodes, fixed positioning in three dimensions should be able to be determined for any active neurons firing within a three dimensional neural network volume. Attenuation would make it impossible for a two dimensional array to accomplish this feat independently for any significantly thick volume, however the planar recording sites provide enough coverage to determine the Z-height along the orthogonal direction of the conductive flexible polymer pillar electrodes.

3. Post CMOS Integration and Full Channel Demonstration

On the path to a completely wireless high density neural recording interface, embedding a custom CMOS die which has a full demonstration neural recording channel into a larger silicon handle and then bonding conductive flexible polymer pillar electrodes to it could demonstrate the whole scheme. This would provide a single channel representation of the envisioned recording interface and recording electronics working in tandem.

4. Comparative Studies to Utah Array

Once significant in vitro work has fully illustrated the utility of the conductive flexible polymer pillar electrodes, one further investigation will be comparative studies against the Utah Array which informed the implementation of the design. Using the wireouts and molds that have already been designed to be compatible with the dual hemisphere animal studies conducted in the Neural Interaction Lab at UCSD, direct comparisons between 16 conductive flexible polymer pillar electrode arrays and 16 electrode Utah Arrays should be possible.

5. Coupled Optical Stimulation of Polymer Electrodes

PDMS is already being investigated[8] as a core and cladding material for optical waveguides, so pillars cast using the scheme described could possibly be used to form an optogenetic stimulation and recording platform. Sylgard 184 without any modifications effectively channels green light in air without a cladding (see Figure 58 and Figure 59). Ideally, optically transparent magnetic conductive particles could be used to make a single pillar capable of both recording and stimulation. Alternatively, the conductive fill could be used in a second coating, leaving a narrower core of nonconductive PDMS to act as a waveguide while the metal bearing conductive PDMS cladding layer could be chemically altered to provide conditions for total internal reflection. In this case, a narrow pillar could be formed using a narrow mold. That pillar could then be inserted into a large mold and the difference in volume could be filled by the conductive cladding material. Without either of these options, independent recording and optogenetic stimulation pillars could be

produced in a staggered array providing both stimulation and recording capabilities within the same plane of neural activity.

Figure 58. PDMS pillar array channeling 530nm light.

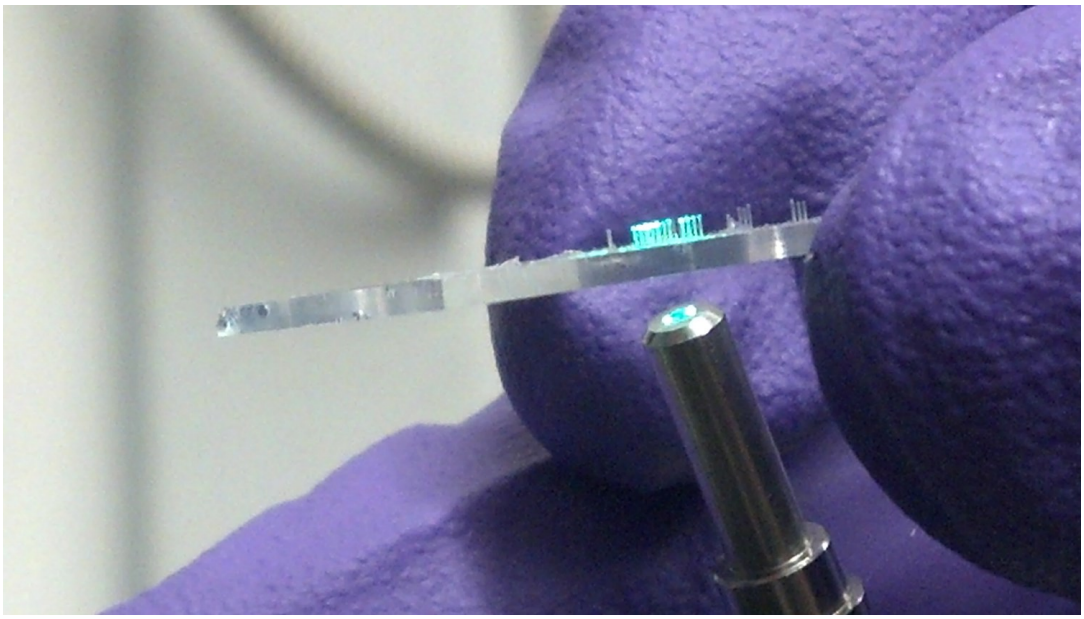

Figure 59. PDMS pillars channeling 530nm light.

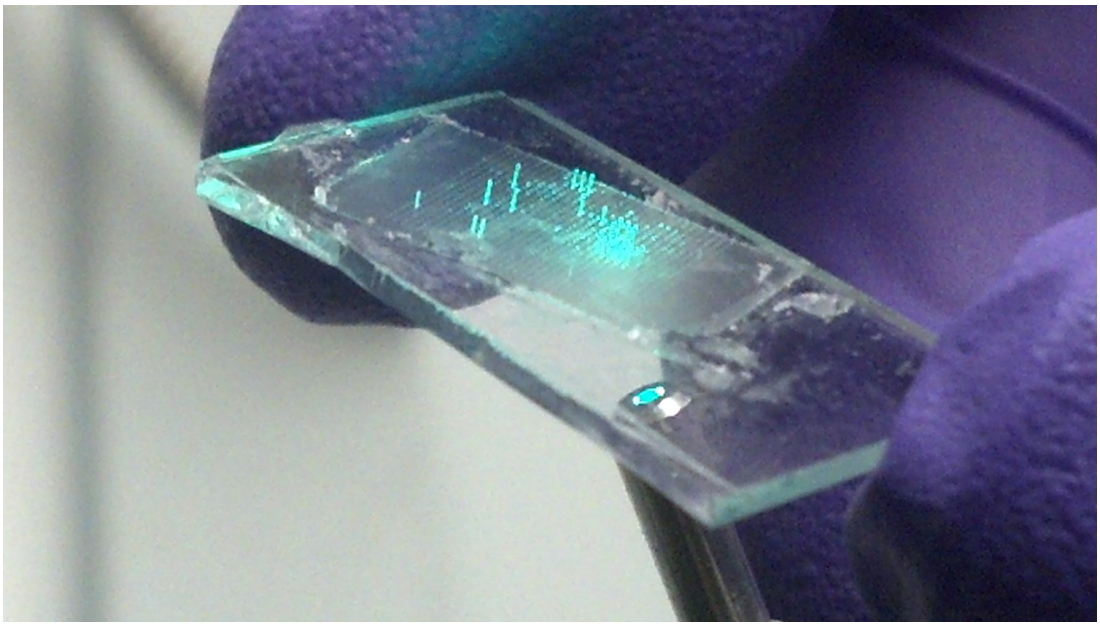

B. Alumina Nanoporous Membranes Arrays

The nanoporous alumina membrane scaffolds that have been developed and demonstrated are robust thin film scaffolds on silicon frames that are ideal for transport studies. When combined with crown ethers, these have demonstrated several different voltage dependent behaviors.

1. Investigation of Crown Behavior

The demonstrative investigations conducted using the fabricated nanoporous alumina have highlighted electric field dependent crown behaviors. These behaviors are interesting, but more characterization is required to better understand and present a more complete model of these observed behaviors. Using a mixture of modeling as well as single nanopores and the fabricated nanoporous alumina membranes, the exact behavior may be completely understood.

2. Development of Improved Tethered Transporters

As the highest observed stable preferential selectivity to potassium versus sodium was 2.8 with meso silica and triethoxysilane terminated 18-crown-6, it is clear that for the envisioned selective electrically gated ion pump devices to operate as intended in the scheme better chemistries will need to be found that provide higher levels of selectivity. Whatever materials are used, it is very likely that the nanoporous alumina membranes will continue to be utilized as a structurally stable scaffold.

3. Development of Sequestration Chemistries and a Sequestration Platform

As the overall neural stimulating interface scheme requires a potassium sequestration mechanism, it is likely that this will be developed moving forward. Due to the similar transport flux, chemical, thermal, and mechanical stability requirements for such a device, it is likely it will also use the same nanoporous alumina membranes that have been described in this work.

References

1. L.S. Theogarajan, R.J. Jensen, and J.F. Rizzo Stimulation of Rabbit Retinal Ganglion Cells by altering K+ Ion Gradients: Dose-Response Curve. Invest. Ophthalmol. Vis. Sci., 45(5):4215 (2004).

2. Joakim Isaksson, Peter Kjäll, David Nilsson, Nathaniel Robinson, Magnus Berggren, Agneta Richter-Dahlfors Electronic control of Ca2+ signaling in neuronal cells using an organic electronic ion pump Nature Materials 6, 673 - 679 (2007).

3. Amarjit Singh, Haixin Zhu, and Jiping He Improving Improving Mechanical Stiffness of Coated Benzocyclobutene (BCB) Based Neural Implant. 26th Annual International Conference of the IEEE EMBS (2004).

4. A.C. Fischer, N. Roxhed, T. Haraldsson, N. Heinig, G. Stemme, F. Niklaus Fabrication of high aspect ratio through silicon vias (TSVs) by magnetic assembly of nickel wires. IEEE 24th Annual International Conference on Micro Electro Mechanical Systems (MEMS) (2011).

5. E. Vasile, F. Dumitru, A. Razvan, O. Opera, and C. Andronescu Novel Ureido-4 '-Aminobenzo-15-Crown-5-Ether Periodic Mesoporous Silicas. Digest Journal of Nanomaterials and Biostructures Vol. 8, No. 1, January - March (2013).

6. Adinela Cazacu, Yves-Marie Legrand, Andreea Pasc, Gihane Nasr, Arie Van der Lee, Eugene Mahon, and Mihail Barboiu. Dynamic hybrid materials for constitutional self-instructed membranes Proceedings of the National Academy of Sciences May 19 (2009).

7. Barbara Platscheck, Andreas Keilbach, and Thomas Bein Mesoporous Structures Confined in Anodic Alumina Membranes Advanced Materials, 23, 2395-2412 (2011).

8. D.K. Cai, A. Neyer, R. Kuckuk, and H.M. Heise Optical absorption in transparent PDMS materials applied for multimode waveguides fabrication. Optical Materials 30 (2008).